A NUMERICAL EXPERIMENT ON A TURBULENCE MODEL

by

Aldo Giorgini

Prepared under support
of the
U.S. Army Materiel Command
Grant DA-AMC-28-043-65-G20
and the
National Center for Atmospheric Research

FLUID MECHANICS PROGRAM
ENGINEERING RESEARCH CENTER
COLLEGE OF ENGINEERING
COLORADO STATE UNIVERSITY
FORT COLLINS, COLORADO

Technical Report

A NUMERICAL EXPERIMENT ON A TURBULENCE MODEL

by

Aldo Giorgini

Prepared under support
of the
U.S. Army Materiel Command
Grant DA-AMC-28-043-65-G20
and the
National Center for Atmospheric Research

Distribution of This Report is Unlimited

Fluid Dynamics and Diffusion Laboratory
College of Engineering
Colorado State University
Fort Collins, Colorado

December 1967

CER67-68AG49

PREFACE AND ACKNOWLEDGMENTS

It is the intention of the author to present in this paper some results of a numerical experiment on a turbulence model performed at the National Center for Atmospheric Research on a CDC 6600 high speed computer, while the author was a Postdoctoral Fellow of the Advanced Study Program of NCAR and an Assistant Professor of Engineering at Colorado State University.

The author wishes to thank:

The operators of the Computing Facility and the technicians of the Microfilm Facility for their invaluable cooperation; to their participation is due the successful completion of the experiment in a relative short amount of time;

Several members of the personnel of the Computing Facility and chiefly Dave Robertson, whose unparalleled attitude of meeting the challenges of any programming difficulties has been not only extremely useful and expedient but highly enlightening to the author;

Maxine Ross, who patiently typed the present paper from a draft partly unreadable with the results visible here.

Part of the financial support for this study was provided by the Integrated Army Meteorological Wind-Tunnel Research Program under Grant DA AMC 28-043-65-G20.

CONTENTS

I. PURPOSE OF THE PRESENT RESEARCH

The purpose of the present research is the numerical integration of Burgers' equation.

As it is well known, Burgers[1] proposed and studied the equation that now bears his name as a one-dimensional model for Navier-Stokes equation.

The fact that such important quantity as the vorticity has no meaning outside a three-dimensional space is a strong limitation to the use that could be made of any results of Burgers equation as indicative of solutions of Navier-Stokes equations. Therefore from the physical viewpoint any inference should be regarded with suspicion.

But the other fact that Burgers equation shares with Navier-Stokes equations two essential mathematical features, namely

a) strong nonlinearity,

b) small coefficient of the highest order derivative,

justifies the use of Burgers equation as a first step in numerical simulation.

In the present numerical experiment Burgers equation has been Fourier-analyzed to obtain a system of a discrete infinity of equations in a discrete infinity of variables, and the numerical techniques have been used for such a system, being the author's belief that the wave-number space yields to a "cleaner" numerical approach.

II. BURGERS' EQUATION AND ITS FOURIER-MATE

If $u(x,t)$ is the velocity field at time t on a one-dimensional space measured by the abscissa x, Burgers' equation can be written

$$\frac{\partial u}{\partial t} + u \frac{\partial u}{\partial x} = \nu \frac{\partial^2 u}{\partial x^2} , \tag{1}$$

where ν is the viscosity of the fluid. In this form Burgers' equation is an approximate model of the real behavior of shock waves in gas dynamics.

If we define

a length scale L

a velocity scale U

and consider the following variables and parameters

adimensional velocity $v = u/U$

adimensional abscissa $\xi = x/L$

adimensional time $\tau = Ut/L$

Reynolds number $R = UL/\nu$,

equation (1) can be rewritten as

$$\frac{\partial v}{\partial \tau} + v \frac{\partial v}{\partial \xi} = \frac{1}{R} \frac{\partial^2 v}{\partial \xi^2} . \tag{2}$$

If the velocity field in its Fourier-expansion

$$v(\xi,\tau) = \sum_{\kappa=1}^{\infty} v(\kappa,\tau) \sin \kappa\xi , \tag{3}$$

which implies a period 2π in the velocity field, is substituted into

equation (2), we get the system of ordinary differential equations

$$(4) \qquad \left\{ \right._{\kappa=1,\infty} \frac{dv(\kappa,\tau)}{d\tau} + \frac{\kappa^2}{R} v(\kappa,\tau) = \frac{\kappa}{2} \sum_{\kappa'=1}^{\infty} v(\kappa',\tau)v(\kappa+\kappa',\tau) - \frac{\kappa}{4} \sum_{\kappa'=1}^{\kappa-1} v(\kappa',\tau)v(\kappa-\kappa',\tau) \ .$$

Because of our definitions and the expansion (3), it is

$$(5) \qquad u(x,t) = \sum_{\kappa=1}^{\infty} Uv(\kappa,\tau) \sin \frac{\kappa}{L} x \ ,$$

which implies that the Fourier-coefficient of u(x,t) is

$$(6) \qquad u(\kappa,t) = Uv(\kappa,\tau) \ ,$$

and the period in physical space is $2\pi L$.

The following are the inverse transforms:

$$(7) \qquad v(\kappa,\tau) = \frac{1}{\pi} \int_0^{2\pi} v(\xi,\tau) \sin(\kappa\xi) d\xi \ ,$$

$$(8) \qquad u(\kappa,t) = \frac{1}{\pi L} \int_0^{2\pi L} u(x,t) \sin \left(\frac{\kappa}{L} x\right) dx \ .$$

The numerical solution of (4) with random initial conditions will be the aim of the present research.

III. DISCUSSION OF THE PROBLEMS ENCOUNTERED IN APPLYING THE NUMERICAL TECHNIQUES

The system (4) being the object of our numerical experiment we will rewrite it, without explicit mention of the time dependence, as follows

$$(4)\quad \left\{ \left(\frac{d}{d\tau} + \frac{\kappa^2}{R} \right) v(\kappa) = \frac{\kappa}{2} \sum_{\kappa'=1}^{\infty} v(\kappa')v(\kappa+\kappa') - \frac{\kappa}{4} \sum_{\kappa'=1}^{\kappa-1} v(\kappa')v(\kappa-\kappa') \right. \quad \kappa=1,\infty \ .$$

Even a cursory look to the above system shows that the numerical approximations we must use are two:

1) finite increments of the time variable,

2) a wave-number cut-off N (to replace the symbol ∞ in the system (4)).

Neglecting the errors introduced by the computer, and provided measures are taken to avoid numerical instabilities, the main sources of errors are just the above approximations.

While the errors introduced by the use of finite increments for τ may be checked by allowing the increments $\Delta\tau$ to become smaller and smaller in subsequent trials; the influence of the wave-number cut-off is much more difficult to assess. By using a method analogous to the one suggested for the errors introduced by $\Delta\tau$, we should use first a very large wave-number cut-off N and decrease it gradually in successive experiments.

This is quite feasible but in this context the knowledge of an exact solution in wave-number space would be invaluable in order to shorten both computer time and programmer time.

Such solution exists and was found by Benton.[2] A short presentation of Benton's solution and a discussion of its merits follow.

III-1. Benton's Solution to Burgers' Equation

Benton finds that a solution to the system (4) is:

$$\tilde{v}(\kappa,\tau) = -\frac{2}{R}\,\mathrm{csch}\,\kappa\,(\alpha + \frac{\tau}{R}) \,, \tag{9}$$

where α determines the initial conditions.*

As it stands, in the solution (9) -- as well as in the equation (4) of which (9) is a solution -- the Reynolds number R is unspecified. In fact the velocity scale U has not been correlated yet with any velocity distribution. We will agree to call U an "initial" velocity scale and precisely we will call U the mean square velocity over the space interval $2\pi L$, that is

---

* The physical meaning of α is evident: for $\tau = -\alpha R$, $\tilde{v}(\kappa,\tau)$ becomes infinite. Therefore $-\alpha$ is the virtual time-origin, measured in Reynolds numbers, of an infinite velocity field which, because of viscosity, decays in time according to the law given by (9).

$$(10) \qquad U^2 = \frac{1}{2\pi L}\int_0^{2\pi L} u^2(x,0)\,dx$$

$$= \frac{U^2}{2\pi}\int_0^{2\pi}\left[\sum_{\kappa=1}^{\infty}\tilde{v}(\kappa,0)\sin\kappa\xi\right]^2 d\xi$$

$$= \frac{U^2}{2\pi}\sum_{\kappa=1}^{\infty}\tilde{v}^2(\kappa,0)\int_0^{-\pi}\sin^2\kappa\xi\,d\xi$$

$$= \frac{U^2}{2}\sum_{\kappa=1}^{\infty}\tilde{v}^2(\kappa,0)\ ,$$

that is

$$2 = \frac{4}{R^2}\sum_{\kappa=1}^{\infty}\operatorname{csch}^2\kappa\alpha$$

or

$$(11) \qquad R^2 = 2\sum_{\kappa=1}^{\infty}\operatorname{csch}^2\kappa\alpha\ .$$

The functional expression (11) allows us to find the initial Reynolds number (according to the criterion defined above) once α is given, or vice versa.

In the figures 1 and 2 the initial Reynolds number is shown versus the parameter α.

Besides being the only known solution in terms of wave-number space, Benton's solution has an additional feature which makes it particularly suitable as a test solution: the absolute value of the velocity amplitude,

$$(12) \qquad |\tilde{v}(\kappa,\tau)| = \frac{2}{R}\operatorname{csch}\kappa\left(\alpha+\frac{\tau}{R}\right)\ ,$$

decreases monotonically with time and with κ.

Due to the effects of viscosity, no matter what initial conditions are given, we would expect to reach such qualitative state after some

time. In fact, the wave-numbers dissipate energy proportional to $\kappa^2 v^2(\kappa)$, and therefore the highest wave-numbers are bound to lose more energy than they can receive through the energy exchange with the other modes.

For these reasons Benton's solution will be used as a reference solution

1) for the determination of the influence of the wave-number cut-off and the perfecting of the numerical techniques,

2) for the determination of the statistical ensemble in the numerical experiment in Burgerlence proper.

III-2. Plan of Approach

Given that we will use a wave-number cut-off N, the system of equations to solve, starting from arbitrary initial conditions

(13) $\qquad v(\kappa,0) \qquad \kappa = 1,N$

is

$$(14) \qquad \left\{ \right._{\kappa=1,N} \quad \frac{dv(\kappa,\tau)}{d\tau} = -\frac{\kappa^2}{R} v(\kappa,\tau) + \frac{\kappa}{2} \sum_{\kappa'=1}^{N-\kappa} v(\kappa')v(\kappa+\kappa') - \frac{\kappa}{4} \sum_{\kappa'=1}^{\kappa-1} v(\kappa')v(\kappa-\kappa') \ .$$

We will consider time increments within which the cubic limited Taylor-expansions of the $v(\kappa)$'s are good approximations to the real functions.

In general the time increments may vary with time and be different for different wave-numbers; we will use for them the notation $\Delta\tau(\kappa,\tau)$, neglecting one of the arguments whenever it is implicitly evident.

We will consider therefore, together with the system above, the systems

$$(15)\left\{\begin{array}{l}\\ \kappa=1,N\end{array}\right. \quad \frac{d^2 v(\kappa,\tau)}{d\tau^2} = -\frac{\kappa^2}{R}\frac{dv(\kappa,\tau)}{d\tau} + \frac{\kappa}{2}\sum_{\kappa'=1}^{N}\left(\frac{dv(\kappa')}{d\tau}\, v(\kappa+\kappa') + v(\kappa')\,\frac{dv(\kappa+\kappa')}{d\tau}\right)$$

$$- \frac{\kappa}{4}\sum_{\kappa'=1}^{\kappa-1}\left(\frac{dv(\kappa')}{d\tau}\, v(\kappa-\kappa') + v(\kappa')\,\frac{dv(\kappa-\kappa')}{d\tau}\right)$$

$$(16)\left\{\begin{array}{l}\\ \kappa=1,N\end{array}\right. \quad \frac{d^3 v(\kappa,\tau)}{d\tau^3} = -\frac{\kappa^2}{R}\frac{d^2 v(\kappa,\tau)}{d\tau^2}$$

$$+ \frac{\kappa}{2}\sum_{\kappa=1}^{N}\left(\frac{d^2 v(\kappa')}{d\tau^2}\, v(\kappa+\kappa') + 2\,\frac{dv(\kappa')}{d\tau}\,\frac{dv(\kappa+\kappa')}{d\tau} + v(\kappa')\,\frac{d^2 v(\kappa+\kappa')}{d\tau^2}\right)$$

$$- \frac{\kappa}{4}\sum_{\kappa'=1}^{N}\left(\frac{d^2 v(\kappa')}{d\tau^2}\, v(\kappa-\kappa') + 2\,\frac{dv(\kappa')}{d\tau}\,\frac{dv(\kappa-\kappa')}{d\tau} + v(\kappa')\,\frac{d^2 v(\kappa-\kappa')}{d\tau^2}\right).$$

Once the quantities

$$(17) \qquad d(\kappa,\tau) = \frac{dv(\kappa,\tau)}{d\tau}, \quad f(\kappa,\tau) = \frac{d^2 v(\kappa,\tau)}{d\tau^2}; \quad g(\kappa,\tau) = \frac{d^3 v(\kappa,\tau)}{d\tau^2},$$

are found for a certain κ and τ the value of $v(\kappa, \tau+\Delta\tau)$ is found by means of

$$(18) \qquad v(\kappa, \tau+\Delta\tau) = v(\kappa,\tau) + d(\kappa,\tau)\Delta\tau(\kappa,\tau) + \frac{1}{2} f(\kappa,\tau)\Delta\tau^2(\kappa,\tau)$$

$$+ \frac{1}{6} g(\kappa,\tau)\Delta\tau^3(\kappa,\tau) .$$

III-3. Criterion for the Determination of the Wave-Number Cut-Off

Several criteria could be devised. The criterion used in the present study is the following:

Consider the initial conditions of the reference solution

(19) $$-\frac{2}{R}\,\mathrm{csch}\,\nu\alpha,$$

where α and R are conjugated with respect to (11).

Call N the wave-number cutoff. Then

$$\frac{4}{R^2}\sum_{\nu=1}^{N}\nu^2\,\mathrm{csch}^2\nu\alpha \qquad \text{and} \qquad \frac{4}{R^2}\sum_{\nu=N+1}^{\infty}\nu^2\,\mathrm{csch}^2\nu\alpha$$

represent respectively the dissipation taking place between wave-number 1 and wave-number N, and the dissipation of the wave-numbers above N.

We will fix a small value ϵ for the ratio

(20) $$\frac{\sum_{\nu=N+1}^{\infty}\nu^2\,\mathrm{csch}^2\nu\alpha}{\sum_{\nu=1}^{\infty}\nu^2\,\mathrm{csch}^2\nu\alpha},$$

and agree that N is the lowest wave number that makes such ratio less than ϵ.

Different values of ϵ may be chosen. In our research we will fix $\epsilon = 0.01$ with the belief that the discard of 1% of the total dissipation should affect very little the total behavior of the solution. The effects of the wave-number cut-off will be studied later.

In the figures 3, 4, 5, 6, 7 the wave-number cut-off is plotted against the Reynolds number.

III-4. Criterion for the Estimate of the Maximum Time Interval of Integration

The most reasonable criterion for the determination of the total time of integration seems to be the following:

Given the initial conditions

$$-\frac{2}{R}\,\mathrm{csch}\ \varkappa\alpha\ ,$$

according to which the initial kinetic energy is

$$\frac{4}{R^2}\sum_{\varkappa=1}^{N}\mathrm{csch}^2\varkappa\alpha\ ,$$

consider the ratio

$$(21)\qquad \frac{\sum_{\varkappa=1}^{\infty}\mathrm{csch}^2\varkappa(\alpha+\frac{T}{R})}{\sum_{\varkappa=1}^{\infty}\mathrm{csch}^2\varkappa\alpha}$$

between the total kinetic energy at $\tau = T$ and $\tau = 0$. T may be calculated if we assign to the above ratio a value $\eta < 1$ and assign a value to R.

It seems reasonable to assign to η the value .1, with the belief that, by the time the kinetic energy has decayed to 1/10 of its original value, the wave-numbers greater than the very first ones will have sufficiently interacted exchanging their energy.

In the figures 8, 9, 10, 11 T has been plotted against R for η = .5, .1, .01, .001.

III-5. Criterion for the Determination of the Time-Increment to Assign to Each Wave-Number

The best criterion seems to be given by the following recipe:

Start from some initial conditions at $\tau = 0$ and find the first three derivatives $d(\varkappa,0)$, $f(\varkappa,0)$, $g(\varkappa,0)$ by means of the systems (14), (15), (16). The linear, quadratic and cubic limited Taylor-expansions around $\tau = 0$ are respectively

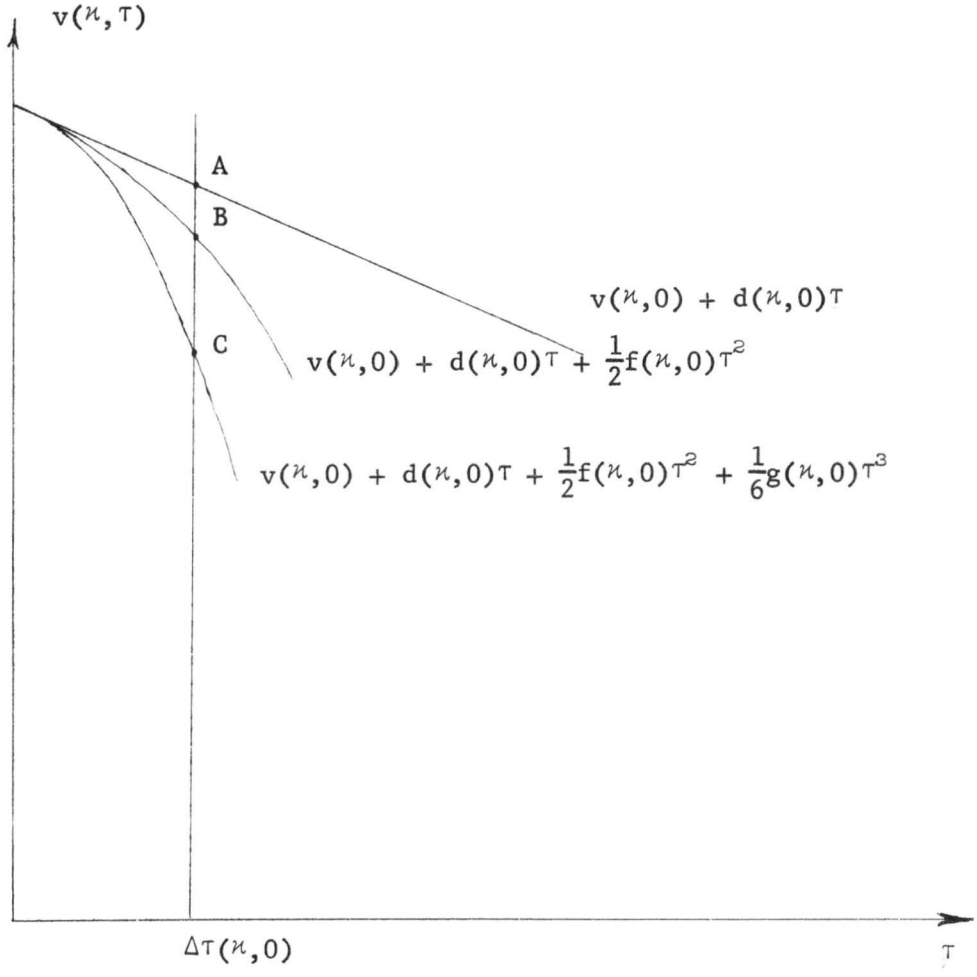

We will consider only time increments within which the cubic limited expansion is a good approximation to the exact solution and therefore we will fix a small number ψ and determine $\Delta\tau$ such that

$$\frac{|CB|}{|BA|} = \psi \tag{22}$$

or

$$\frac{1}{6}\left|g(\kappa,0)\Delta\tau^3(\kappa,0)\right| = \psi\,\frac{1}{2}\left|f(\kappa,0)\Delta\tau^2(\kappa,0)\right|$$

$$\Delta\tau(\kappa,0) = 3\psi\left|\frac{f(\kappa,0)}{g(\kappa,0)}\right| \tag{23}$$

We will find that there is a $\kappa = \kappa_1$ for which the above expression is a minimum. Take $\Delta\tau(\kappa_1,0)$ as the reference time step and calculate $n(\kappa,0)$ as the lower integer approximating $\Delta\tau(\kappa,0)/\Delta\tau(\kappa_1,0)$.

For all those κ's for which $n(\kappa,0) = 1$ the cubic limited expansion is a good approximation for the first time interval $\Delta\tau(\kappa_1,0)$; for all those κ's for which $n(\kappa,0) = 2$ the cubic limited expansion is a good approximation till time $\tau = 2\Delta\tau(\kappa_1,0)$, and so on.

For those κ's for which $n(\kappa,0) \neq 1$ then

$$g(\kappa,\Delta\tau) = g(\kappa,0)$$

$$f(\kappa,\Delta\tau) = f(\kappa,0) + g(\kappa,0)\Delta\tau$$

$$d(\kappa,\Delta\tau) = d(\kappa,0) + f(\kappa,0)\Delta\tau + \frac{1}{2}\,g(\kappa,0)\Delta\tau^2$$

We want to calculate now $\Delta\tau(\kappa,\Delta\tau)$ for $\kappa = \kappa_n$, a κ for which we had $n(\kappa_n,0) = n$.

In this case

$$\Delta\tau(\kappa_n,0) = 3\psi\left|\frac{f(\kappa_n,0)}{g(\kappa_n,0)}\right| = n\Delta\tau \tag{24}$$

and

$$\Delta\tau(\varkappa_n,\Delta\tau) = 3\psi\left|\frac{f(\varkappa_n,\Delta\tau)}{g(\varkappa_n,\Delta\tau)}\right|$$

$$= 3\psi\,\frac{|\,f(\varkappa_n,0) + g(\varkappa_n,0)\Delta\tau\,|}{|\,g(\varkappa_n,0)\,|}$$

$$< 3\psi\,\frac{|\,f(\varkappa_n,0)\,|}{|\,g(\varkappa_n,0)\,|} + 3\psi\Delta\tau$$

$$= n\Delta\tau + 3\psi\Delta\tau \tag{25}$$

if ψ is very small then

$$\Delta\tau(\varkappa_n,\Delta\tau) \tilde{=} n\Delta\tau$$

$$\Delta\tau(\varkappa_n,\Delta\tau) = \Delta\tau(\varkappa_n,0). \tag{26}$$

We will therefore compare the newly calculated $\Delta\tau(\varkappa_1,\Delta\tau)$'s with $\Delta\tau(\varkappa,\Delta\tau) - \Delta\tau$ (for $\varkappa \neq \varkappa_1$); we choose the minimum of them and go as in the previous step.

By this criterion, at each step we have to solve the systems (14), (15), (16) only for some of the N wave-numbers and the computer time is considerably reduced.

While it is thought that this criterion should be utilized for cases of three-dimensional turbulence in order to avoid numerical instabilities, for our case it has been deemed expedient to devise a criterion which could be used for all realizations, in the sense of using standard $\Delta\tau$'s, in order that the computed values of different realizations be ready for averaging without having to go through the process of interpolations.

The following criterion has been devised as an alternate.

It seems evident that we cannot use Benton's solution as it stands. In fact in this solution the amplitude of the wave-numbers is a "smooth" function of κ and therefore the energy exchange among the wave-numbers is already in a sort of equilibrium.

In order to find the characteristic relaxation time of each wave-number we will put ourselves in the most demanding conditions for each wave-number. We will assume that at $\tau = 0$ all the wave-numbers have zero amplitude but the κth, which is of our concern.

In this case the equation for κ at $\tau = 0$ is

$$\left.\frac{dv(\kappa)}{d\tau}\right|_{\tau=0} = -\frac{\kappa^2}{R} v(\kappa) .$$

We will assume that the characteristic time of decay for each wave-number is inversely proportional to the above expression, that is

$$\Delta\tau(\kappa) \tilde{=} \frac{R}{\kappa^2 |v(\kappa)|}$$

or, relative to $\Delta\tau(1)$ assumed to be 1,

$$\Delta\tau(\kappa) = \frac{1}{\kappa^2} \left| \frac{v(1)}{v(\kappa)} \right| .$$

Being interested in the statistical properties of Burgers equation, the v's appearing in the above expression will be random. We will therefore assign to v(1) and $v(\kappa)$ the value of the respective standard deviations (see Chapter V), obtaining in so doing

$$\Delta\tau(\kappa) = \frac{1}{\kappa^2} \frac{e^{\kappa\alpha} - e^{-\kappa\alpha}}{e^{\alpha} - e^{-\alpha}} . \tag{27}$$

The figures 12-16 show the results for several Reynolds numbers. The number of time intervals per $\Delta\tau(1)$ is linear with κ in the beginning and reaches a maximum for roughly N/2.

A program according to this scheme has been worked out and used for one realization. The time saving with respect to the constant time increment scheme has been 15%. Nevertheless this criterion has not been used for the generation of the statistical ensemble because some realizations had already been taped with a modified equal-increment method (to be explained just below) and the reworking of them would have not brought to an appreciable saving in computer-time.

The criterion mentioned has been the following: the time increment has been set equal for all wave-numbers but the last 50 (for R = 90 and N = 200) for which the time increment has been halved in order to take into account the effects of the wave-number cut-off.

The time increment has been allowed to vary in time according to the following.

III-6. Criterion for the Determination of the Variation of the Time Increment with Time

This problem is strictly connected with the one of the preceding paragraph in the case we used the second or third method. For reasons already mentioned it seems advisable to find a general rule that can be used for all realizations of the ensemble. We will take therefore as a "representative" amplitude

$$u = \sqrt{\sum_{\kappa=1}^{N} \tilde{v}^2(\kappa)} \,, \tag{28}$$

where $$\tilde{v}(\kappa) = -\frac{2}{R} \operatorname{csch} \kappa\left(\alpha + \frac{\tau}{R}\right) \,,$$

and consider its derivative in time as proportional to the inverse of the time increment $\Delta\tau$.

With respect to a unit time increment for $\tau = 0$, we have

$$(29) \qquad \Delta\tau = \sqrt{\frac{\sum_{\kappa=1}^{N} \tilde{v}^2(\kappa,\tau)}{\sum_{\kappa=1}^{N} \tilde{v}^2(\kappa,0)} \; \frac{\frac{d}{dt}\sum_{\kappa=1}^{N} \tilde{v}^2(\kappa,\tau)}{\frac{d}{dt}\sum_{\kappa=1}^{N} \tilde{v}^2(\kappa,\tau)}}_{\tau=0}$$

$$= \sqrt{\frac{\sum_{\kappa=1}^{N} \operatorname{csch}^2 \kappa(\alpha + \frac{\tau}{R})}{\sum_{\kappa=1}^{N} \operatorname{csch}^2 \kappa\alpha} \; \frac{\sum_{\kappa=1}^{N} \kappa \frac{\cosh \kappa\alpha}{\sinh^2 \kappa\alpha}}{\sum_{\kappa=1}^{N} \kappa \frac{\cosh \kappa(\alpha+\tau/R)}{\sinh^2 \kappa(\alpha+\tau/R)}}} \; .$$

For $\eta = 0.1$ $\Delta\tau$ has been plotted against τ for R = 90 in figure 17. Figure 18 shows the total number of time steps required in order to cover the total time of integration T = 4. as a function of the initial time step. $\Delta\tau = .0017$, corresponding to 1000 time steps, has been chosen and verified for the generation of the statistical ensemble.

IV. INFLUENCE OF THE WAVE-NUMBER CUT-OFF

In this chapter, as well as in the following ones, we will present some results of the numerical experiments. We will avoid the tendency of preambling with theoretical considerations and showing later how well the numerical experience matches the results of our speculations. On the contrary we will present the results of our numerical experiments and try to justify them by means of analytical arguments.

For the study of the effects of the wave-number cut-off a low Reynolds number ($R \tilde{=} 17$, conjugated to $\alpha = .1$) has been chosen so that it would be possible to integrate the systems (14), (15), (16) for a very large time interval taking only 40 minutes of computer-time.

The reference exact solution has been plotted, for several instants in the figures 19-23. The ratio $v(\kappa)/\tilde{v}(\kappa)-1$, where $\tilde{v}(\kappa)$ is the exact solution and $v(\kappa)$ the numerical experiment, has been plotted in figure 24, for several instants.

At the very beginning of the numerical experiment a build-up of energy is noticed with respect to the exact solution, especially at the highest wave-number (where the error introduced by the wave-number cut-off may be as high as 70%). The wave-numbers below 37th (49 is the wave-number cut-off) present an error less than 1%. The error tends to decrease in time and become negative for the lowest wave-number. Toward the end of the integration the error is confined to .0001%.

In order to justify such behavior, we will assume that a true energy cascade from lower to higher wave-numbers takes place at high wave-numbers (close to the wave-number cut off).

We will call

$E_1(\tau)$ the energy contained in the first N wave-numbers;

$D_1(\tau)$ the dissipation of the same wave-numbers;

$E_2(\tau)$ the energy contained in the wave-numbers above N;

$D_2(\tau)$ the dissipation of the same wave-numbers;

$T(\tau)$ the energy flux through N.

We will add an index ES or NE to make reference either to the exact solution or to the numerical experiment.

At $\tau = 0$, a configuration similar to the following exists:

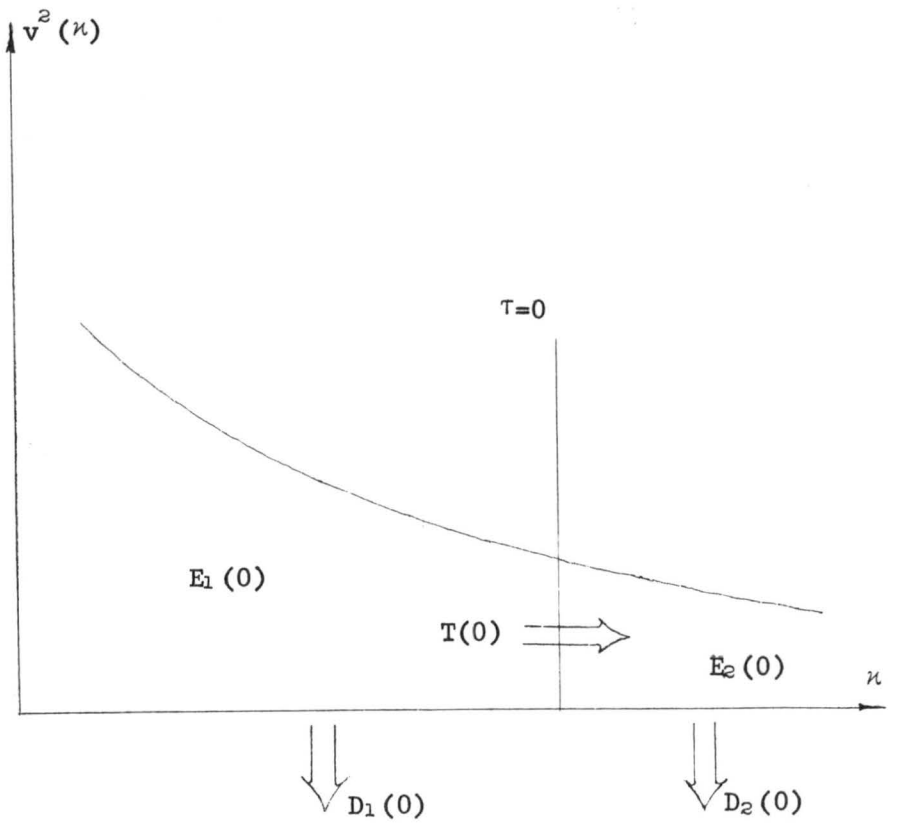

For the exact solution it is

$$\frac{dE_1(0)}{d\tau} = -D_1(0) - T(0) , \tag{30}$$

$$\frac{dE_2(0)}{d\tau} = -D_2(0) + T(0) . \tag{31}$$

For the numerical experiment it is

$$\frac{dE_1(0)}{d\tau} = -D_1(0) . \tag{32}$$

Therefore:

$$\left(\frac{dE_1(0)}{d\tau}\right)_{ES} < \left(\frac{dE_1(0)}{d\tau}\right)_{NE} \qquad \text{(both negative).}$$

This means that for a short time $E_1(\tau)_{NE}$ is larger than $E_1(\tau)_{ES}$ and, because of the cascade, this extra energy will be accumulated around N.

Call τ any instant of this new configuration. Obviously the configuration of the numerical experiment requires more energy dissipation than the coinstantaneous configuration of the exact solution and therefore it will be

$$\left(D_1(\tau)\right)_{NE} > \left(D_1(\tau)\right)_{ES} .$$

Because of the continuous accumulation due to the cascade in the NE it will eventually be, at a later time,

$$\left[D_1(\tau) + T(\tau)\right]_{ES} = D_1(\tau)_{NE} ,$$

that is

$$\left.\frac{dE_1(\tau)}{d\tau}\right|_{E} = \left.\frac{dE_1(\tau)}{d\tau}\right|_{NE} ,$$

always with

$$E_1(\tau)_E < E_1(\tau)_{NE} .$$

and, at a later time still

$$\left|\frac{dE_1(\tau)}{d\tau}\right|_E > \left|\frac{dE_1(\tau)}{d\tau}\right|_{NE} . \tag{33}$$

We will eventually reach a time for which

$$E_1(\tau)_E = E_1(\tau)_{NE} .$$

In the meanwhile energy has been accumulated around N; therefore by now we should have the following configuration

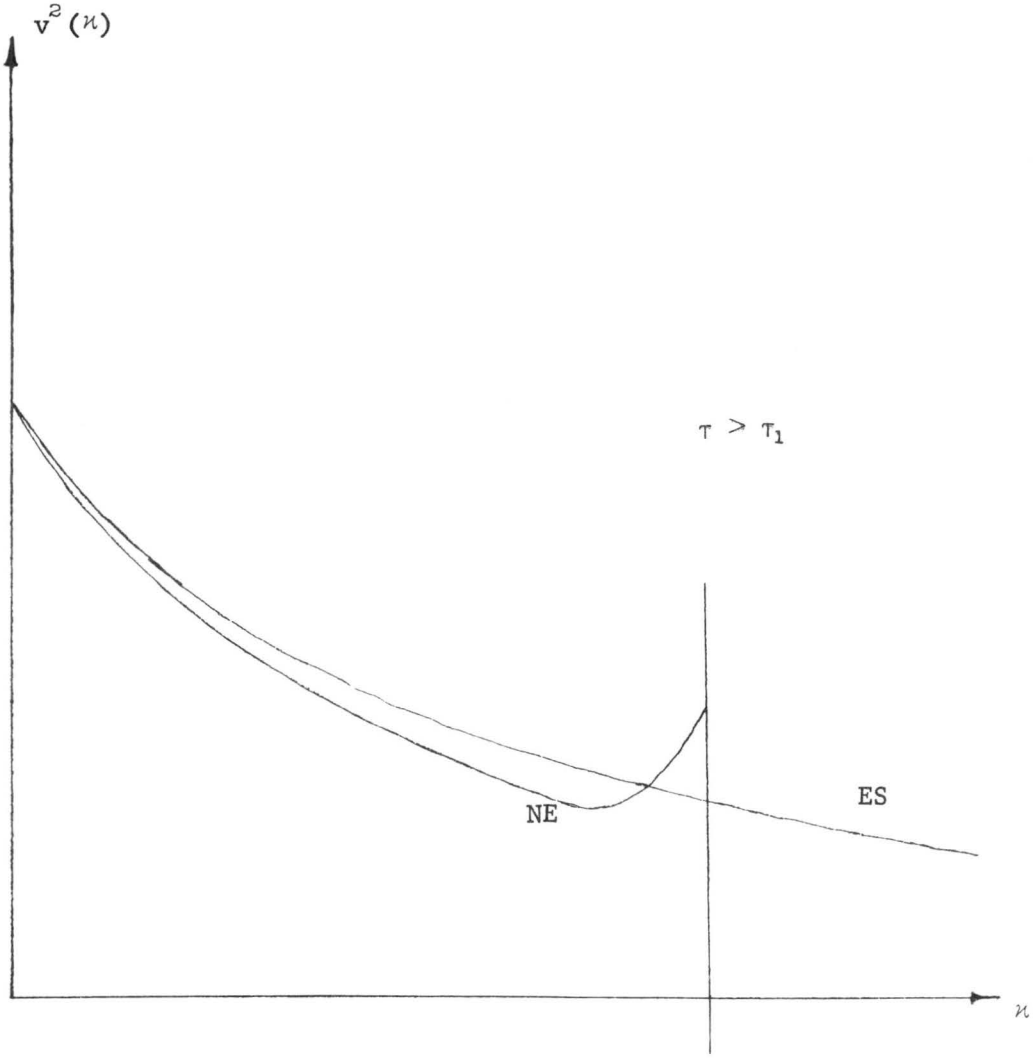

We will call τ_1 the instant at which the graph for NE has started to cross the graph for ES.

If the sense of (33) persists we will eventually have

$$E_1(\tau)_{ES} > E_1(\tau)_{NE}$$

and if, by this time, the field has decayed enough such that a cut-off is ineffectual, then we will reach a point where the whole NE curve is below the ES curve and will stay like that forever.

The effect of the wave-number cut-off in the whole is such as to accelerate the process of decay, and the result of the numerical experiment will be retarded with respect to the coetaneous exact solution.

We might calculate the amount of such delay by means of the following considerations. By the time the wave-number cut-off is ineffectual, the time T is so large that the exact solution

$$-\frac{2}{R}\,\mathrm{csch}\,\varkappa(\alpha + \frac{T}{R})$$

may be approximated by

$$-\frac{4}{R}\,e^{-\varkappa(\alpha+T/R)} \quad .$$

A solution retarded of ΔT will be therefore

$$-\frac{4}{R}\,e^{-\varkappa(\alpha + T/R + \Delta T/R)}$$

and the ratio of their difference to the first

$$e^{-\varkappa\frac{\Delta T}{R}} - 1$$

which, if ΔT is small and R large, can be approximated by

$$-\frac{\varkappa\Delta T}{R} \quad .$$

A behavior like this is in fact shown (not much evidently because of the particular scale of the ordinate) in the figure mentioned above.

In our case the time delay of NE with respect to ES is $\Delta\tau = .35(10^{-6})$, which is indeed very small with respect to 78., instant at which the delay has been measured.

As a conclusion we may say that, provided a sufficiently high wave-number cut-off is given (according to the criterion presented in this paper), its effects are limited to the last few wave-numbers close to the wave number cut-off.

V. THE STATISTICAL EXPERIMENT

We have seen that with a proper choice of the wave-number cut-off, it is possible to limit its influence to the wave-numbers close to it.

Once the maximum time of integration T is chosen (almost invariable with R), the number of time steps (varying in time) will generally be an increasing function of R.

At this point, we should choose a Reynolds number. Our only upper limit is given by considering the computer time. In our case, the total core utilized is very small. With the experimental knowledge that the computer time grows roughly as the square of the wave-number cut-off and with a prefixed maximum of 40 minutes per realization, we have found that we could use a maximum Reynolds number of 90 with a wave-number cut-off of 200. The total adimensional time of integration is T = 4., at which instant the energy has decayed to one tenth of its original value.

V-1. Criterion for the Choice of the Initial Conditions

The initial amplitudes of the wave-numbers are independently and Gaussianly distributed with zero mean and standard deviation

$$\sigma(\kappa) = \frac{2}{R} \operatorname{csch} \kappa\alpha ,$$

α and R being conjugated according to (11).

The number of realizations considered in this report is 60.

The reason for the choice of the standard deviation has been given in paragraph III-1.

V-2. Check of the Random Number Generator

The random number generator of the computer's library furnishes random numbers uniformly distributed between -1 and 1. A subroutine has been used to transform the uniform distribution into a Gaussian distribution with mean 0. and variance 1..

The results of the tests are shown in figures 25-28 for samples of increasing sizes.

The random number generator seems satisfactory, but, due to the small size of our ensemble, it has been deemed opportune to develop the following.

V-3. Criterion for the Determination of the Best Quasi-Gaussian Distribution Fitting a Certain Sample

With reference to the above mentioned figures, we see that for a sample of size 10,000 picked from a much larger population, the Gaussian distribution seems to fit very well. If we now consider a sample of size 60, we can argue that, notwithstanding its having been picked from a normally distributed population, there might be density distribution functions that better fit the particular sample. By this, we mean that the sample might have non-zero mean, non-one variance, non-zero skewness, non-three flatness, and so on, while there might be probability distribution functions satisfying these requirements.

Being interested in the development of a certain distribution we will be mainly interested in the development of the moments of this distribution and, therefore, if we wish to fit the particular histogram of our sample with a smooth curve, it is better to take into account the "significant" moments of our sample and from them to build up a smooth density distribution.

In our case we will call "significant" the moments from the zeroth to the fourth. We will try to fit a distribution of the type

$$(34) \qquad f(x) = \frac{1}{\sqrt{2\pi}\,\sigma}\left(A_0 + A_1\frac{x}{\sigma} + A_2\frac{x^2}{\sigma^2} + A_3\frac{x^3}{\sigma^3} + A_4\frac{x^4}{\sigma^4}\right) e^{-x^2/2\sigma^2},$$

where

$$x = y-\mu, \quad \mu = \langle x \rangle, \quad \text{and} \quad \sigma^2 = \langle x^2 \rangle,$$

on our sample's histogram.

The fit will be accomplished by saturating the five unknown parameters $A_0,\ldots,A_4$ with the relations

$$(35) \qquad \int_{-\infty}^{\infty} x^n f(x)\,dx = \langle x^n \rangle, \qquad n = 0,4 \text{ where } \langle x^0 \rangle = 1.$$

From them we obtain the system

$$A_0 + A_2 + 3A_4 = 1$$

$$A_0 + 3A_2 + 15A_4 = 1$$

$$3A_0 + 15A_2 + 105A_4 = \langle x^4 \rangle / \sigma^4$$

$$A_1 + 3A_3 = 0$$

$$3A_1 + 15A_3 = \langle x^3 \rangle / \sigma^3$$

and from it

$$A_0 = \frac{1}{8}\left(5 + \frac{\langle x^4 \rangle}{\sigma^4}\right)$$

$$A_2 = \frac{1}{8}\left(6 - 2\frac{\langle x^4 \rangle}{\sigma^4}\right)$$

$$A_4 = \frac{1}{24}\left(-3 + \frac{\langle x^4 \rangle}{\sigma^4}\right)$$

$$A_1 = -\frac{1}{2}\frac{\langle x^3 \rangle}{\sigma^3}$$

$$A_3 = \frac{1}{6}\frac{\langle x^3 \rangle}{\sigma^3} .$$

In order that f(x) be a probability density distribution function it should be everywhere non-negative. We should therefore check that the polynomial

$$g(x) = A_0 + A_1\frac{x}{\sigma} + A_1\frac{x^2}{\sigma^2} + A_3\frac{x^3}{\sigma^3} + A_4\frac{x^4}{\sigma^4}$$

has no real zero, or, equivalently, that its derivative

$$g'(x) = \frac{A_1}{\sigma} + 2\frac{A_2}{\sigma^2}x + 3\frac{A_3}{\sigma^3}x^2 + 4A_4\frac{x^3}{\sigma^4}$$

has zeros corresponding to which g(x) has positive value.

This notwithstanding, for purposes of illustration, we may neglect the unrealistic fact of slightly negative densities. By this means we may visualize the progress of a probability density distribution function in time.

V-4. Presentation and Discussion of the Realizations

As first in figure 29 we present Benton's solution for R = 90 at several instants.

The ordinate is

$$\frac{\tilde{v}(\kappa,\tau)}{\tilde{v}(\kappa,0)} .$$

The figures 30-35 present the development of one realization in Fourier space while the figures 36-41 the corresponding development

in physical space. Four different patterns for the final configuration are clearly distinguishable:

1 M	one shock-wave	figures 35 and 41
1 F	one shock wave	figures 42 and 43
2 F	two shock-waves	figures 44 and 45
2 M	two shock-waves	figures 46 and 47.

Few realizations show the trend toward a configuration with three shock-waves.

We list here our observations and comments.

I. From the respective figures it is clear that the configurations 1F and 1M (and 2F and 2M) are only translated one with respect to the other of half a period.

II. It seems worthy asking which are the factors in the initial random conditions that determine the development toward one of the above configurations. With this problem in mind we have plotted in figure 48 the initial values of $v(1)$ and $v(2)$ for all the realizations and in figure 49 their trajectory in time. From this plot one can see that the trajectories tend to remain in the same quadrant in which the initial point is. And, if at the final time T,

$|v(1,T)| < |v(2,T)|$ we have two shock-waves,

$|v(1,T)| > |v(1,T)|$ we have one shock-wave.

More specifically, for each of the above configurations:

1 F when $v(1,T) < 0$ and $|v(2,T)| < |v(1,T)|$

1 M when $v(1,T) > 0$ and $|v(2,T)| < |v(1,T)|$

2 F when $v(2,T) > 0$ and $|v(2,T)| > |v(1,T)|$

2 M when $v(2,T) < 0$ and $|v(2,T)| > |v(1,T)|$.

In the long run we would expect that, unless $v(1,0)$ is very close to zero, the final configuration presented only one shock. When $v(1,0) \sim 0$ then the second wave-number becomes the leading one and (because of the higher dissipation of the higher wave-number) the odd wave-numbers will have very rapidly zero amplitude. The period of the phenomenon is therefore one-half of the original. For similar reasons we would expect a final configuration with three shocks when both $v(1,0)$ and $v(2,0)$ are very close to zero and $v(3,0)$ is not. This explains the relative rarity of the three-shock final configurations and the absence of four-shock ones in our experiment. The fact that two-shock configurations are less frequent than one-shock configurations is explained instead by the fact that the joint probabiltiy density distribution function of $v(1,0)$ and $v(2,0)$ is the product of the probability density distribution function of $v(1,0)$ and of the probability density distribution function of $v(2,0)$ and $v(2,0)$ has a smaller variance than $v(1,0)$ because of our criterion used for the initial conditions.

V-5. The Statistical Averages

60 different realizations of the field $v(\xi,\tau)$ with period $0,2\pi$ have been computed. Such ensemble will not in general be homogeneous in ξ. An artifice for obtaining a homogeneous ensemble is the following. Consider a particular realization (the nth)

$$v_n(\xi,\tau),$$

and all the realizations obtained by translating such realization of η in the ξ axis

$$v_n(\xi+\eta,\tau).$$

η will be our second parameter, creating a more general ensemble, (of which the first ensemble will be a subensemble) and will be distributed uniformly from 0 to 2π.

If $g_n(\xi + \eta, \tau)$ is a physical quantity with ensemble parameters of n and η the ensemble average will be

$$g(\xi,\tau) = \frac{1}{N}\sum_{n=1}^{N} \frac{1}{2\pi} \int_0^{2\pi} g_n(\xi + \eta, \tau)d\eta$$

$$= \frac{1}{2\pi}\int_0^{2\pi} [g(\xi + \eta)^{\circ}\tau]d\eta$$

where [ ] represent the subensemble average.

For the particular case of the two-point correlation

$$v(\xi,\tau)v(\xi+\zeta,\tau)$$

$$= \frac{1}{2\pi}\int_0^{2\pi}\left(\sum_{\kappa=1}^{\infty} v(\kappa,\tau)\sin\kappa(\xi+\eta)\sum_{\kappa'=1}^{\infty} v(\kappa',\tau)\sin\kappa'(\xi+\zeta+\eta)\right)d\eta$$

$$= \left(\sum_{\kappa=1}^{\infty}\sum_{\kappa'=1}^{\infty} v(\kappa,\tau)v(\kappa',\tau)\frac{1}{2\pi}\int_0^{2\pi}\sin\kappa(\xi+\eta)\sin\kappa'(\xi+\zeta+\eta)d\eta\right)$$

$$= \frac{1}{2}\left(\sum_{\kappa=1}^{\infty} v^2(\kappa,\tau)\cos\kappa\zeta\right)$$

$$= \frac{1}{2}\sum_{\kappa=1}^{\infty}[v^2(\kappa,\tau)]\cos\kappa\zeta \quad :$$

and the correlation coefficient

$$f(\zeta,\tau) = \frac{\sum_{\kappa=1}^{\infty}[v^2(\kappa,\tau)]\cos\kappa\zeta}{\sum_{\kappa=1}^{\infty}[v^2(\kappa,\tau)]} \quad .$$

V-6. The following results are presented:

I. Figures 50-55. Development of the mean amplitudes. If the size of the subensemble had been sufficiently large the mean amplitudes would have been zero. Due to the limited number of realizations a deviation from zero is noticeable.

II. Figures 56-61. Development of the average energy spectrum with comparison to the parallel development of the energy spectrum of the reference exact solution.

The final stage (see figures 60 and 61) shows a behavior like κ^{-2} for the first 16 wave-numbers and a behavior at least like κ^{-16} for high wave-numbers.

At this point it would seem mandatory to discuss about "inertial subrange," "dissipation range," and so on.

With our numerical experiment (and we believe that it is representative of decaying Burgerlence) the dissipation curve versus wave-number does show a maximum at $\kappa=1$. It is therefore impossible to determine an "inertial subrange" and therefore Kolmogoroff's dimensional argument for it (which leads to a $\kappa^{-5/3}$ law) would not be applicable in principle.

III. Figures 62-67. Skewness factor. There seems to be a clear tendency for the low wave numbers to have positive skewness and for the high wave-numbers to have negative skewness. In both cases the even wave-numbers have a skewness with absolute value greater than the absolute value of the skewness of the odd wave numbers.

IV. Figures 68-73. Flatness factor. The flatness factor tends to be less than 3 for the smallest wave-numbers and greater than 3 for the largest. Different patterns for even and odd wave-numbers are clearly discernible.

V. Figures 74-79. Correlation function. The correlation function of the general ensemble is shown together with the initial correlation based on variances according to the reference solution. An increase of the microscale in time is evident.

VI. Figures 80-85 and figures 86-91. The development of the histogram and of the probability density distribution function for wave-number 1 and wave-number 2 is shown.

All time-dependent results have been recorded on a computer generated movie. Copies are available at the author's present address: School of Civil Engineering, Purdue University, West Lafayette, Indiana 47907.

References

1. Burgers, J. M.: Advances in Applied Mechanics (Academic Press Inc., New York, 1948), Vol. 1, p. 171.
Burgers, J. M.: Proc. Roy. Netherl. Acad. Sci. (Amsterdam), 43, 2 (1940); 53, 247 (1950); B57, 403 (1954).
Burgers, J. H.: Nonlinear Problems in Engineering (Academic Press Inc., New York, 1964), p. 123.

2. Benton, E. R.: Phys. Fluids, 9, 5, 1247 (1966).

F I G U R E S

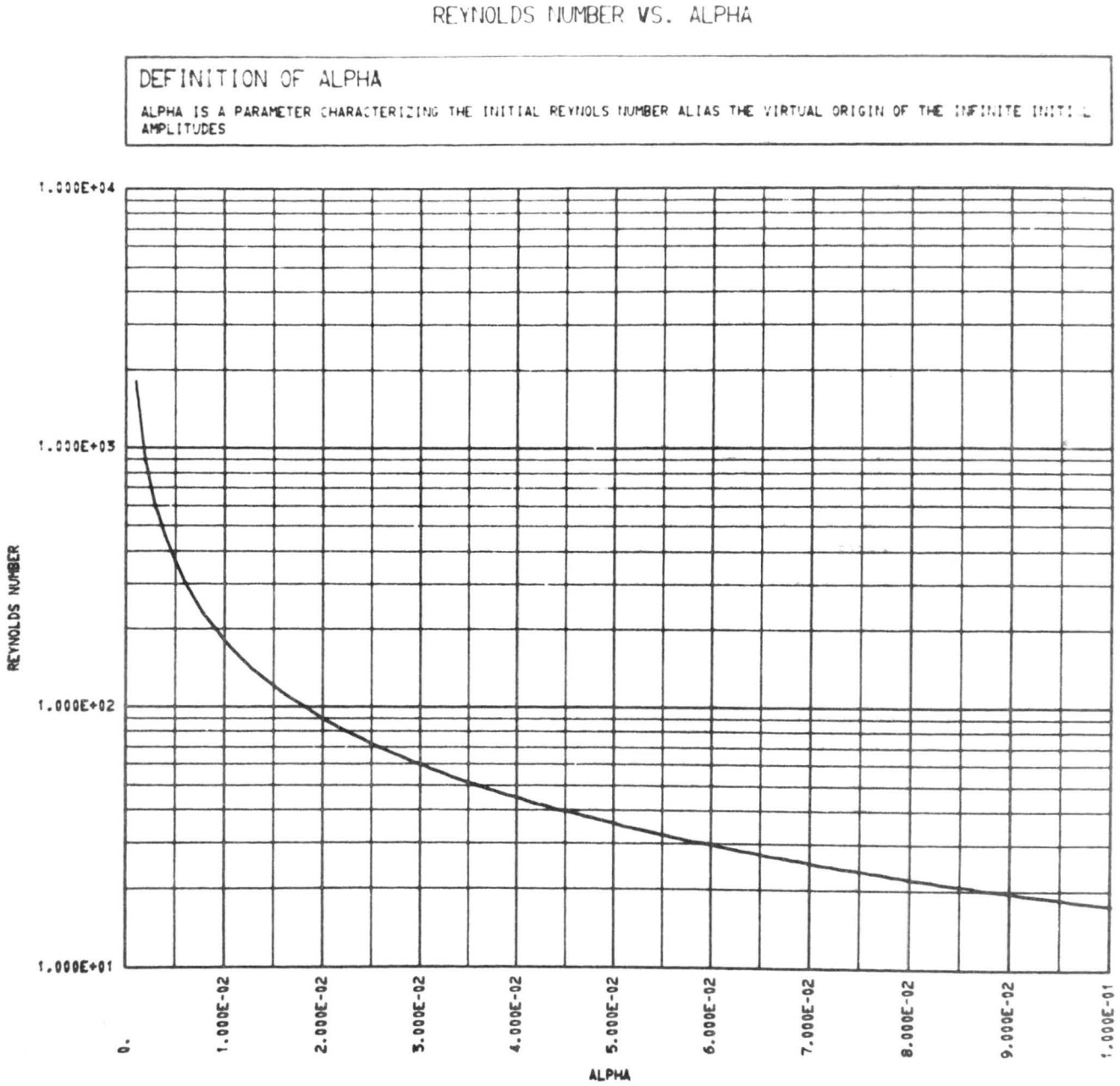
REYNOLDS NUMBER VS. ALPHA
DEFINITION OF ALPHA
ALPHA IS A PARAMETER CHARACTERIZING THE INITIAL REYNOLS NUMBER ALIAS THE VIRTUAL ORIGIN OF THE INFINITE INITIAL AMPLITUDES
1.000E+04
1.000E+03
1.000E+02
1.000E+01
REYNOLDS NUMBER
0.
1.000E-02
2.000E-02
3.000E-02
4.000E-02
5.000E-02
6.000E-02
7.000E-02
8.000E-02
9.000E-02
1.000E-01
ALPHA

Figure 1.

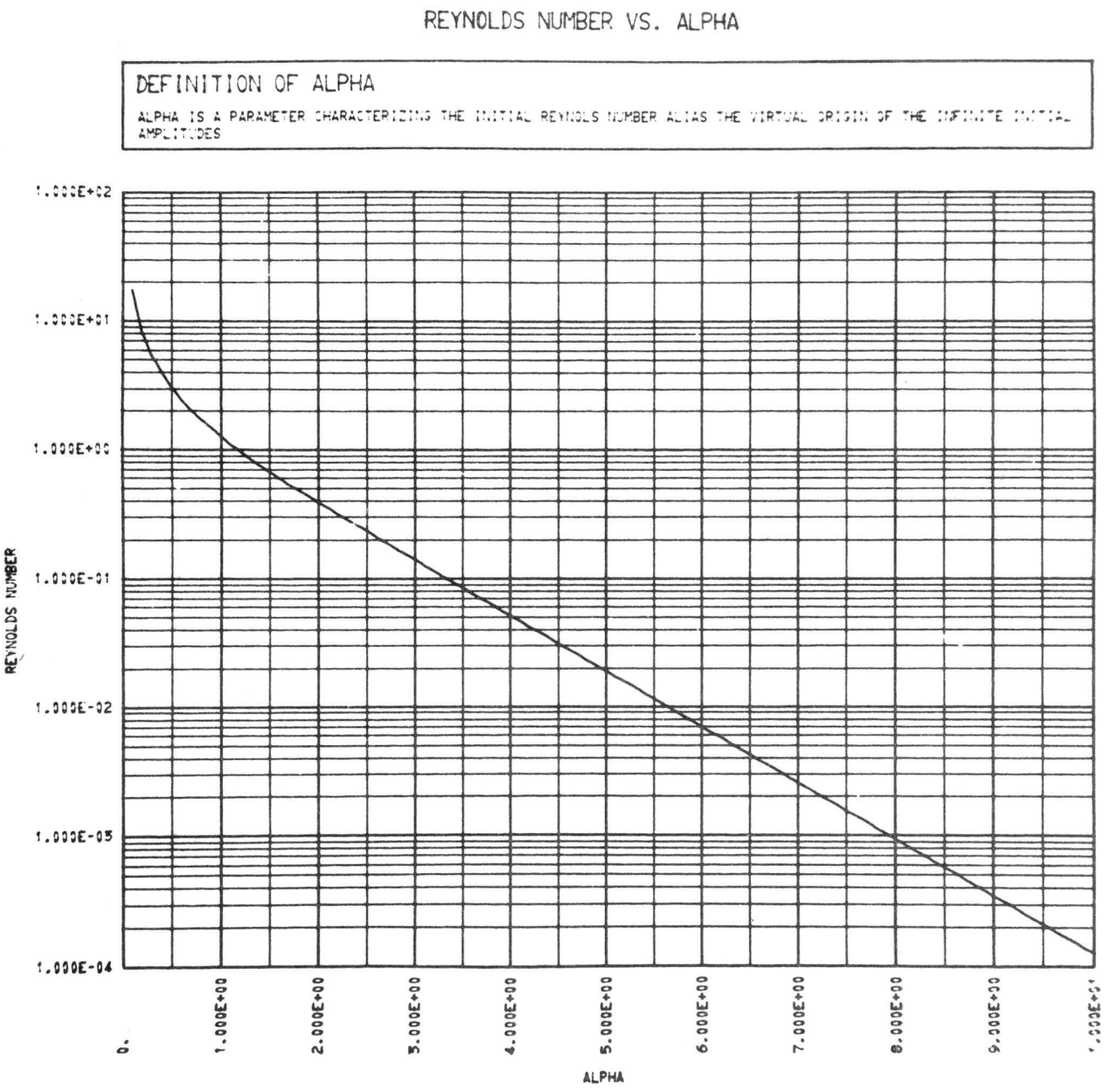
REYNOLDS NUMBER VS. ALPHA
DEFINITION OF ALPHA
ALPHA IS A PARAMETER CHARACTERIZING THE INITIAL REYNOLDS NUMBER ALIAS THE VIRTUAL ORIGIN OF THE INFINITE INITIAL AMPLITUDES
1.000E+02
1.000E+01
1.000E+00
1.000E-01
1.000E-02
1.000E-03
1.000E-04
REYNOLDS NUMBER
0.
1.000E+00
2.000E+00
3.000E+00
4.000E+00
5.000E+00
6.000E+00
7.000E+00
8.000E+00
9.000E+00
ALPHA

Figure 2.

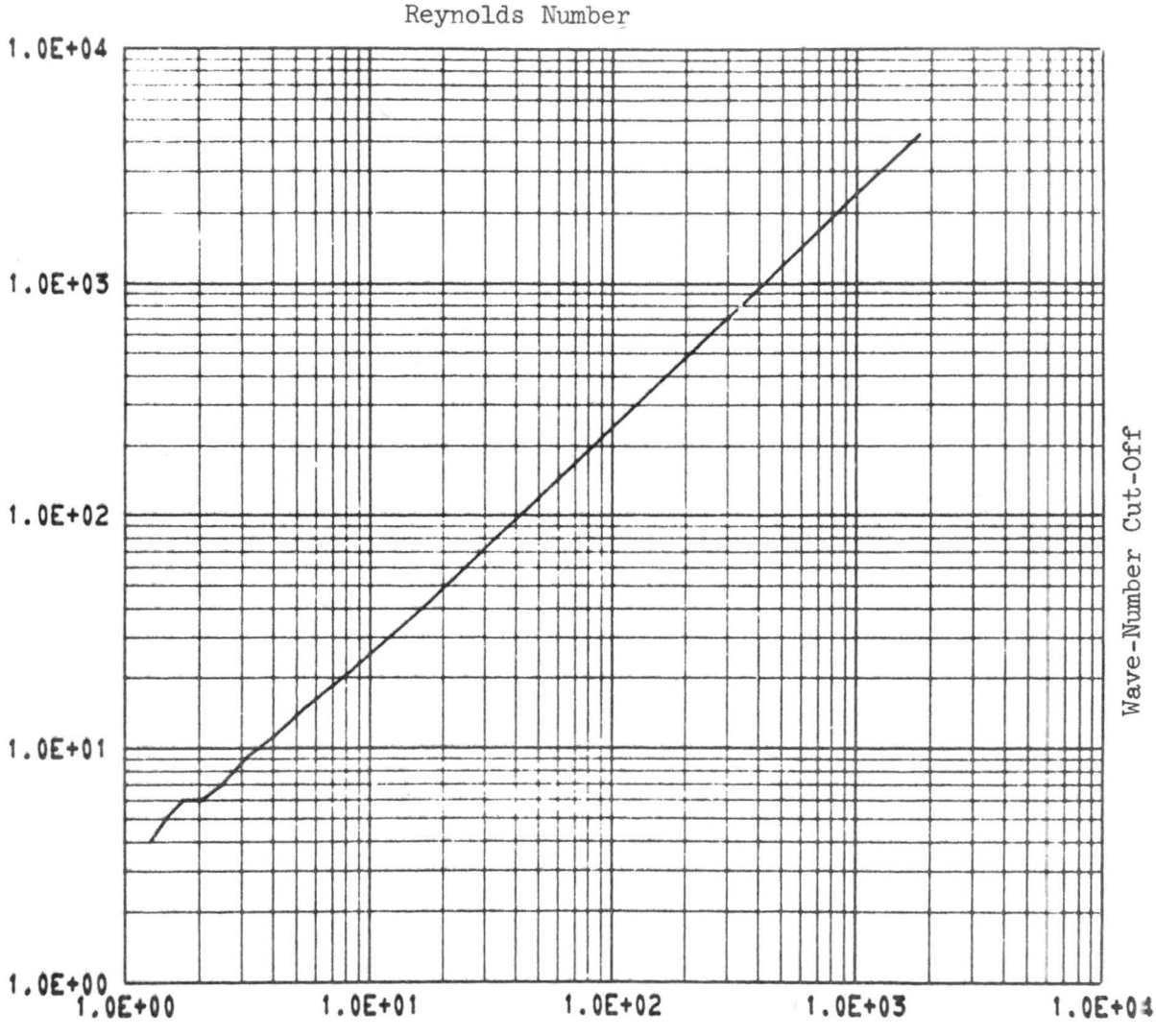

Figure 3. Wave-number cut-off versus Reynols number for $\varepsilon = .005$.

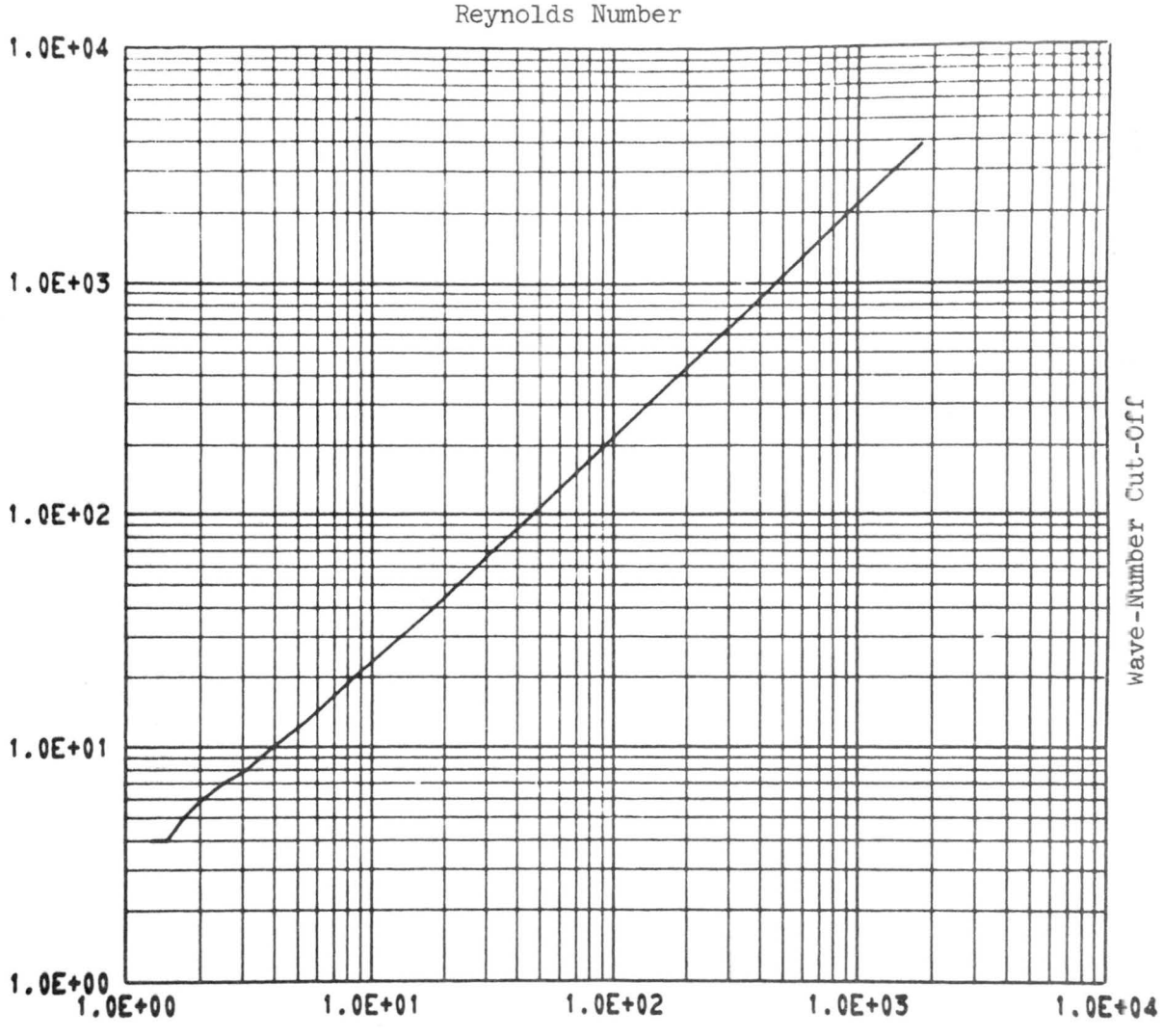

Figure 4. Wave-number cut-off versus Reynolds number for $\mathcal{E}$ =.01.

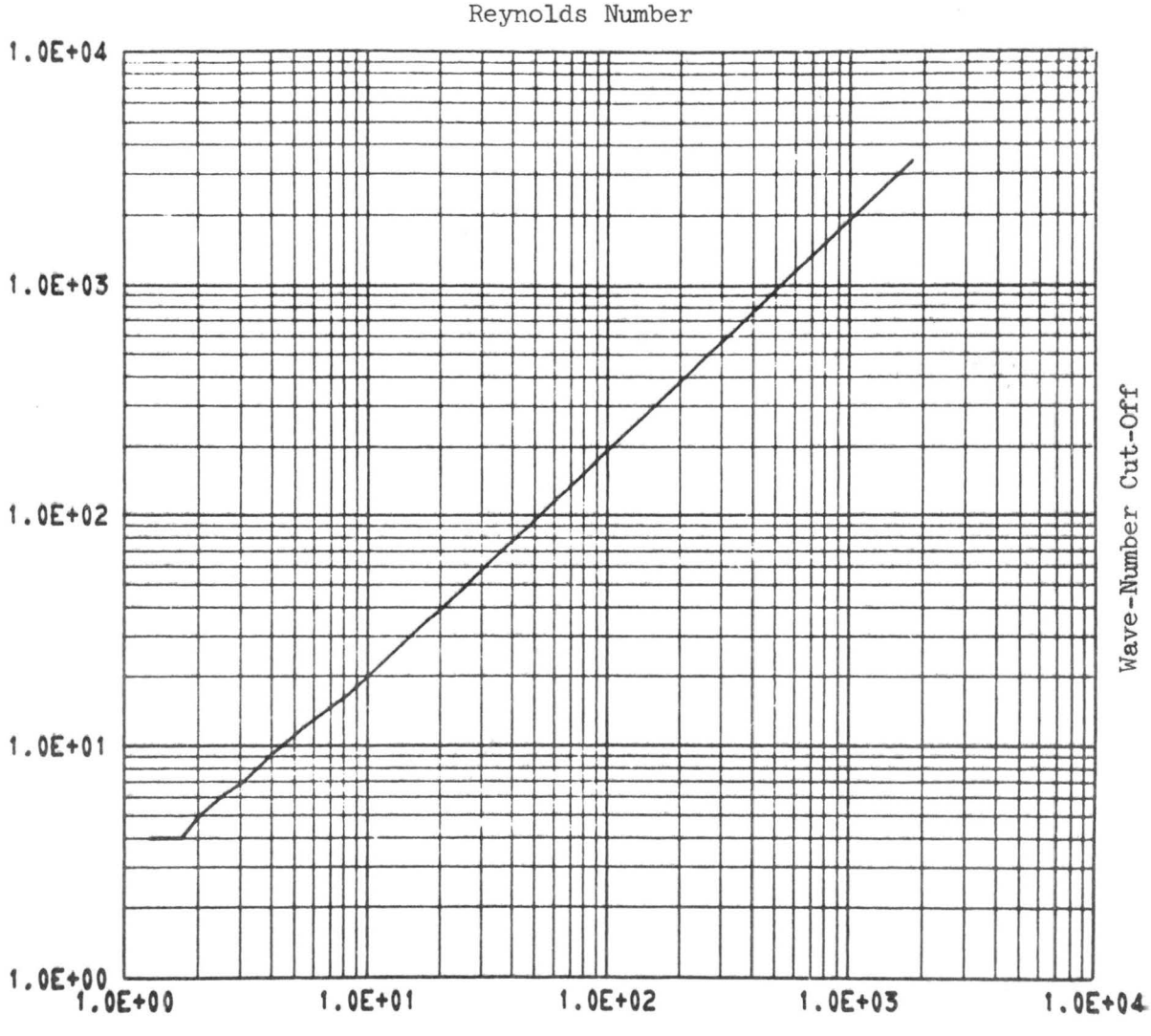

Figure 5. Wave-number cut-off versus Reynolds number for $\mathcal{E}$ =02.

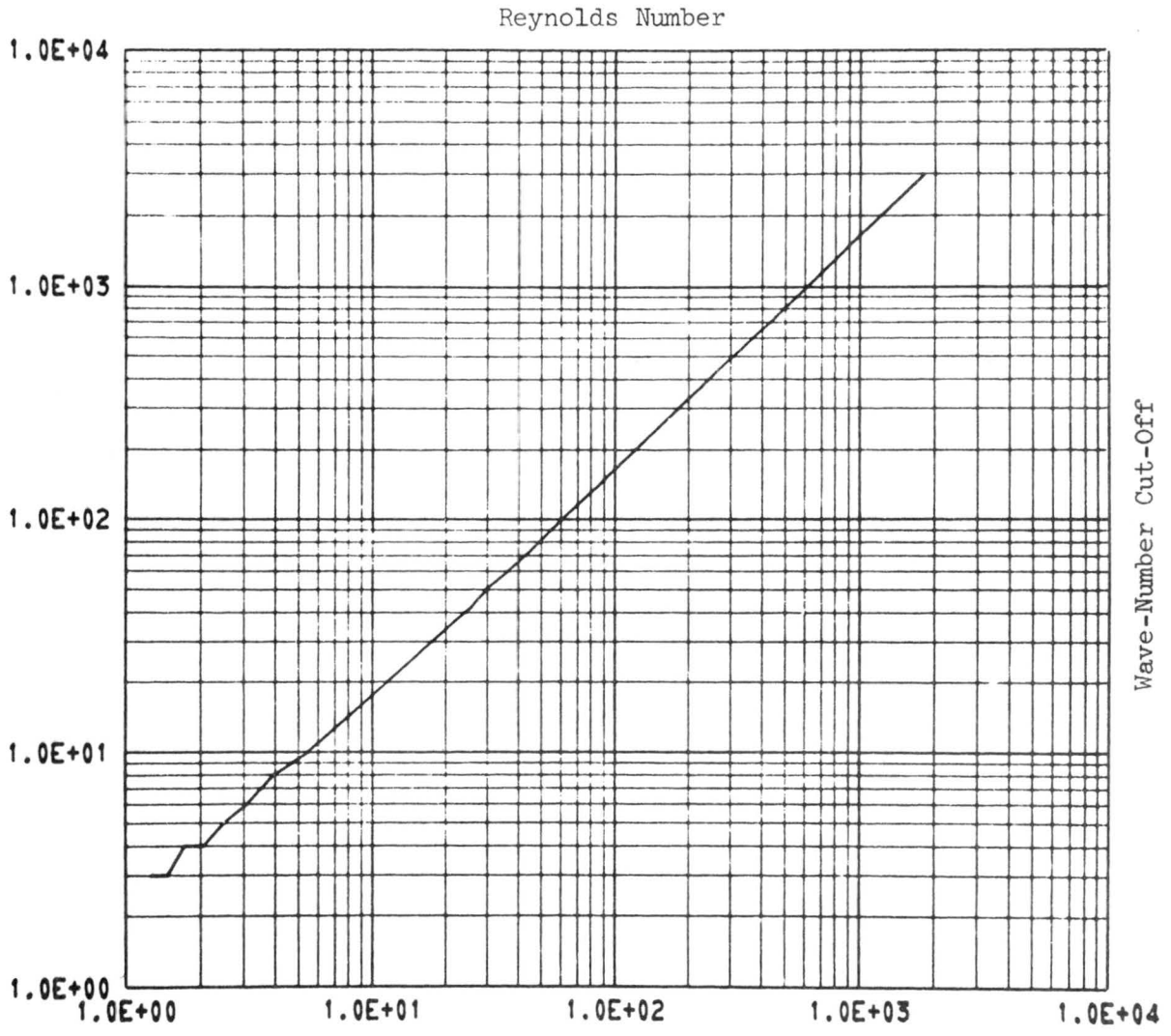

Figure 6. Wave-number cut-off versus Reynolds number for $\mathcal{E}$ =.04.

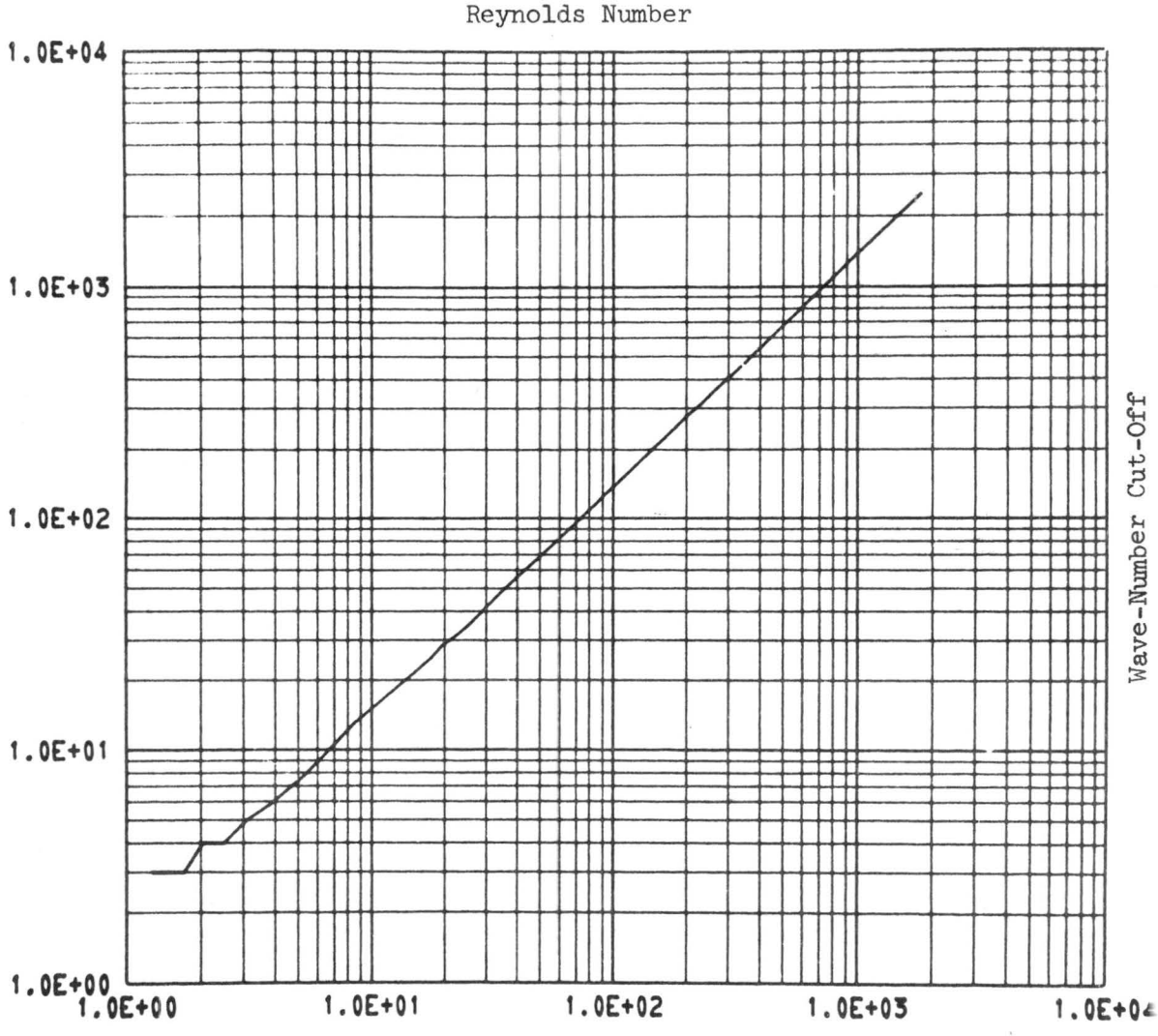

Figure 7. Wave-number cut-off versus Reynolds number for $\mathcal{E}=.08$.

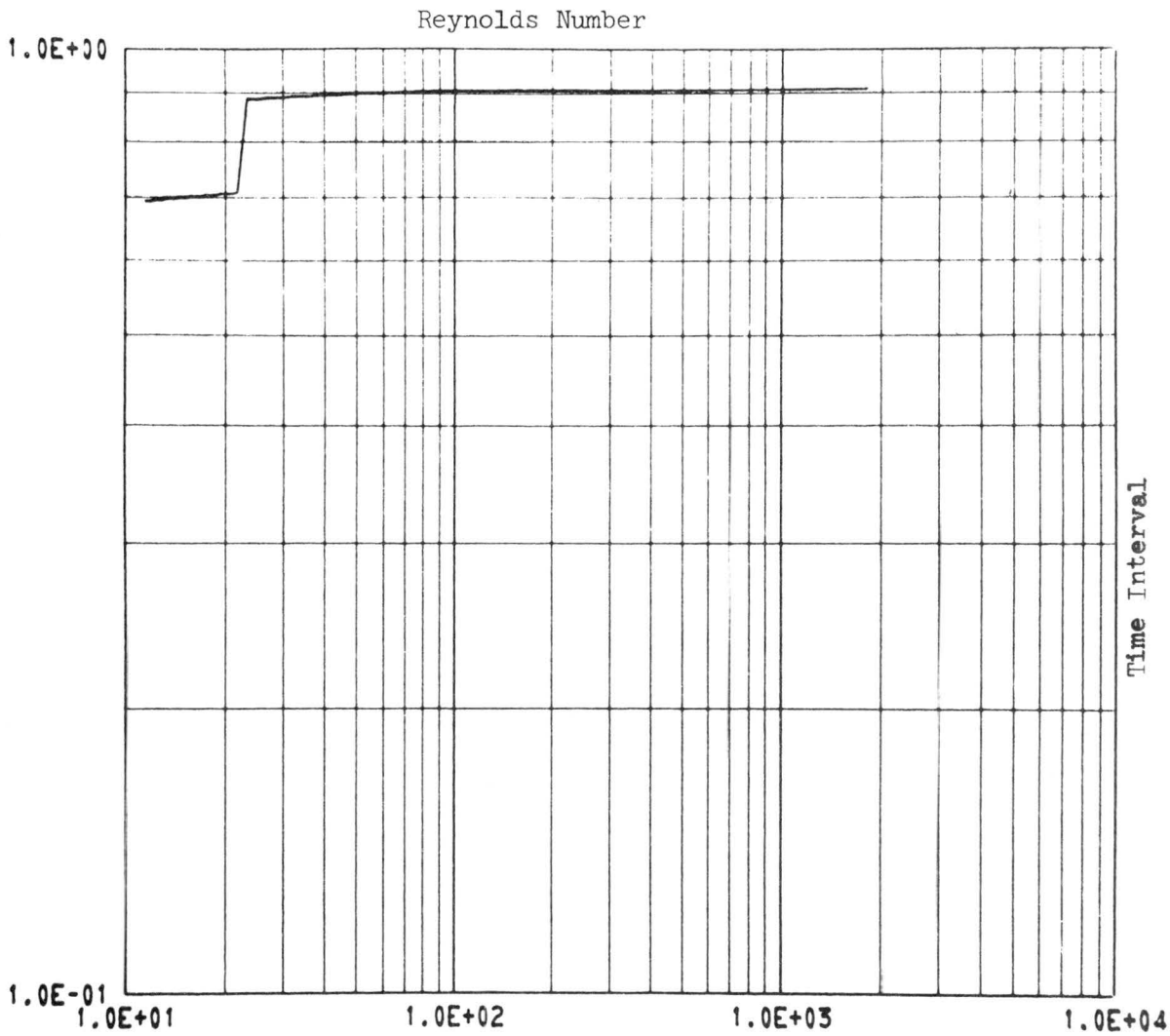

Figure 8. Time interval of integration versus Reynolds number for $\eta = .5$.

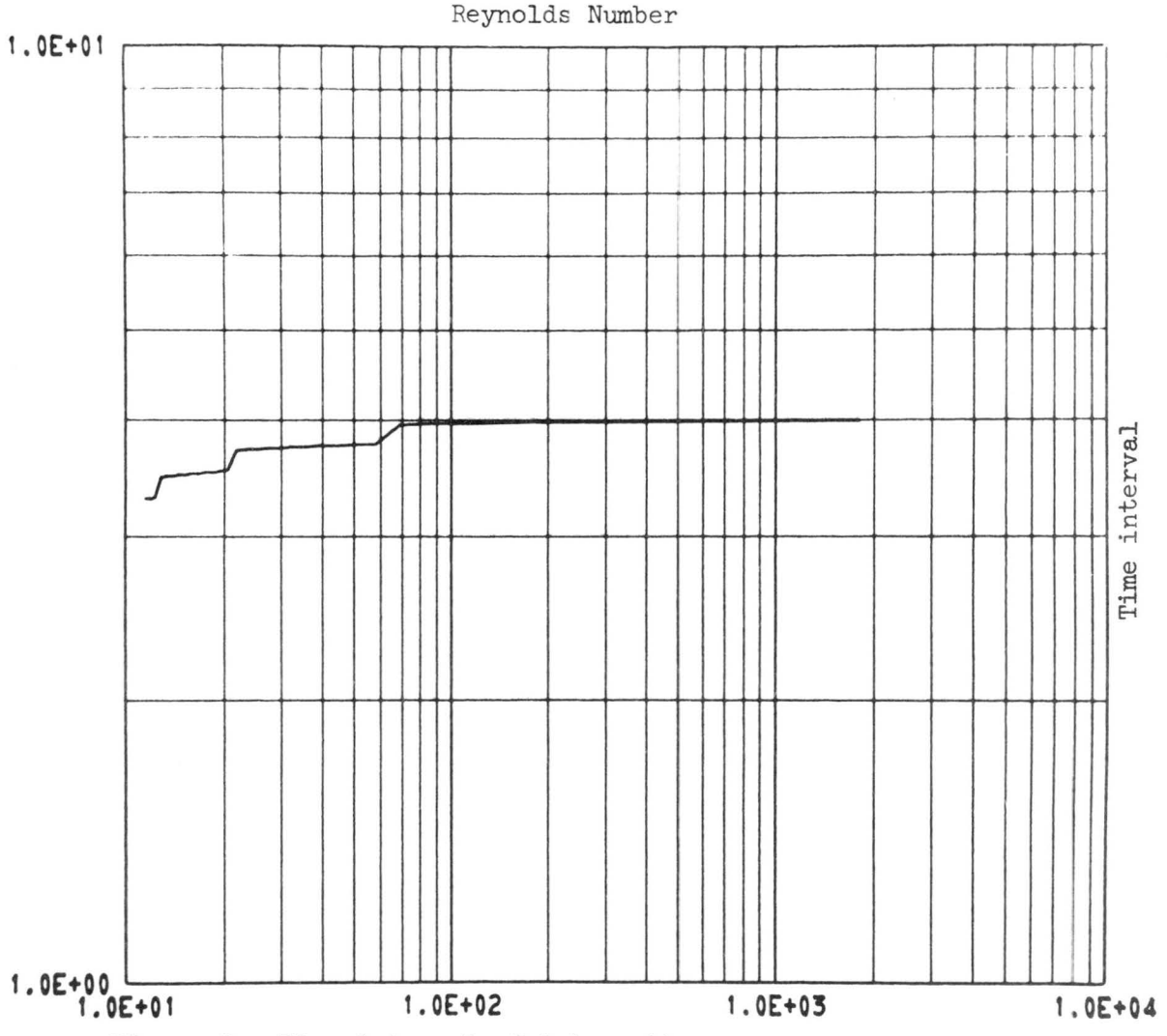

Figure 9. Time interval of integration versus Reynolds number for $\eta = .1$.

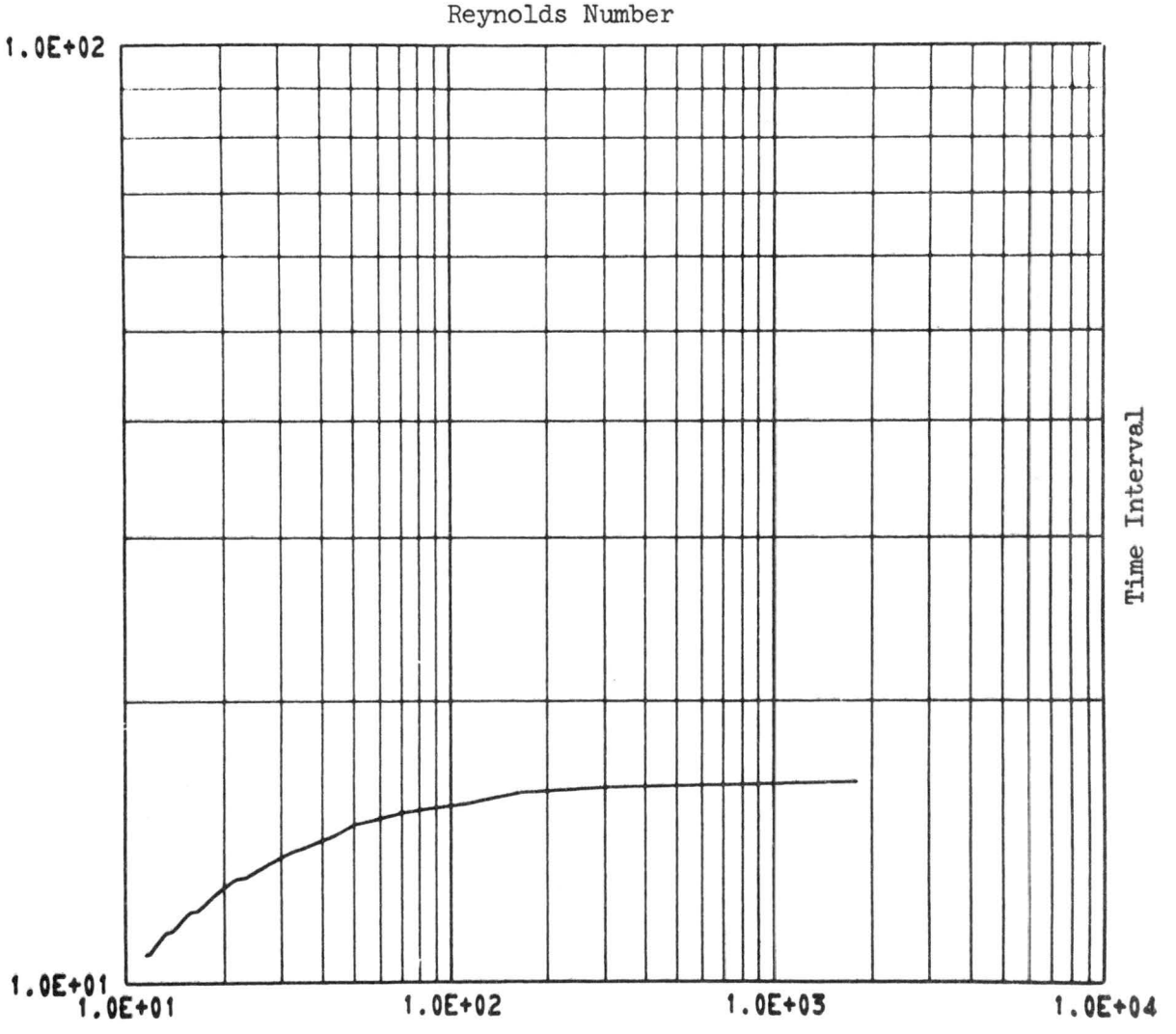

Figure 10. Time interval of integration versus Reynolds number for η =.01.

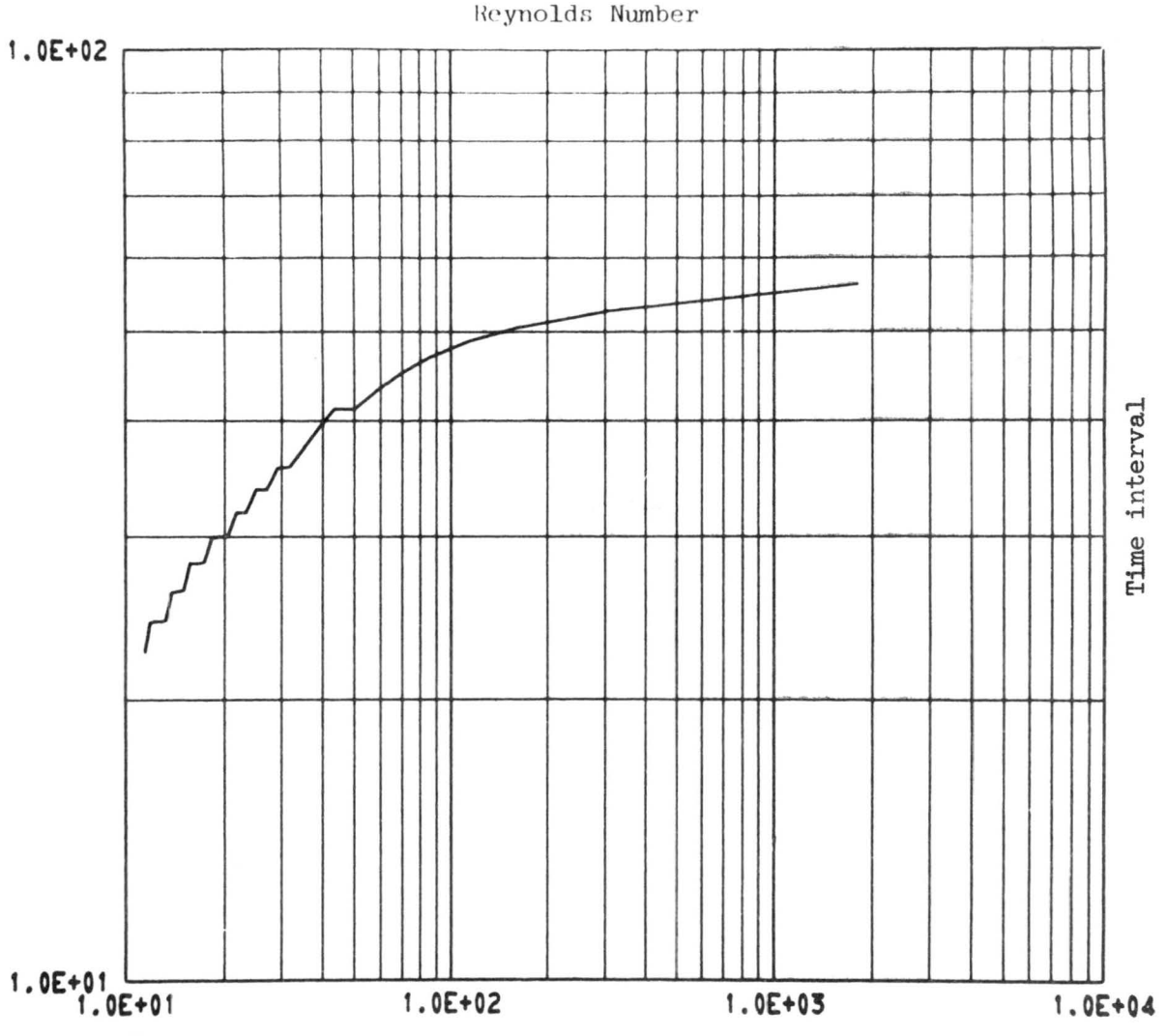

Figure 11. Time interval of integration versus Reynolds number for η =001.

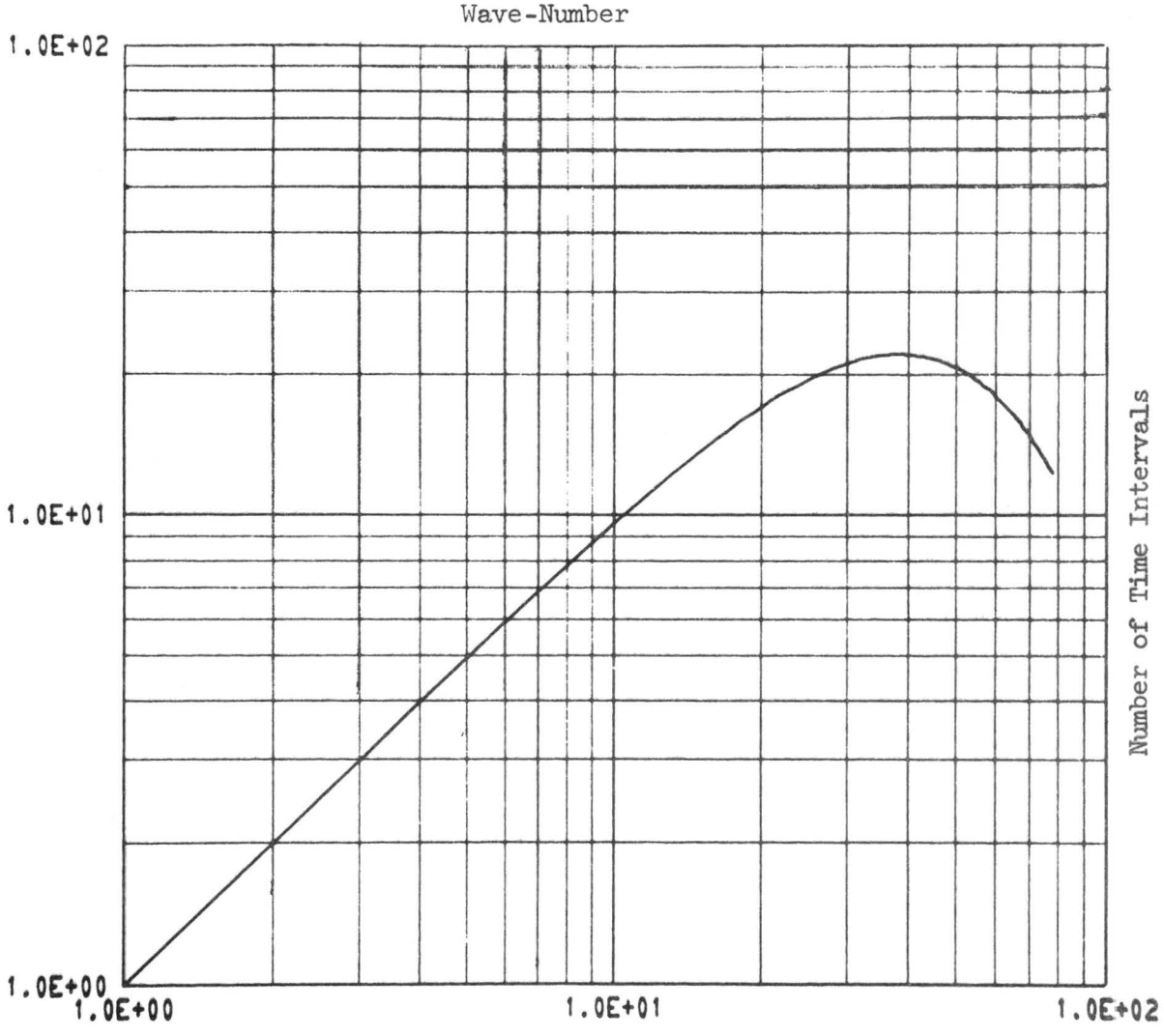

Figure 12. Number of time intervals per time interval of wave-number 1. (R=35.72)

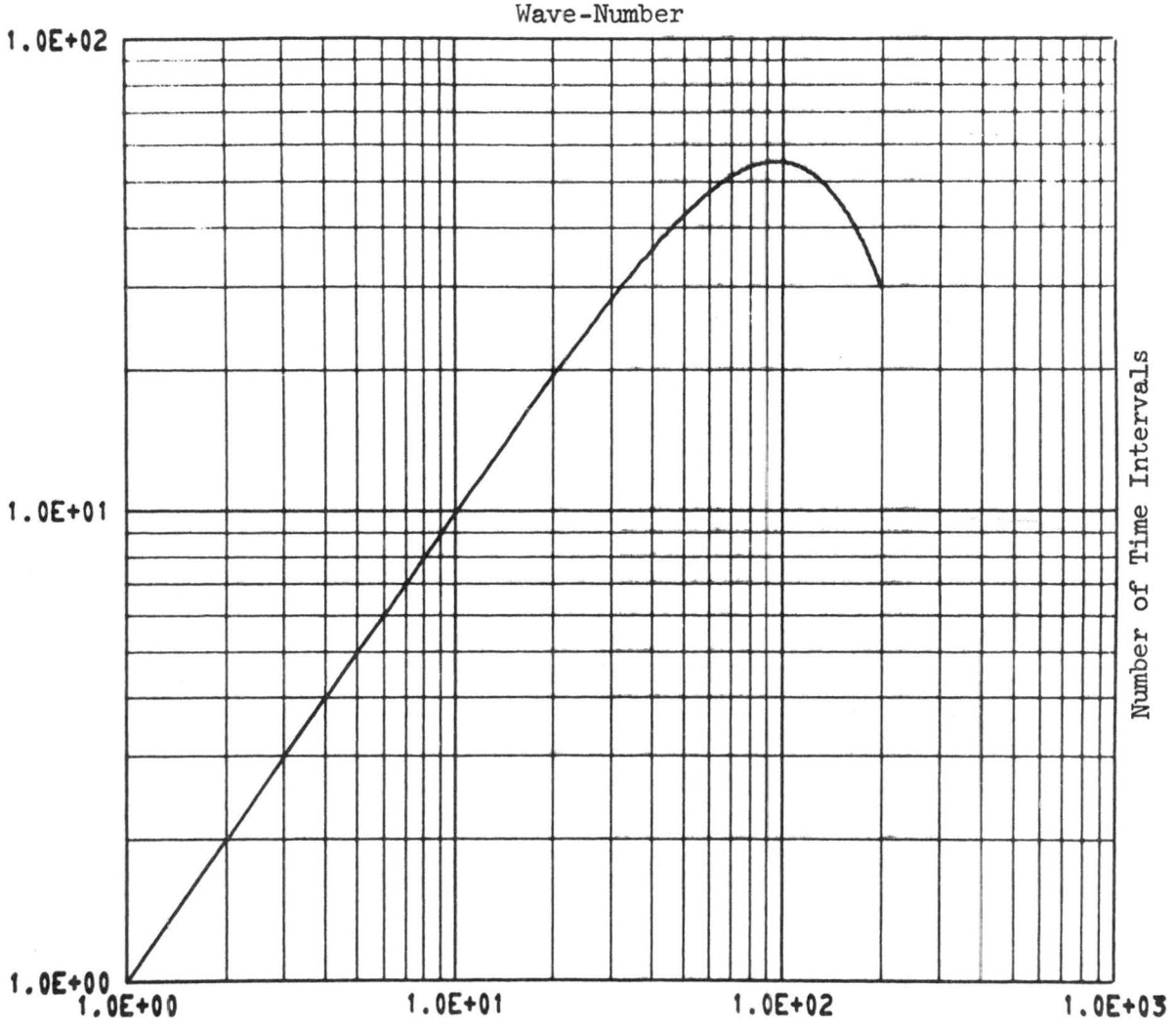

Figure 13. Number of time intervals per time interval of wave-number 1. (R=90.14)

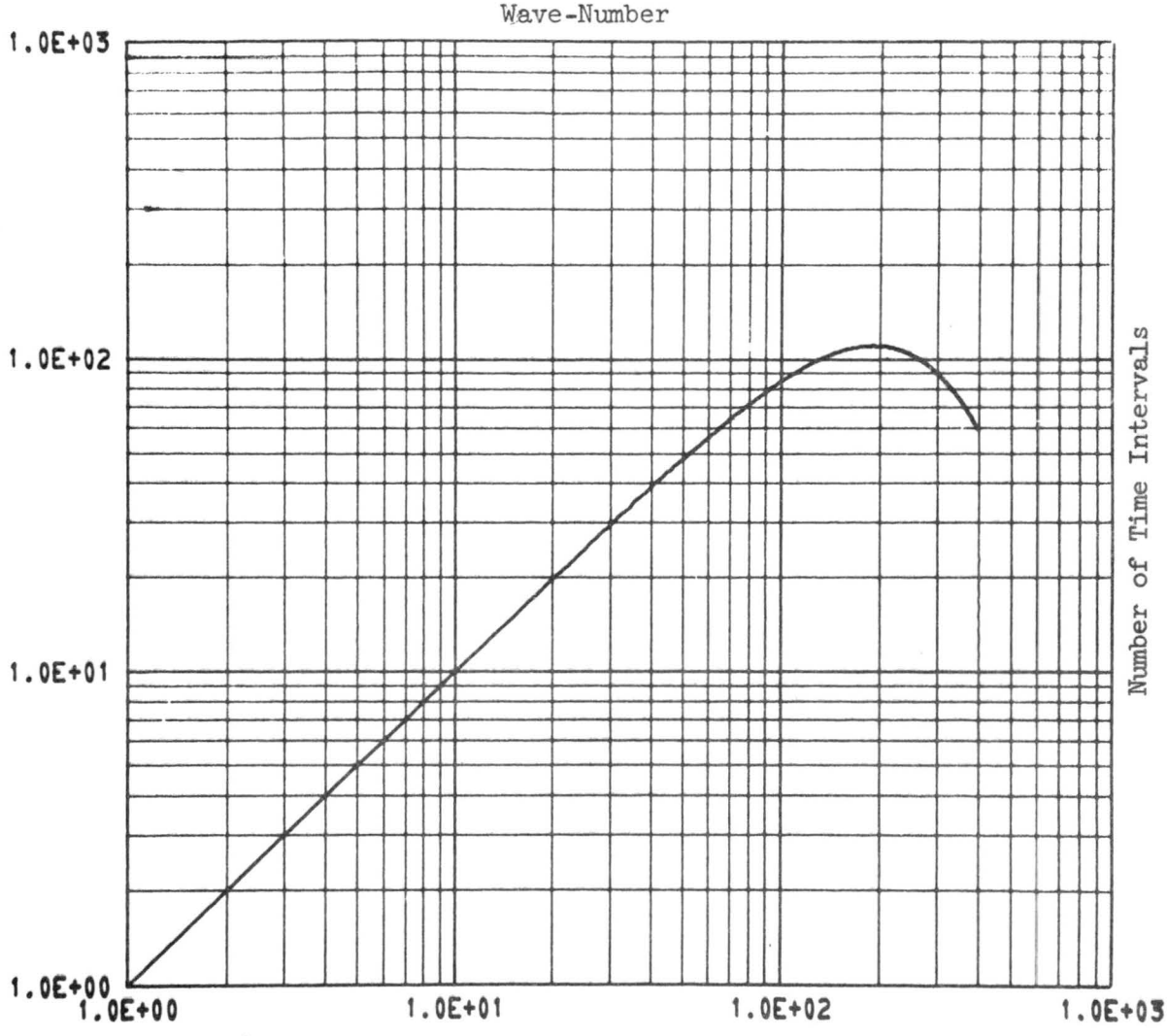

Figure 14. Number of time intervals per time interval of wave-number 1. (R=180.830)

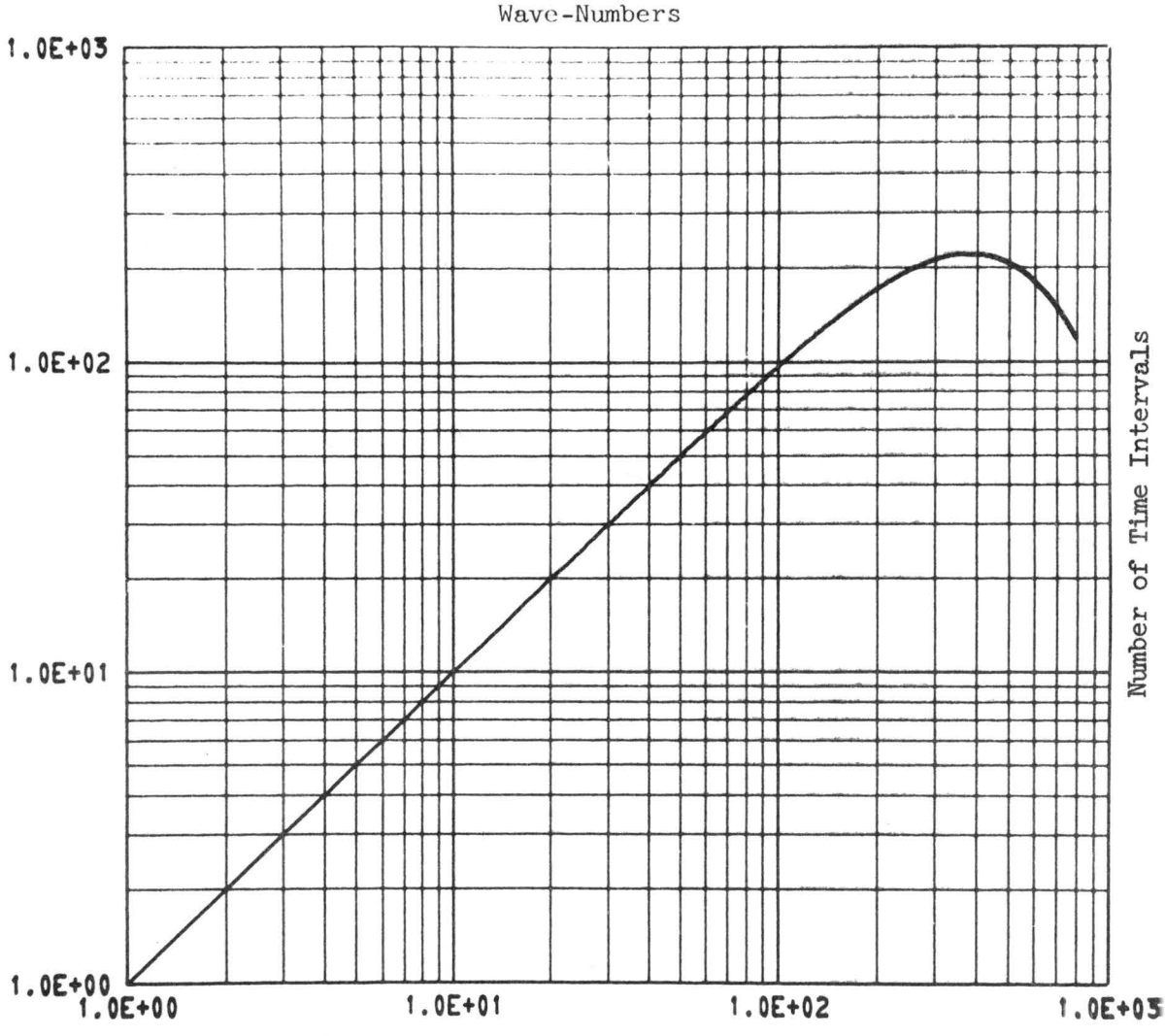

Figure 15. Number of time intervals per time interval of wave-number 1. (R=362.21)

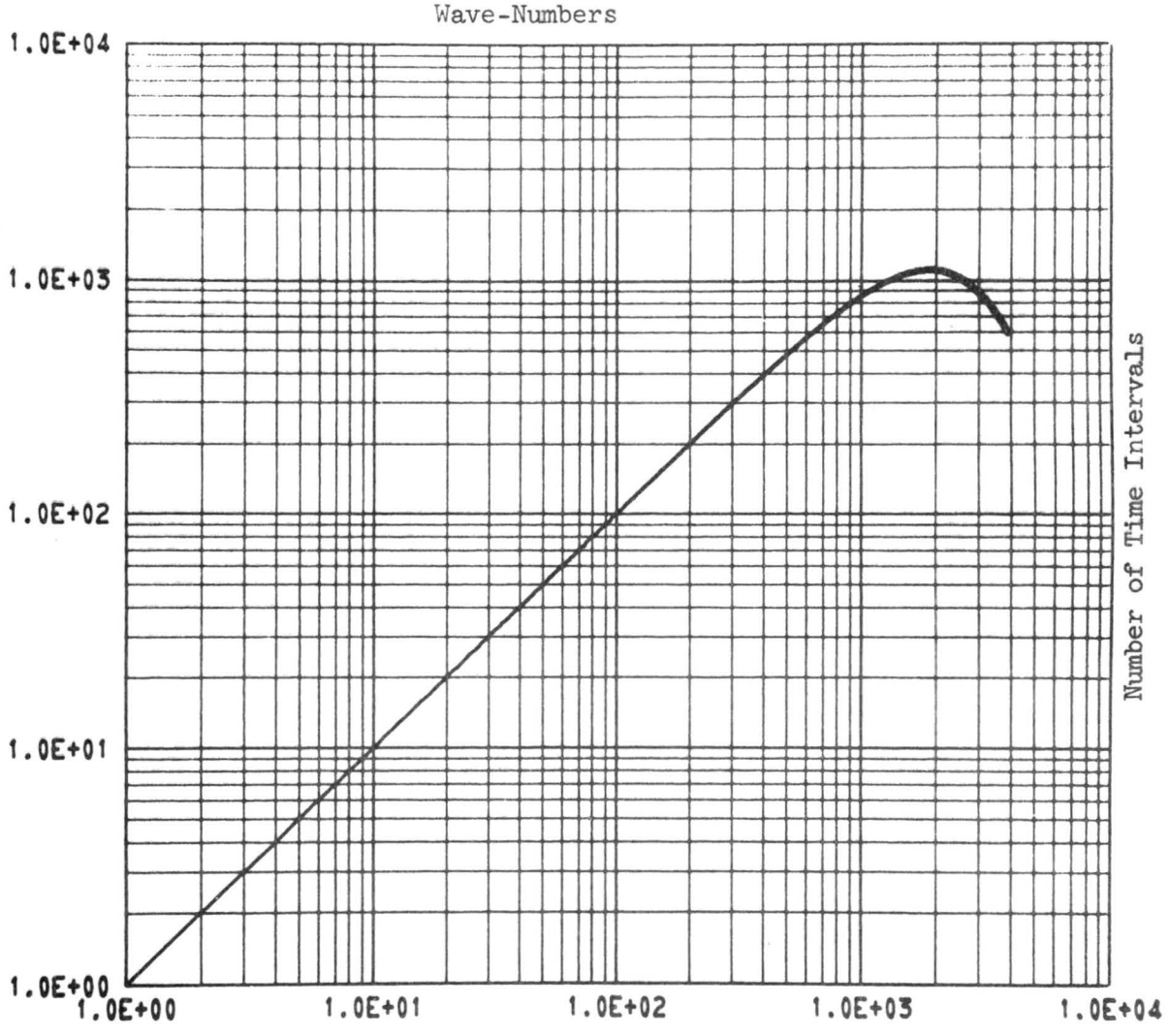

Figure 16. Number of time intervals per time interval of wave-number 1. (R=1813.25)

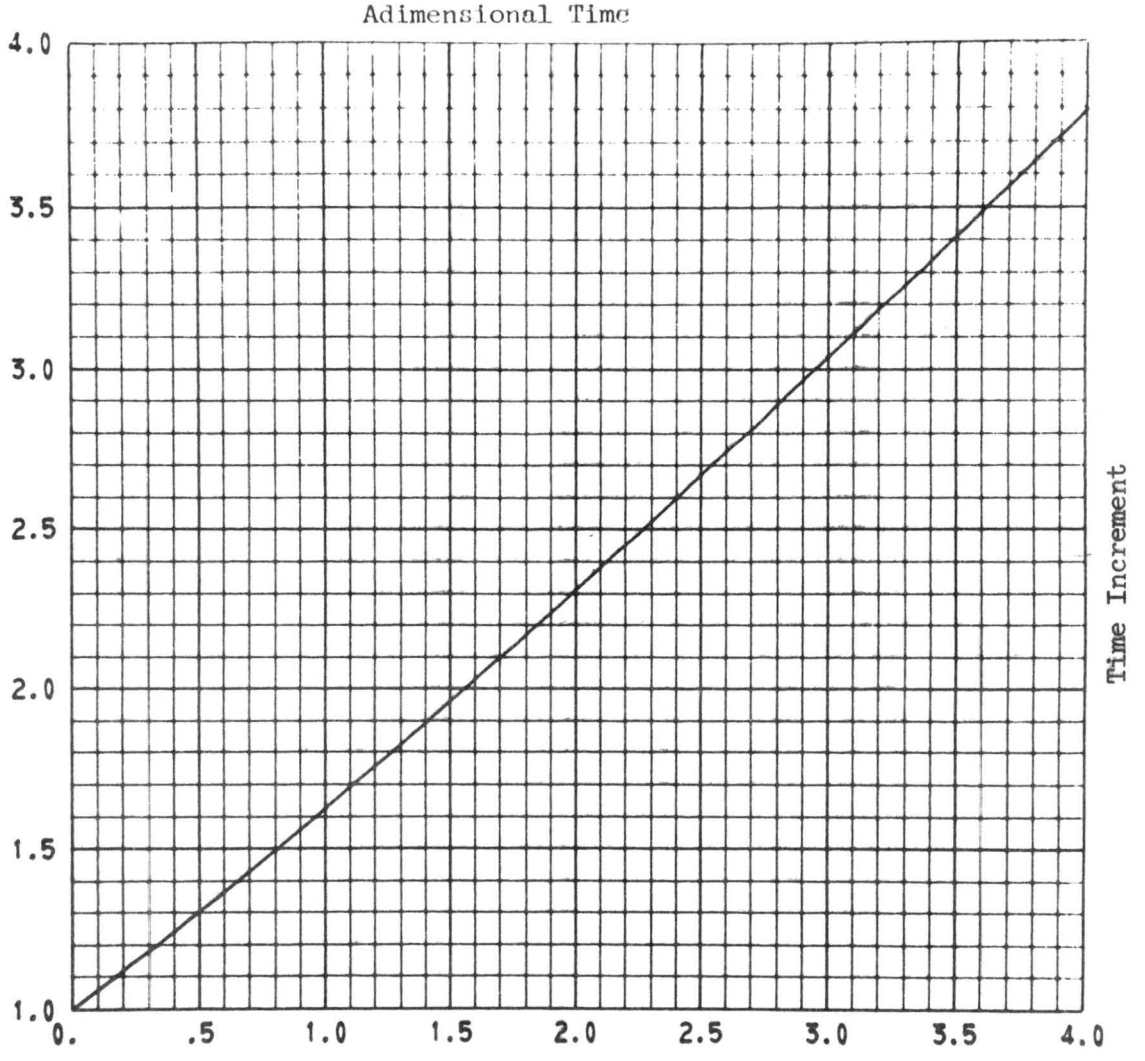

Figure 17. Variation of the time increment in time.

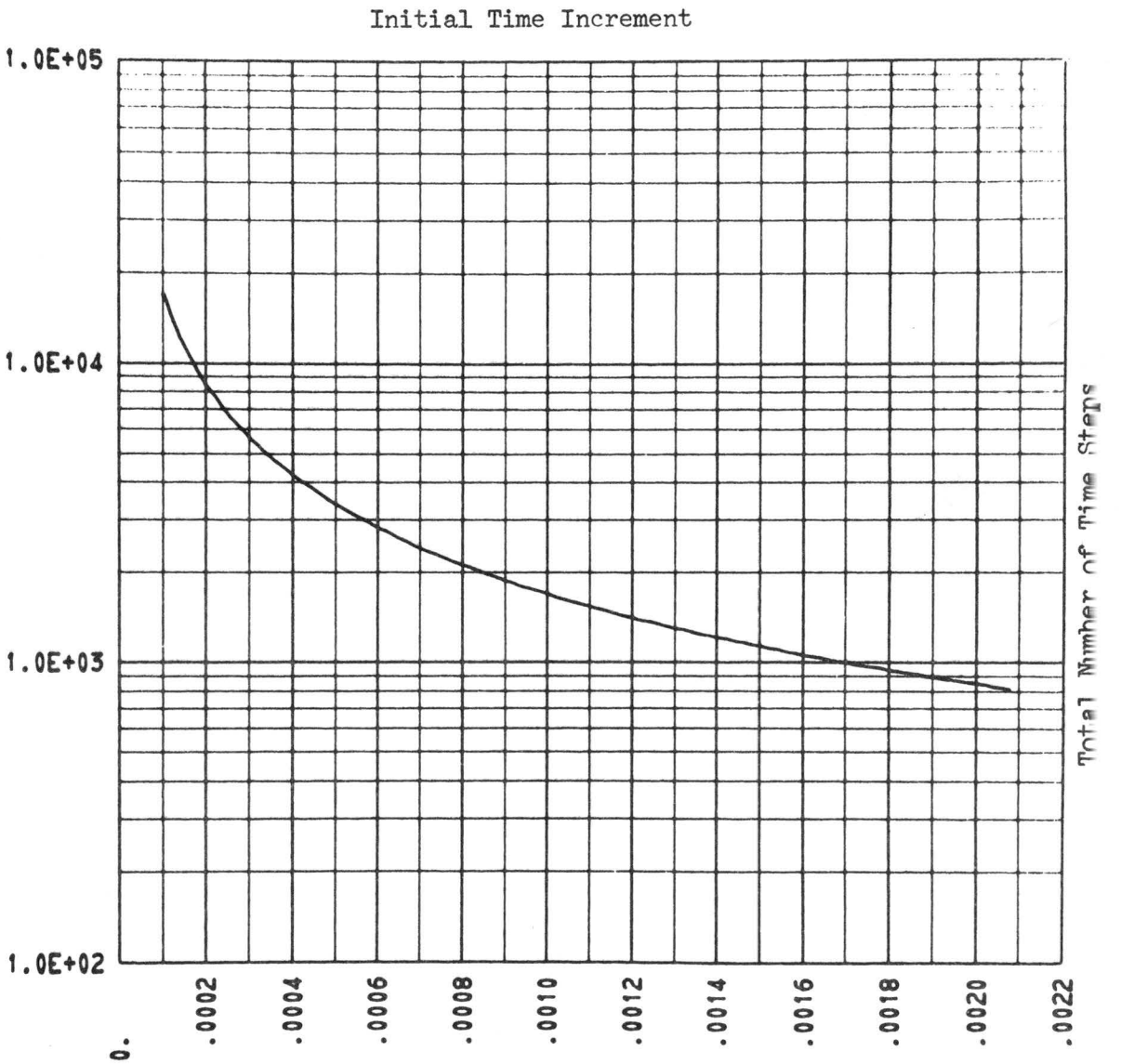

Figure 18. Total number of time steps as a function of the initial time increment for R=90 and T=4..

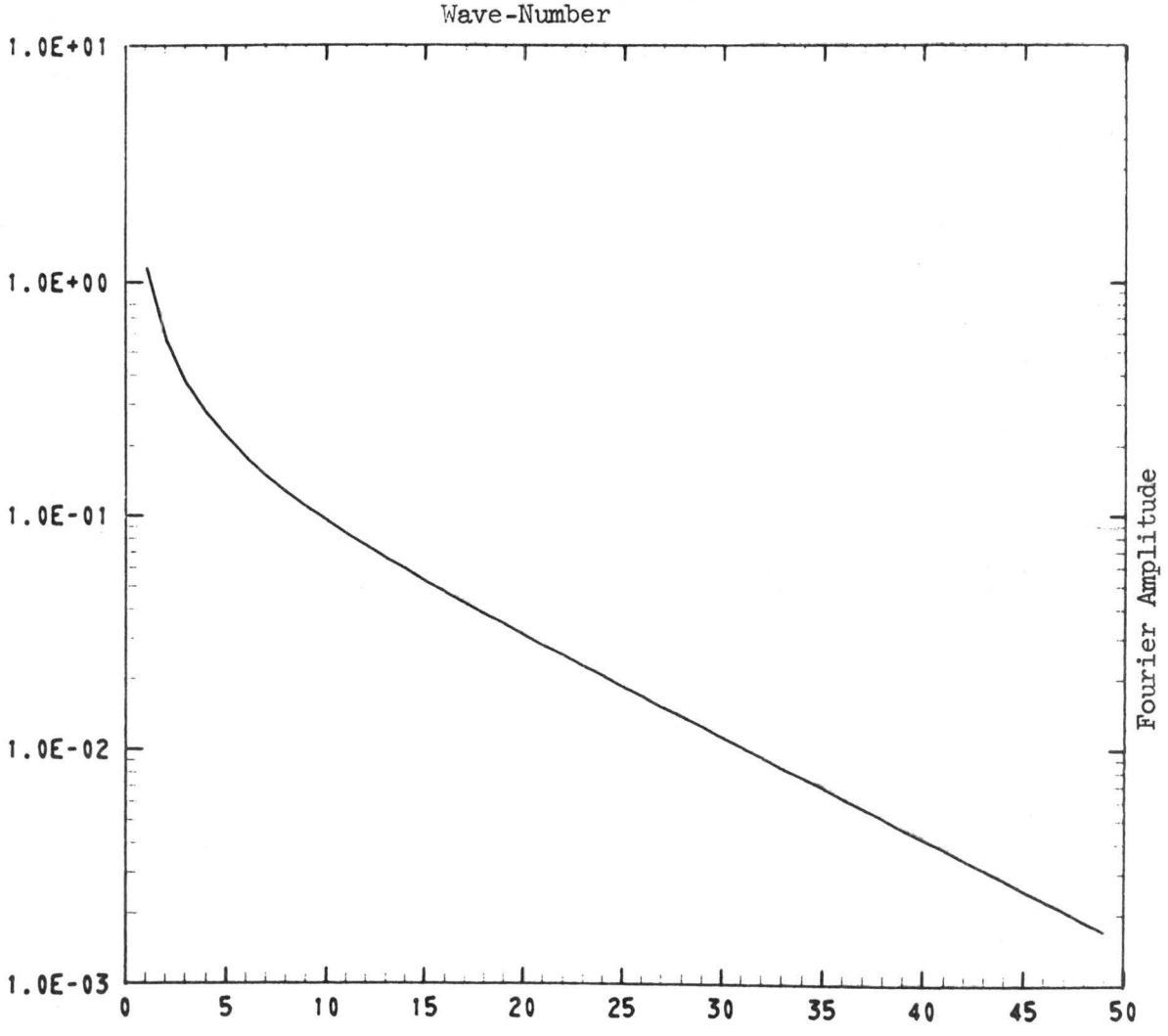

Figure 19. Reference exact solution for R=17 at $\tau = .0$.

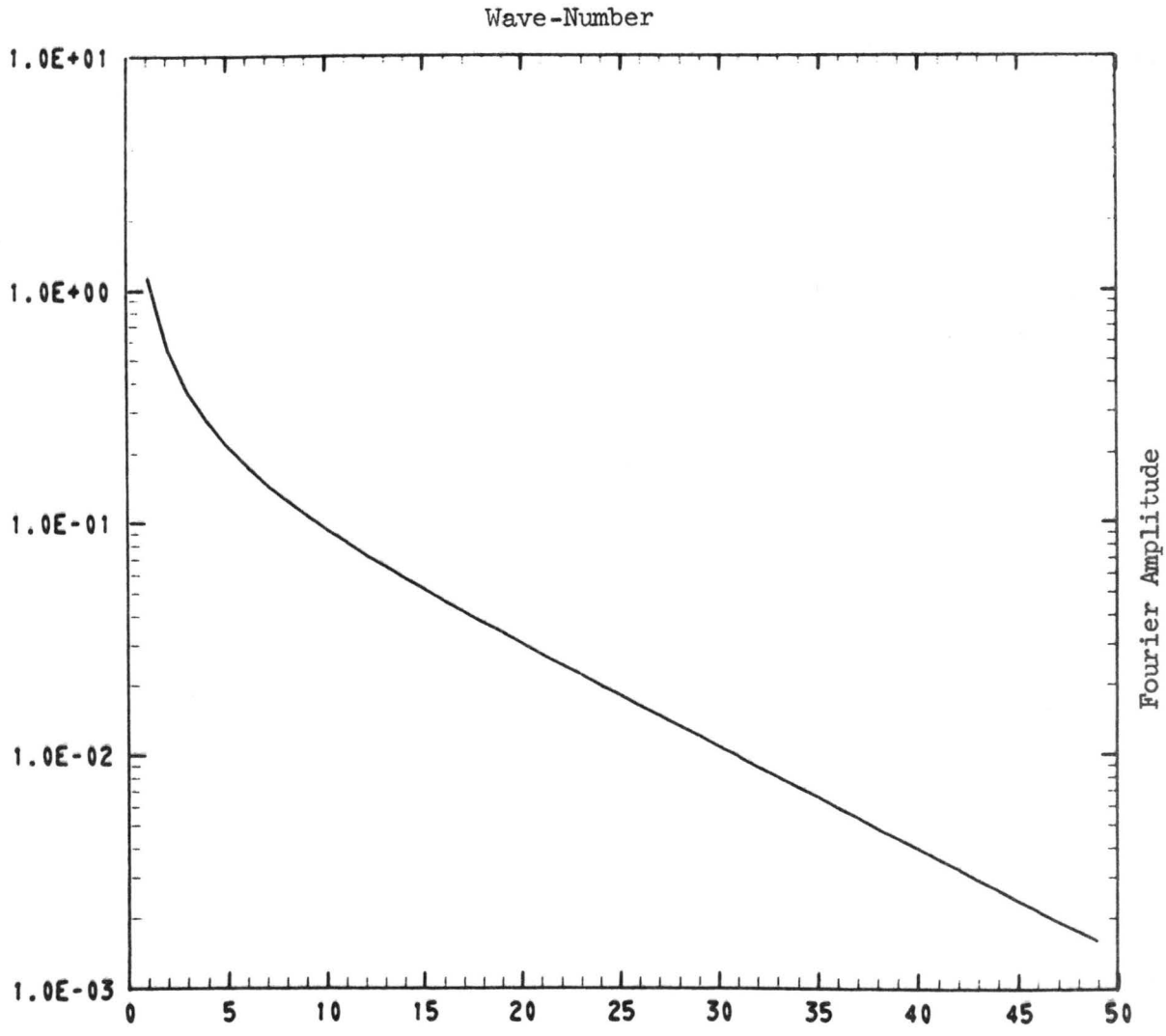

Figure 20. Reference exact solution for R=17 at τ =.0225.

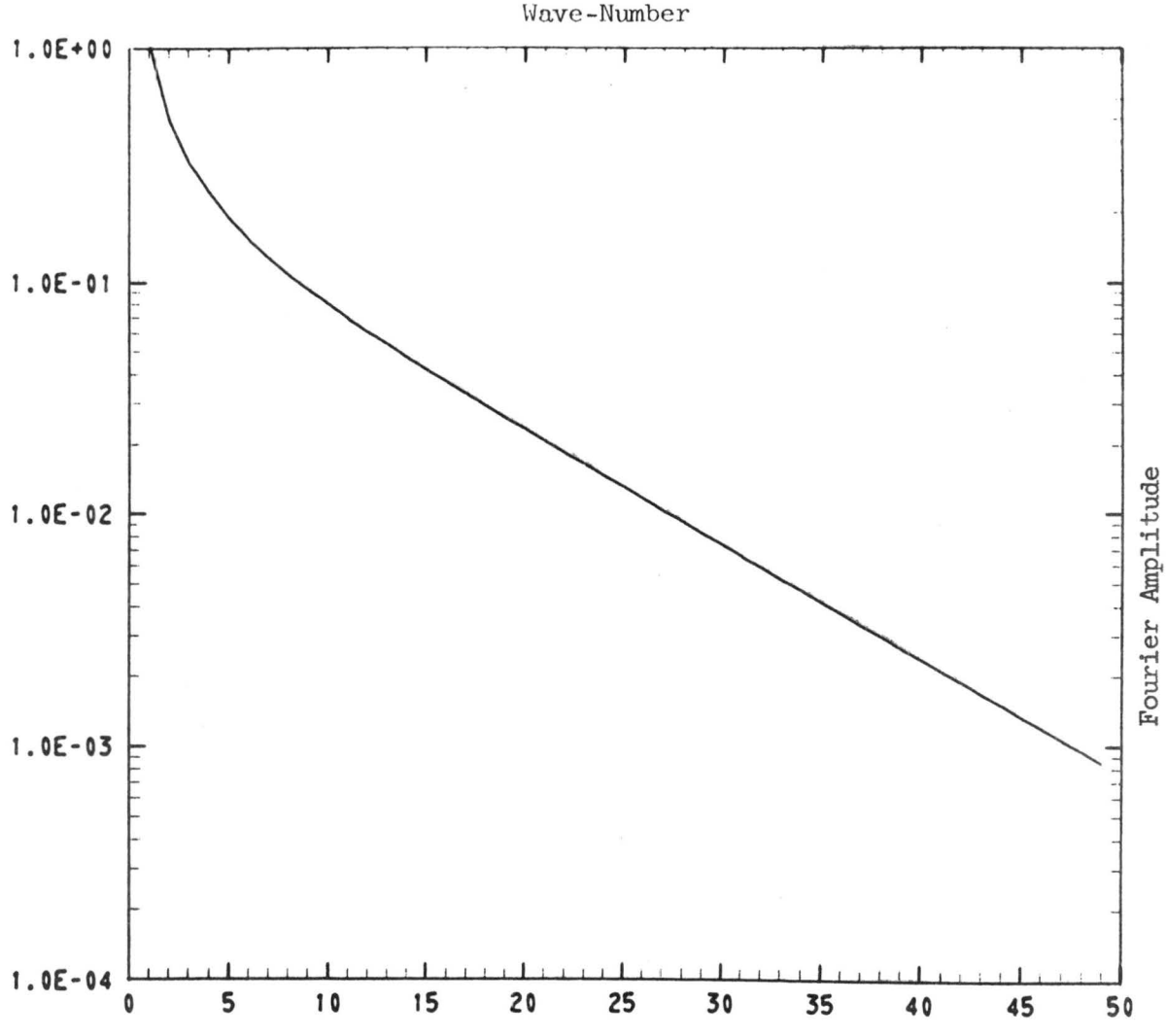

Figure 21. Reference exact solution for R=17 at $\tau = .2475$

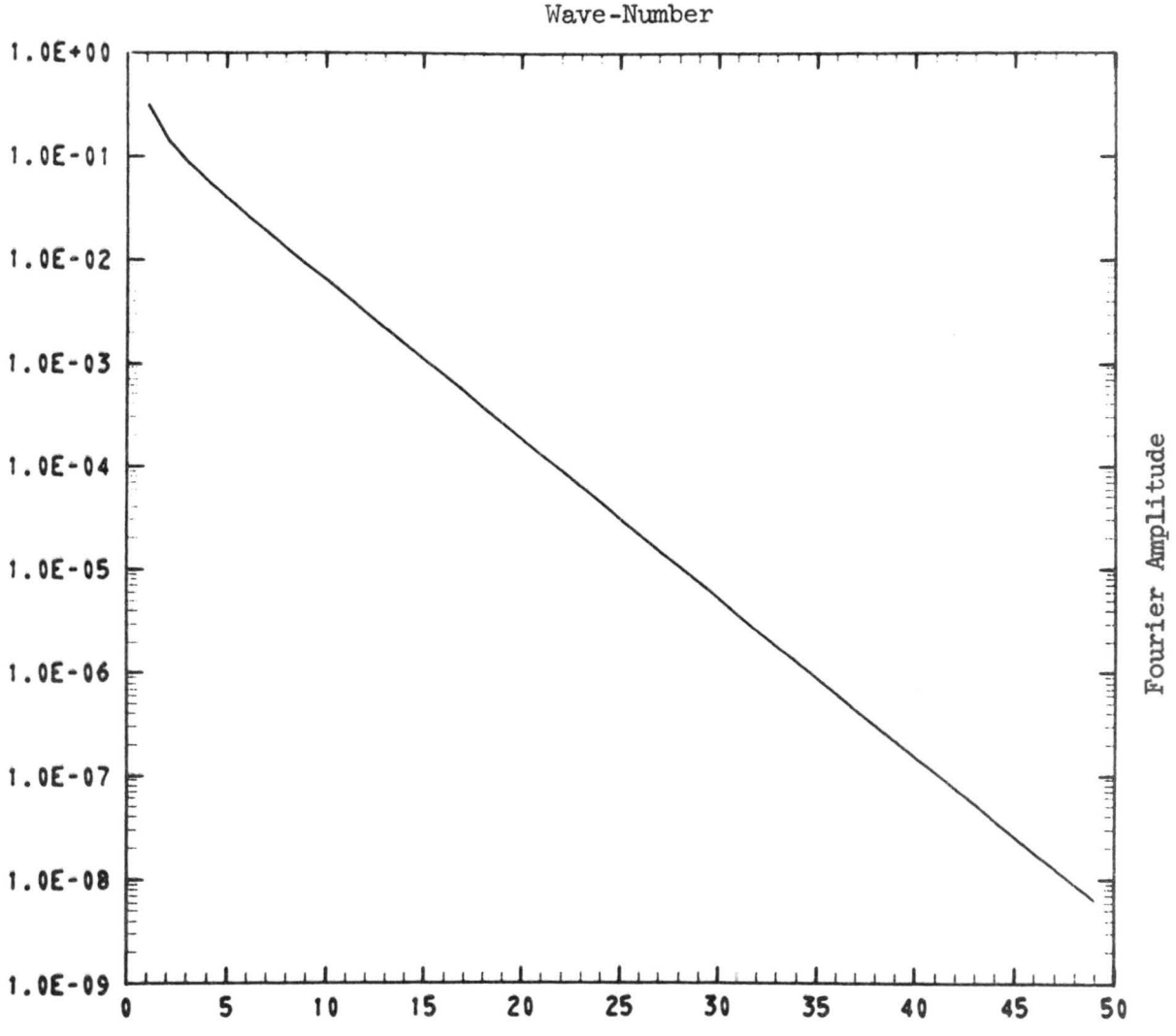

Figure 22. Reference exact solution for R=17 and τ =4.4925.

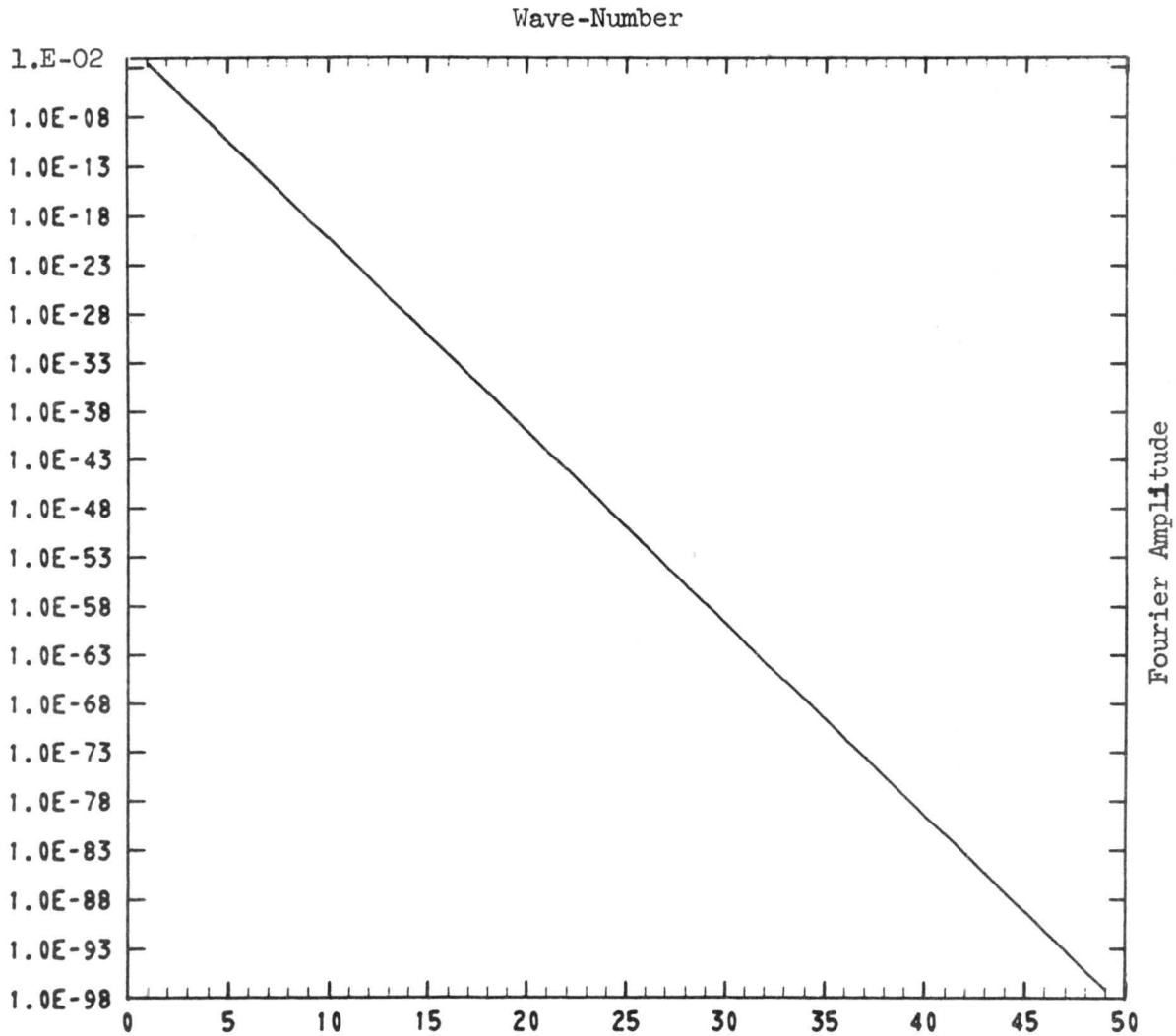

Figure 23. Reference exact solution for R=17 at τ=78..

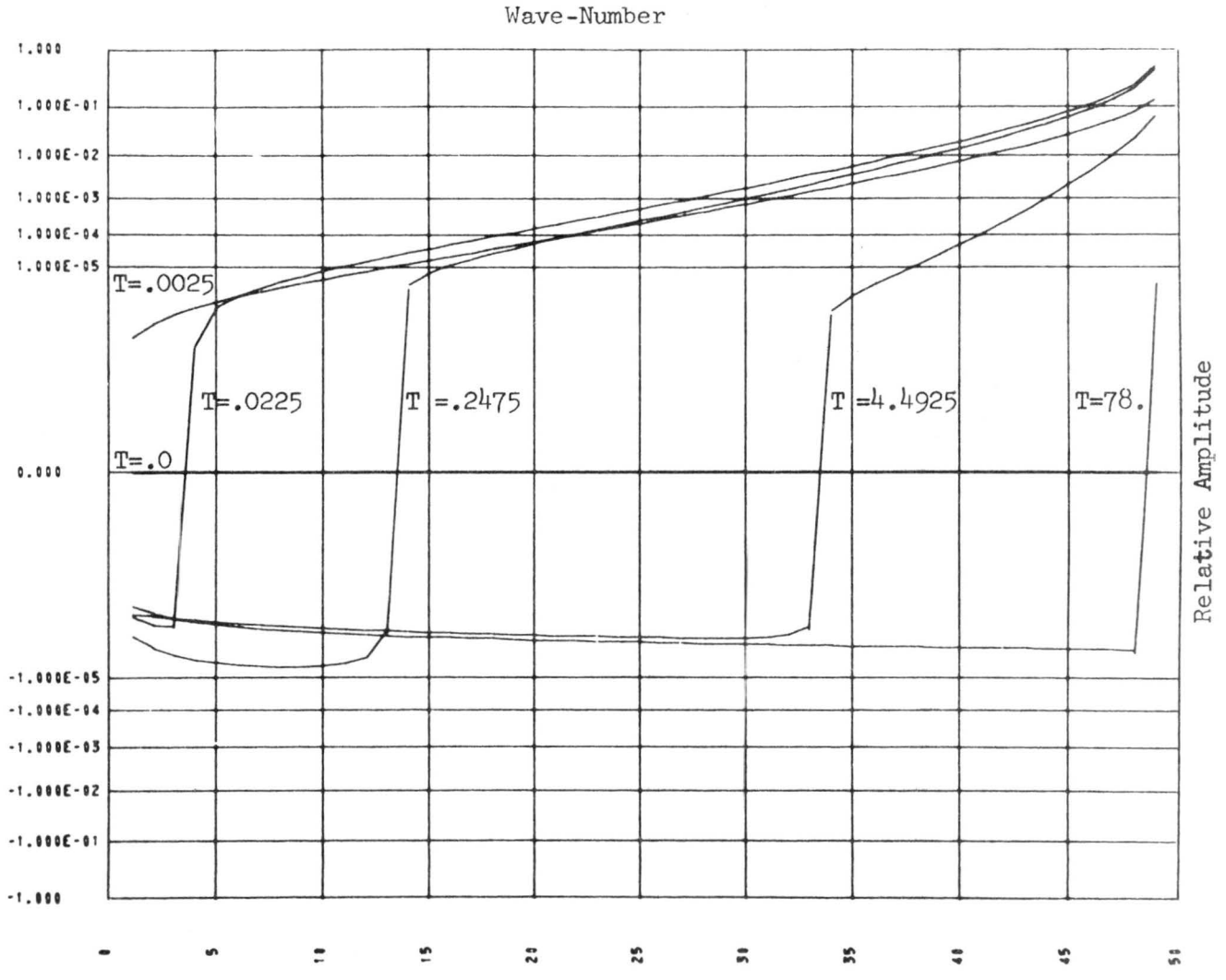

Figure 24. Influence of the wave-number cut-off.

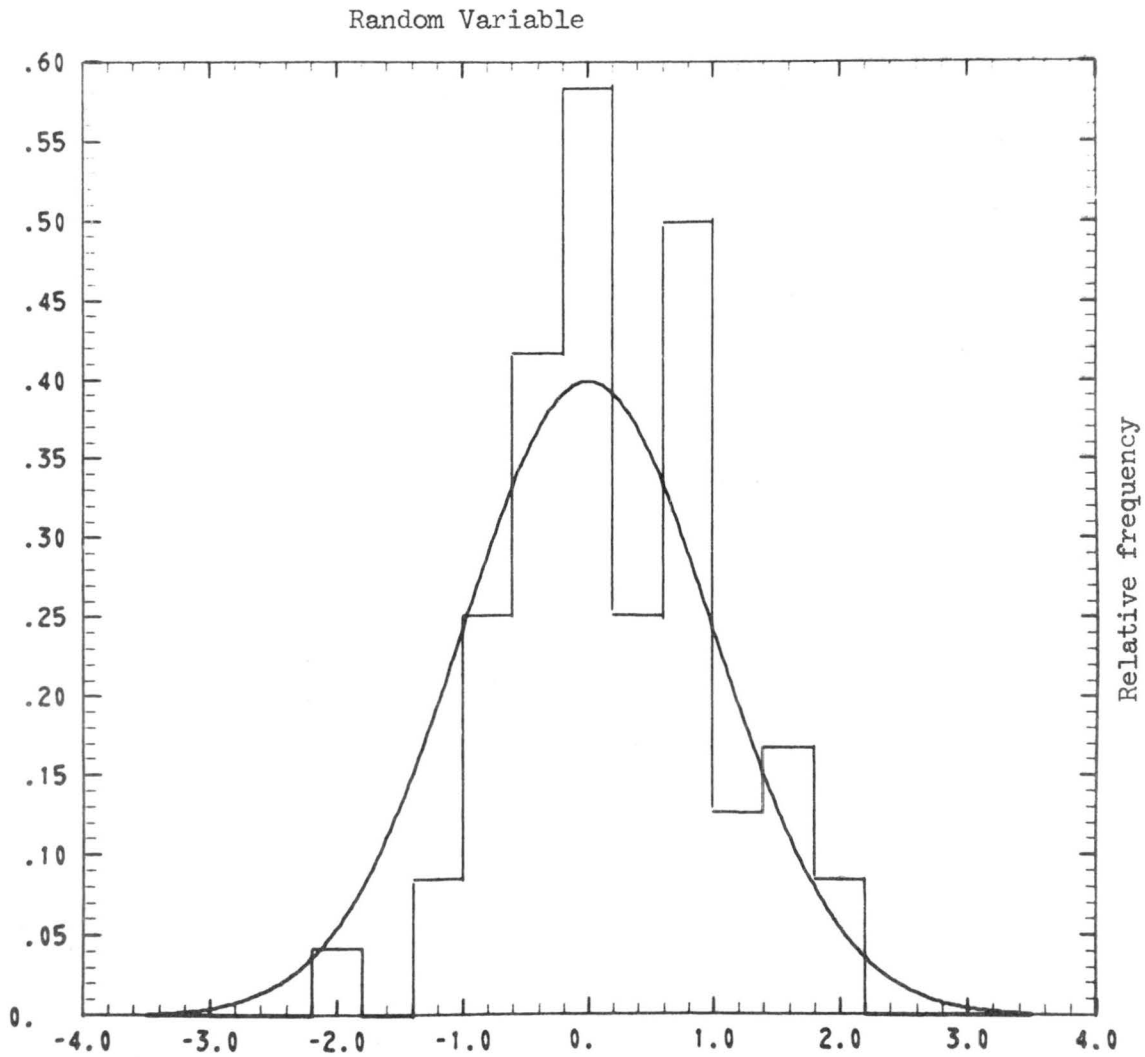

Figure 25. Histogram for a sample of size 60.

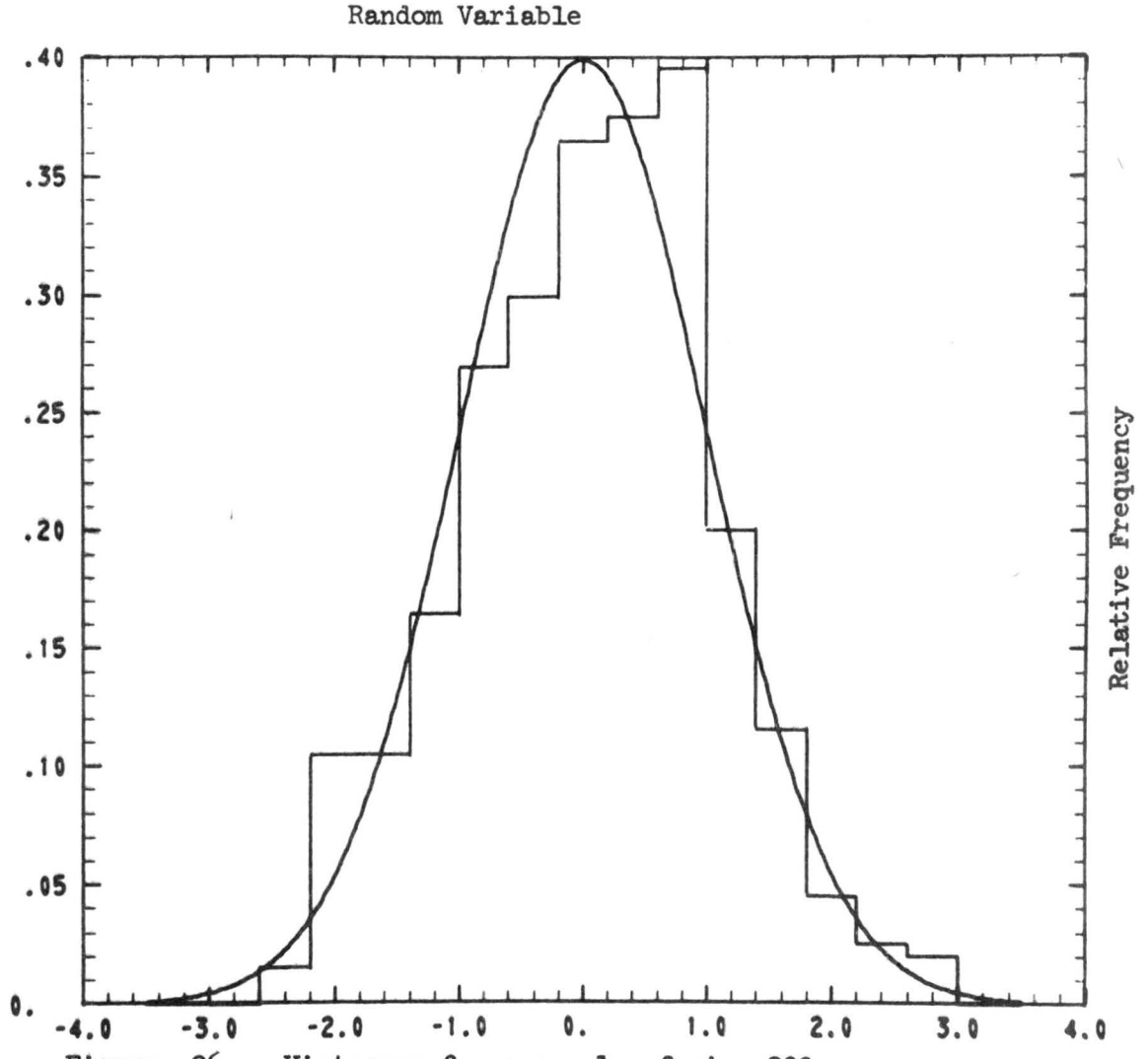

Figure 26. Histogram for a sample of size 200.

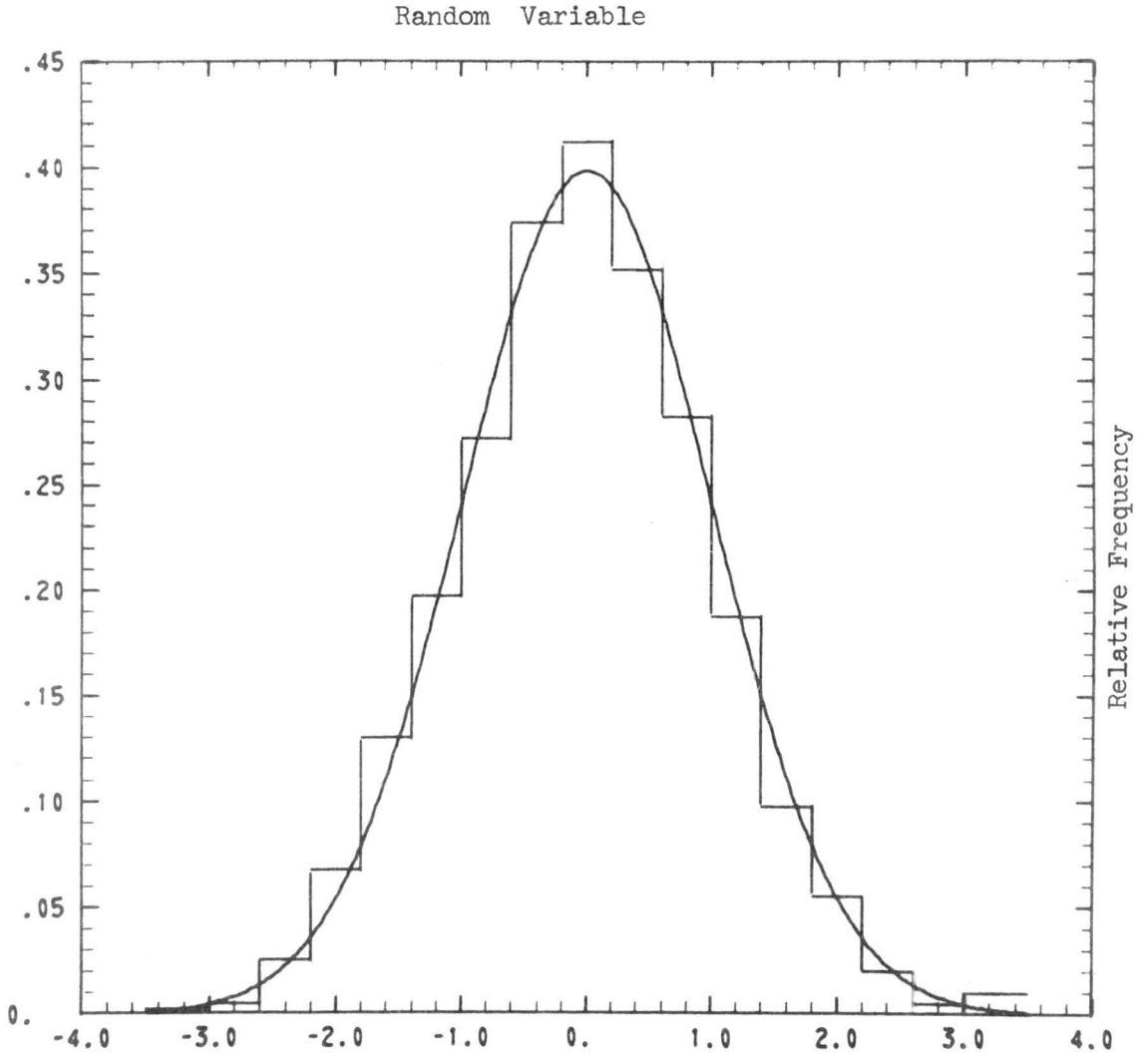

Figure 27. Histogram for a sample of size 1000.

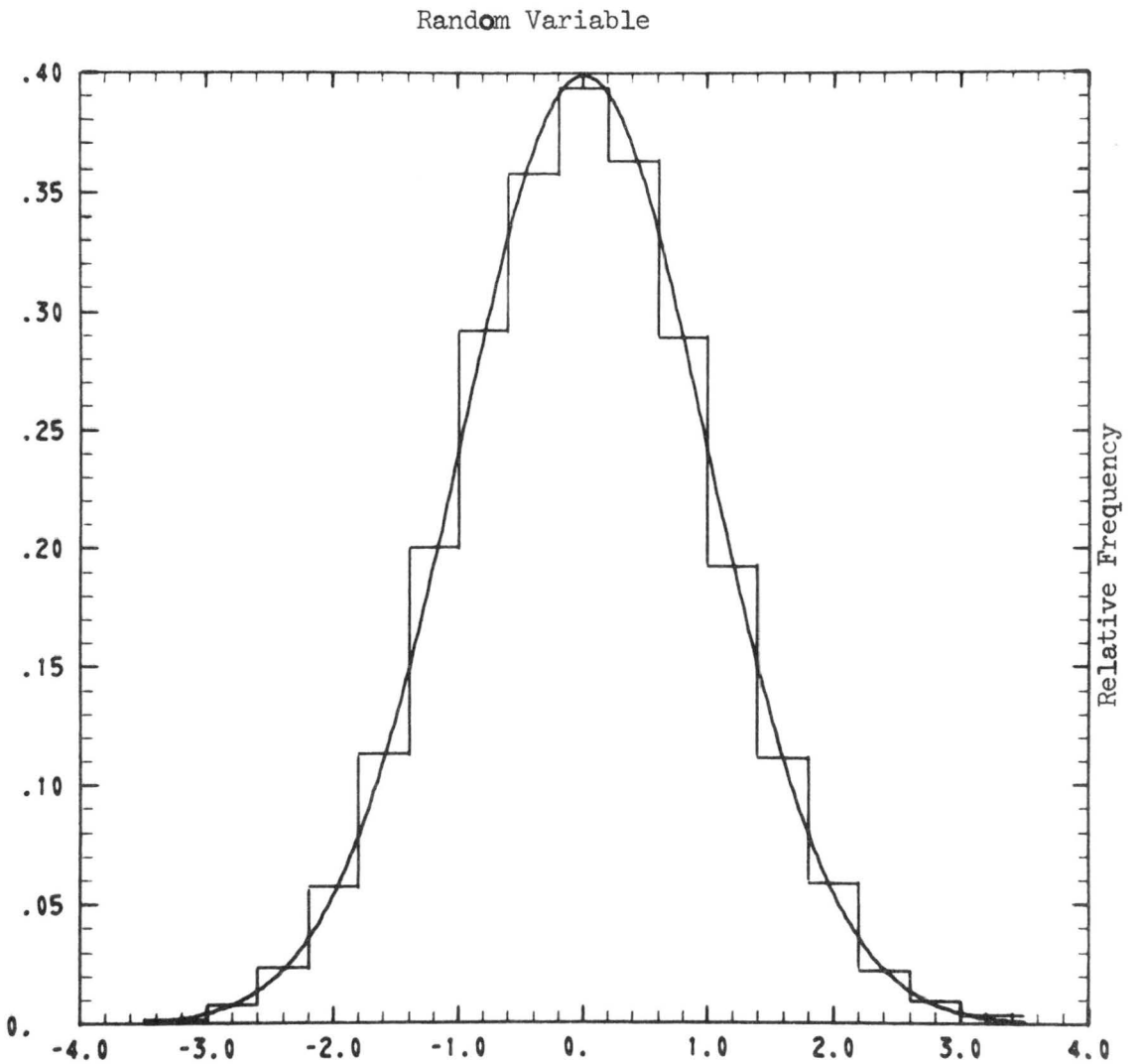

Figure 28. Histogram for a sample of size 10000.

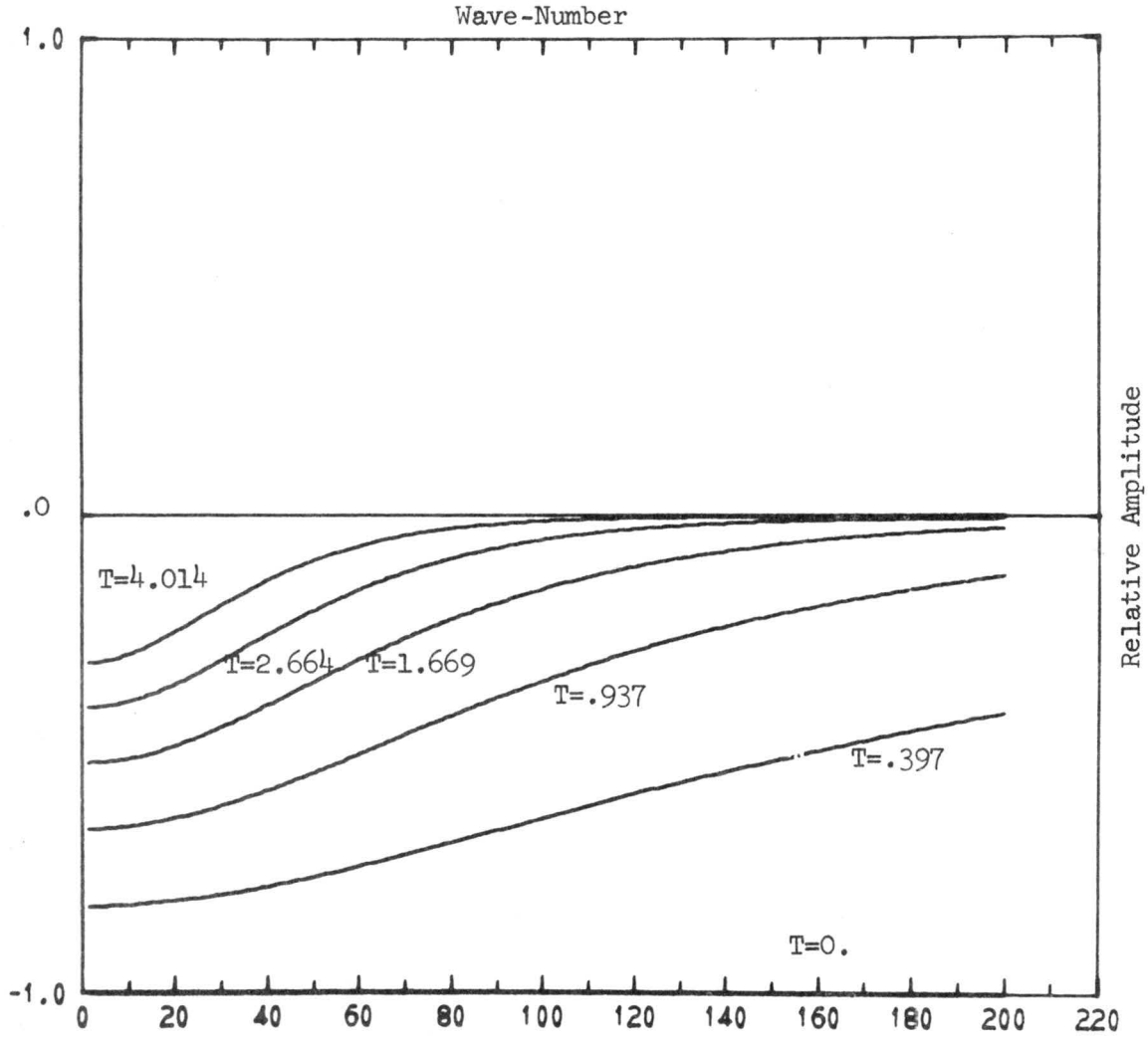

Figure 29. Reference exact solution for R=90.

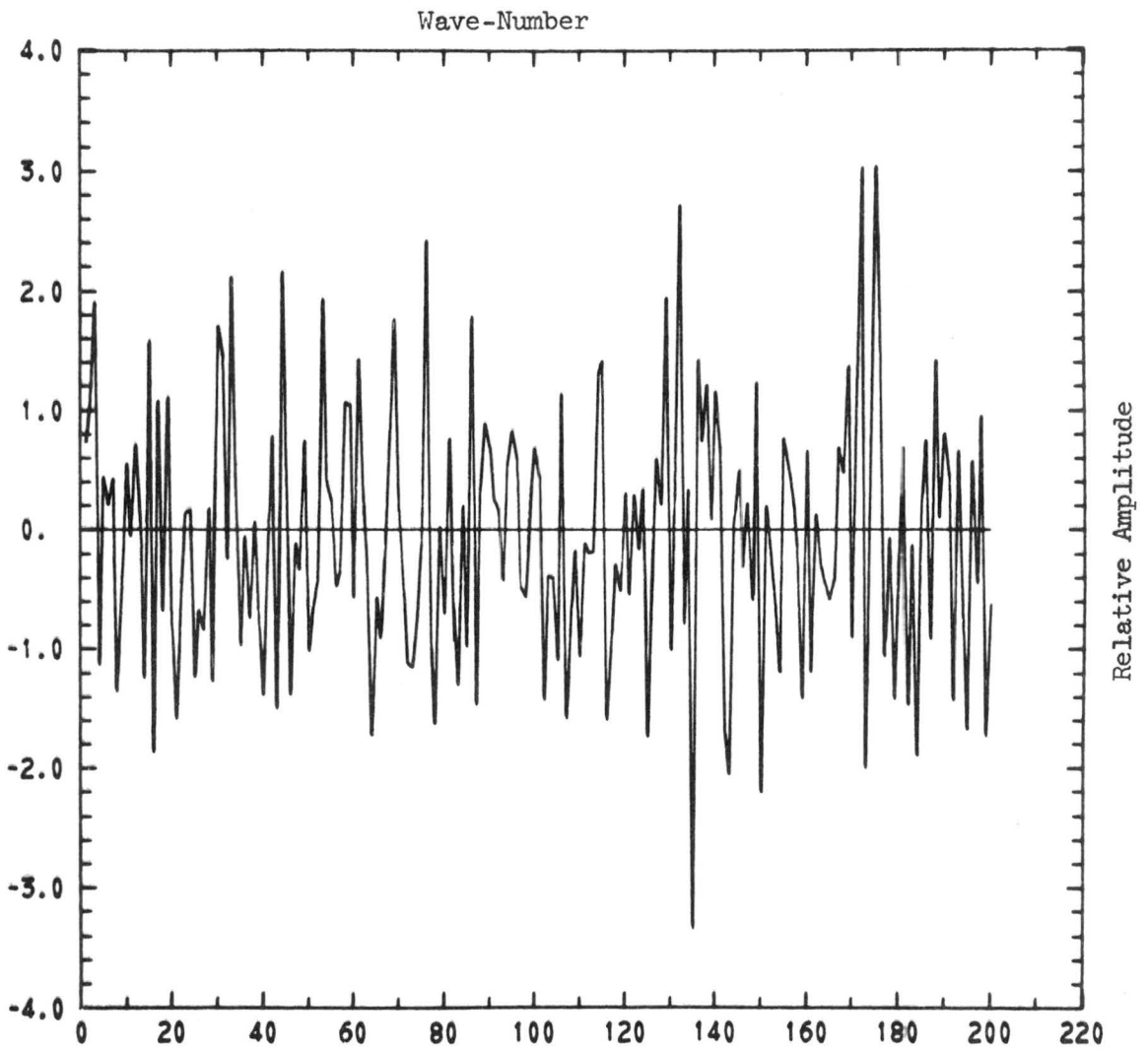

Figure 30. First realization in Fourier space at τ =.0.

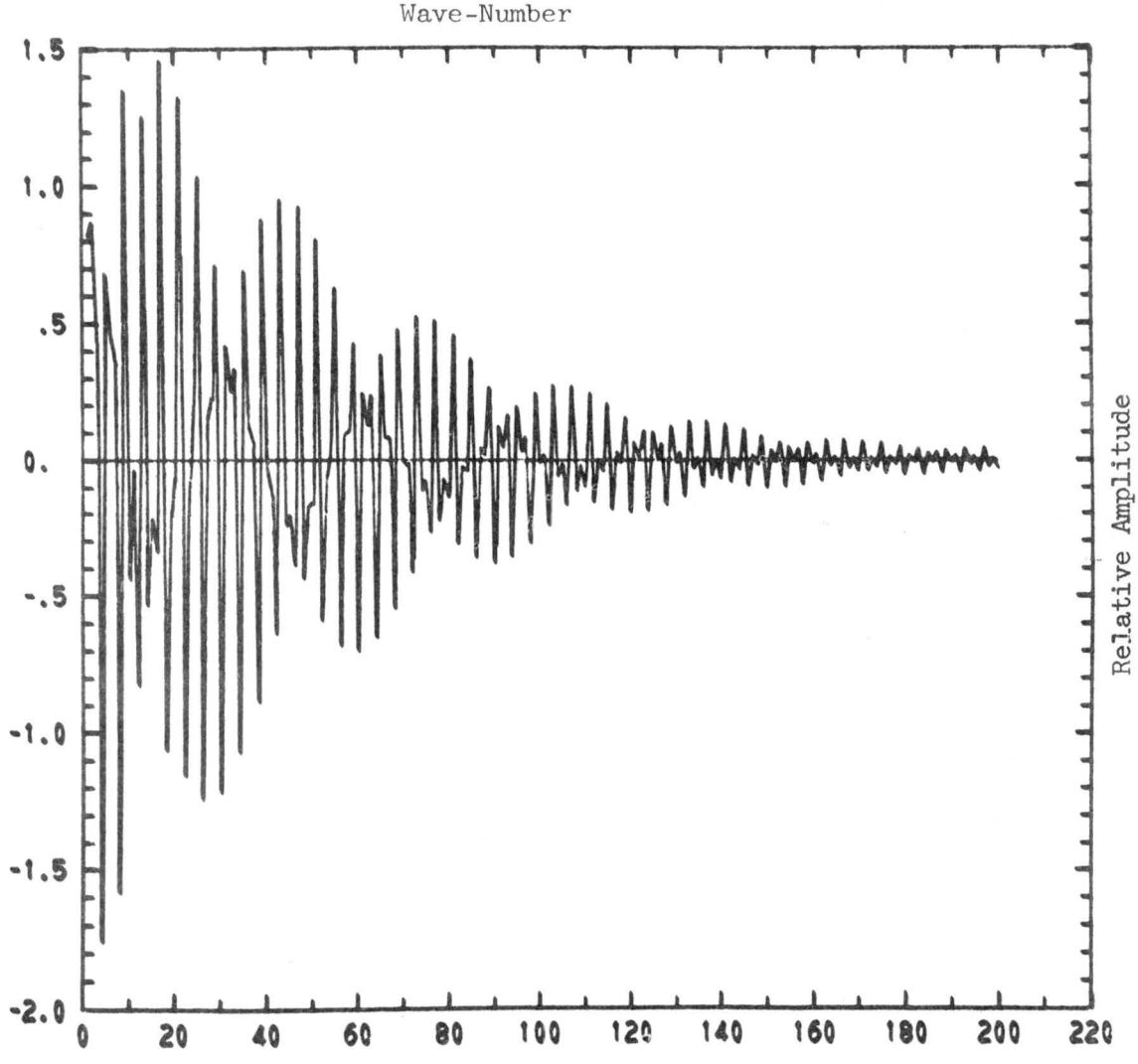

Figure 31. First Realization in Fourier space at τ =.397.

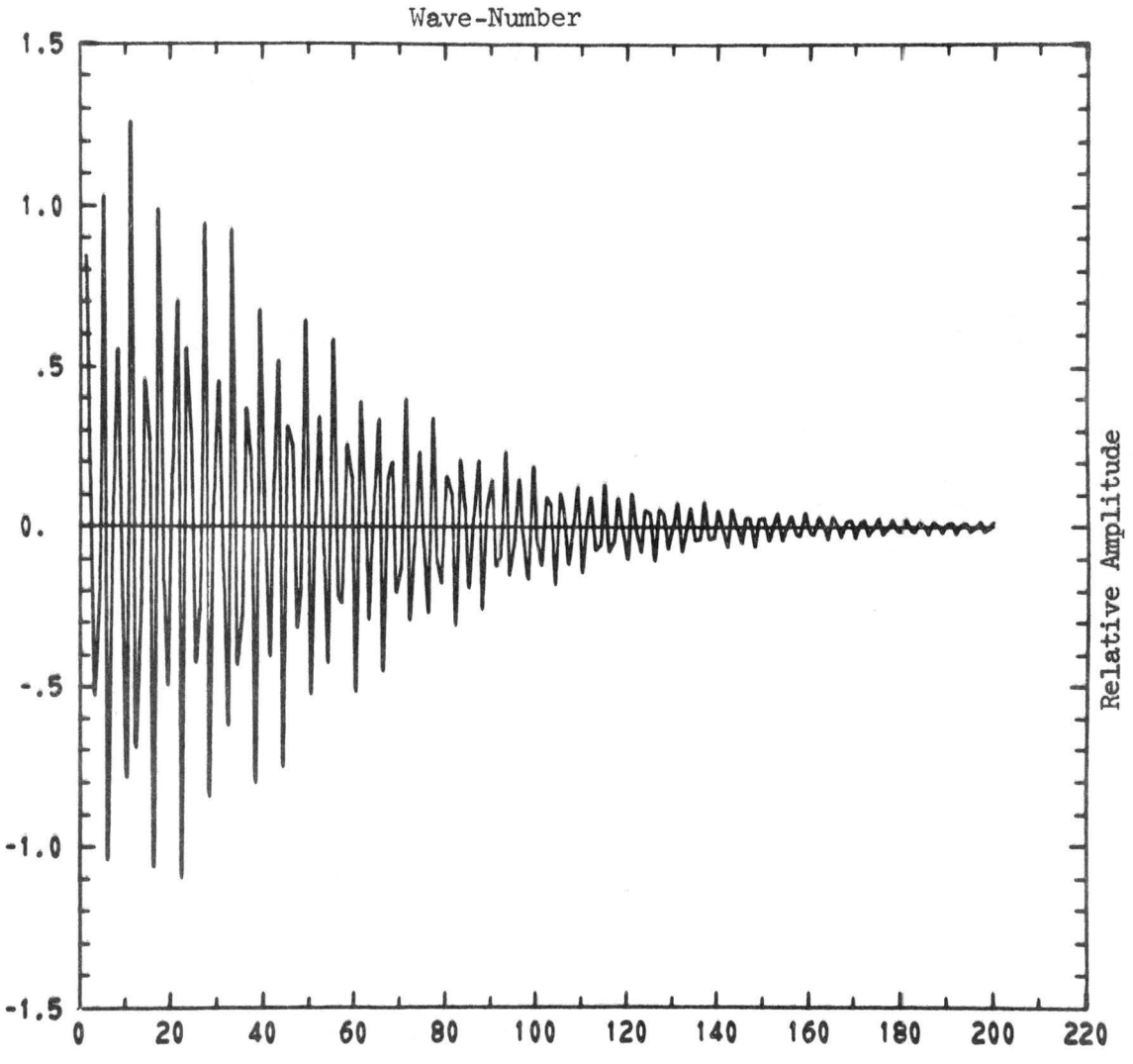

Figure 32. First realization in Fourier space at τ =.937.

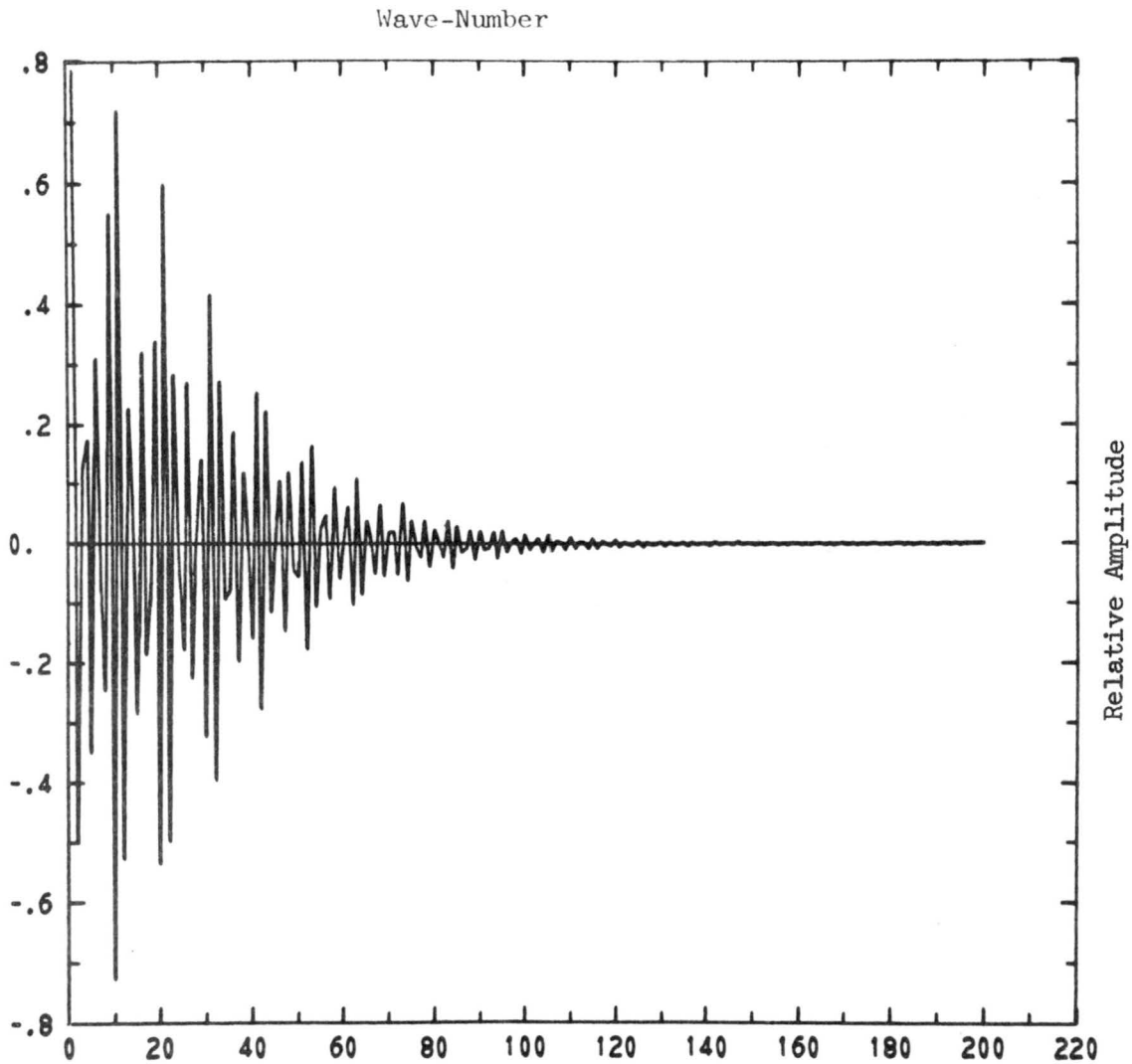

Figure 33. First realization in Fourier space at τ=1.669.

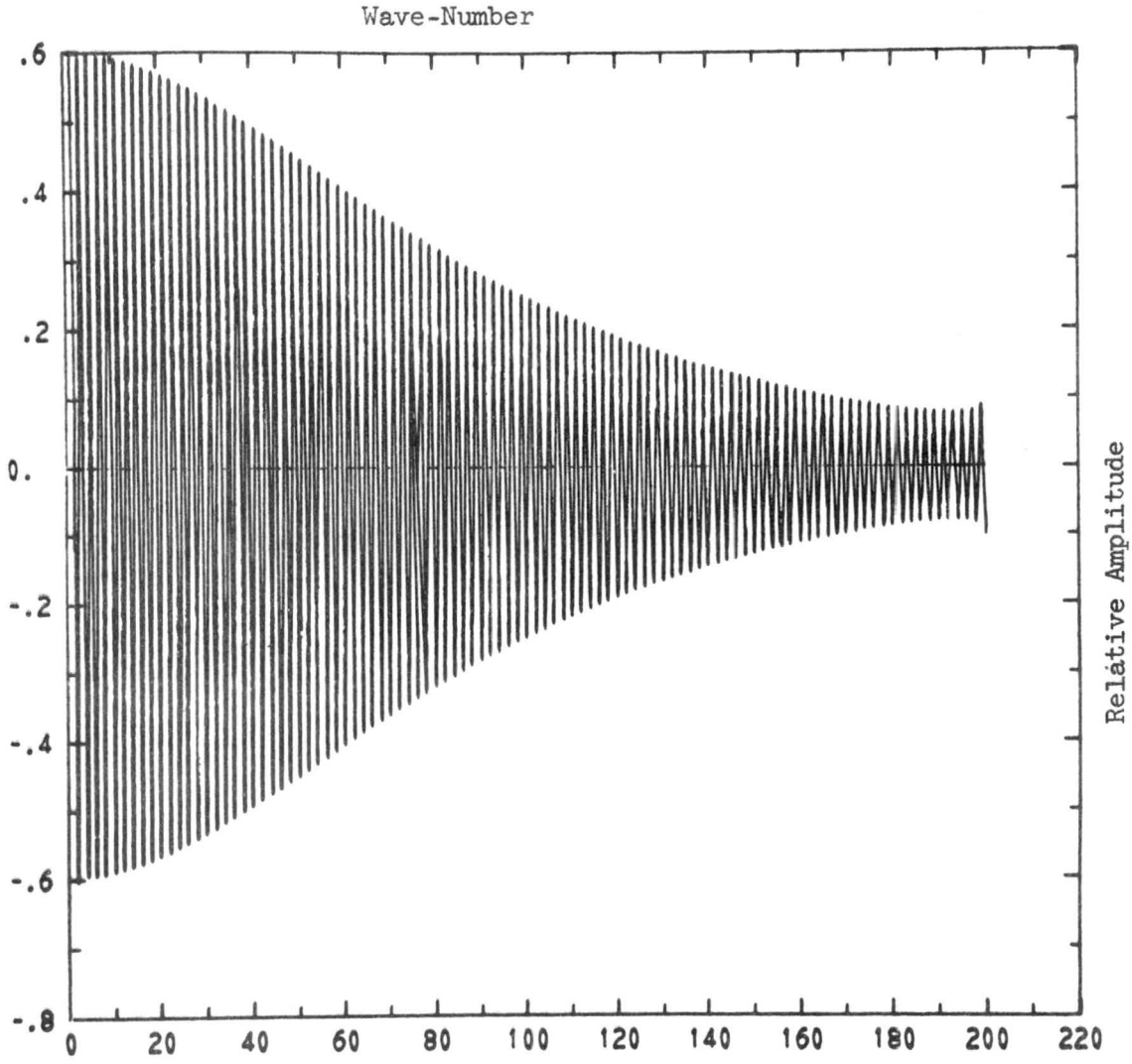

Figure 34. First realization in Fourier space at $\tau = 2.664$.

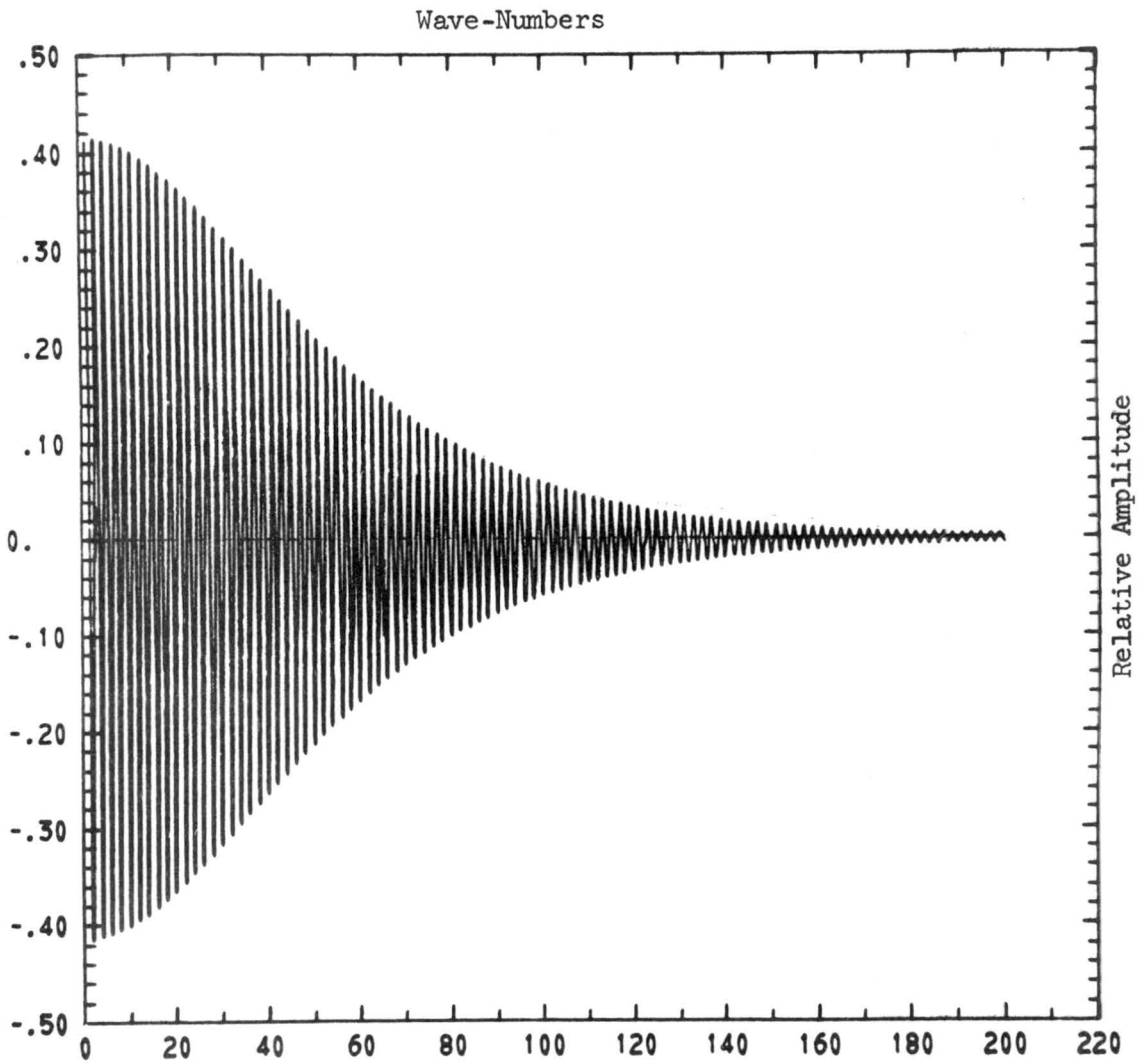

Figure 35. First realization in Fourier space at $\tau = 4$..

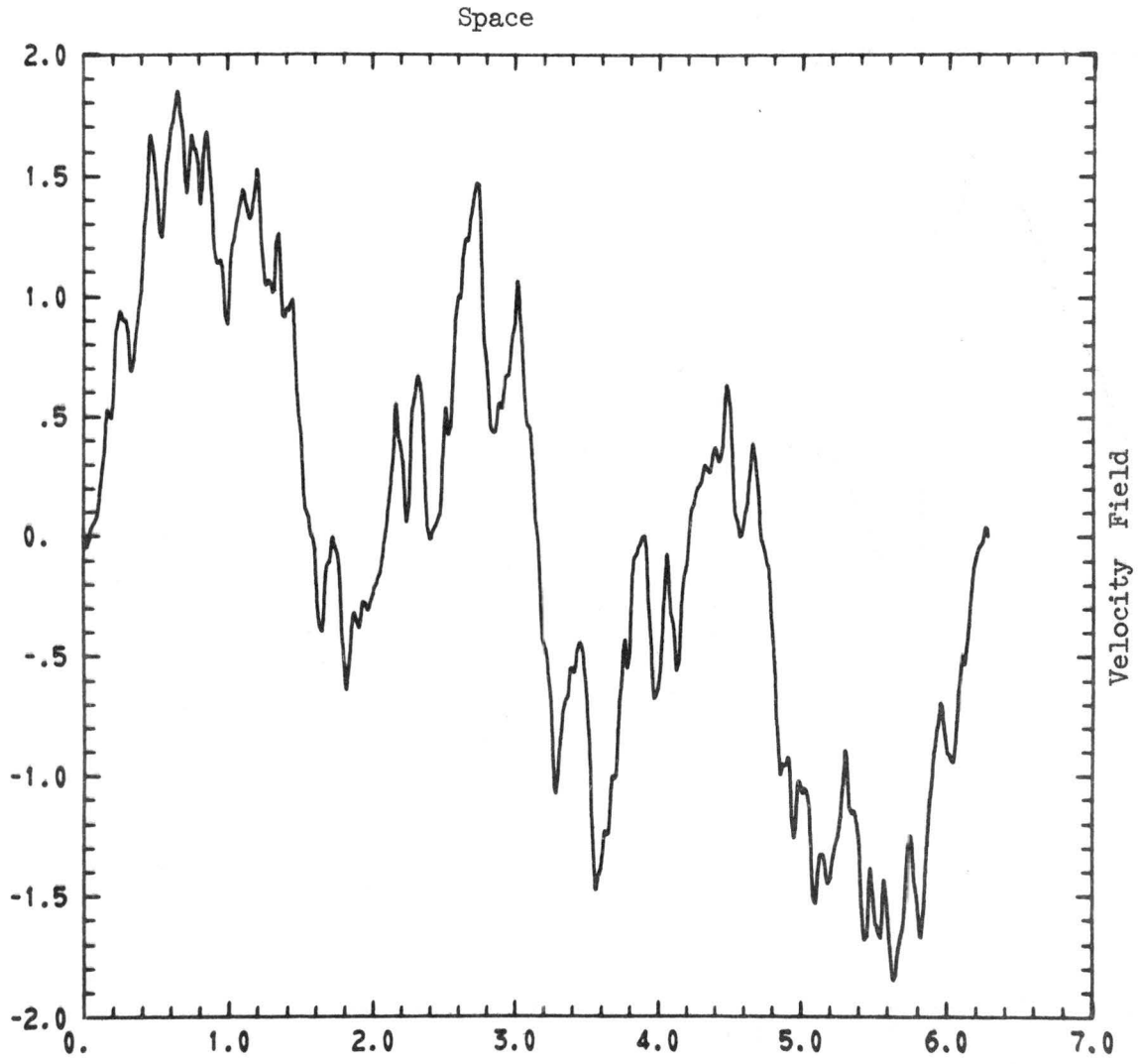

Figure 36. First realization in physical space at $\tau = .0$.

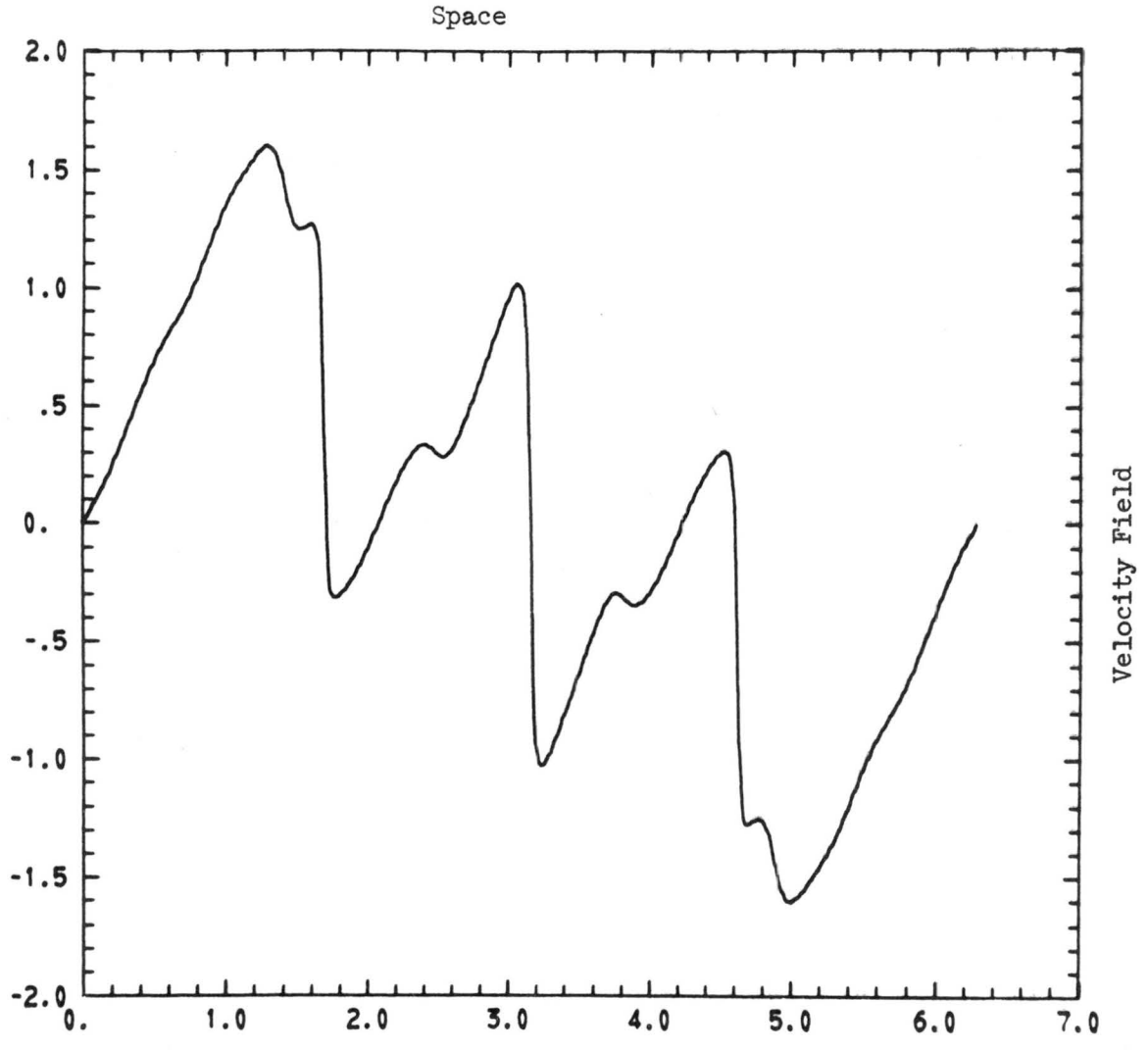

Figure 37. First realization in physical space at τ =.397.

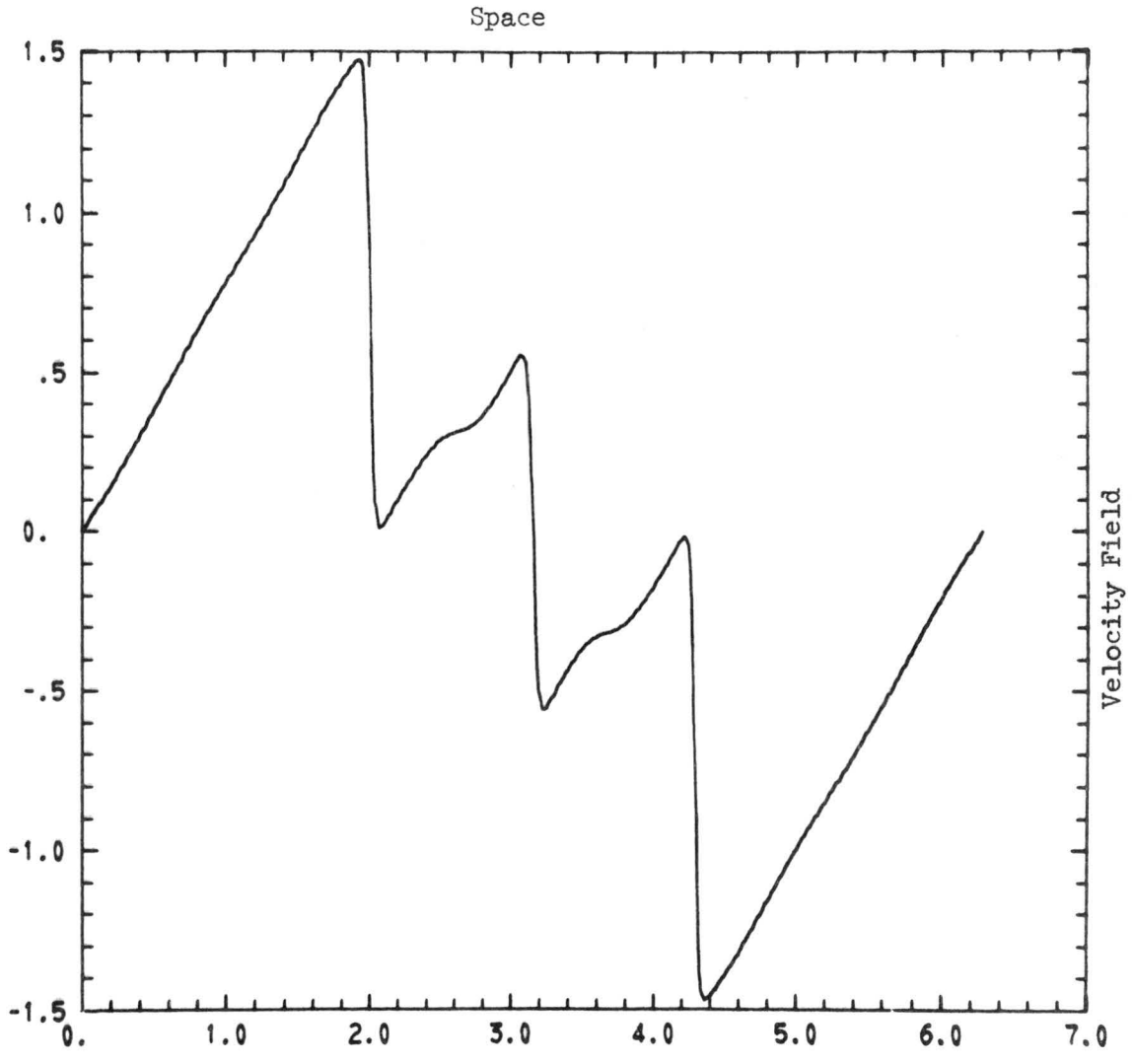

Figure 38. First realization in physical space at τ =.937.

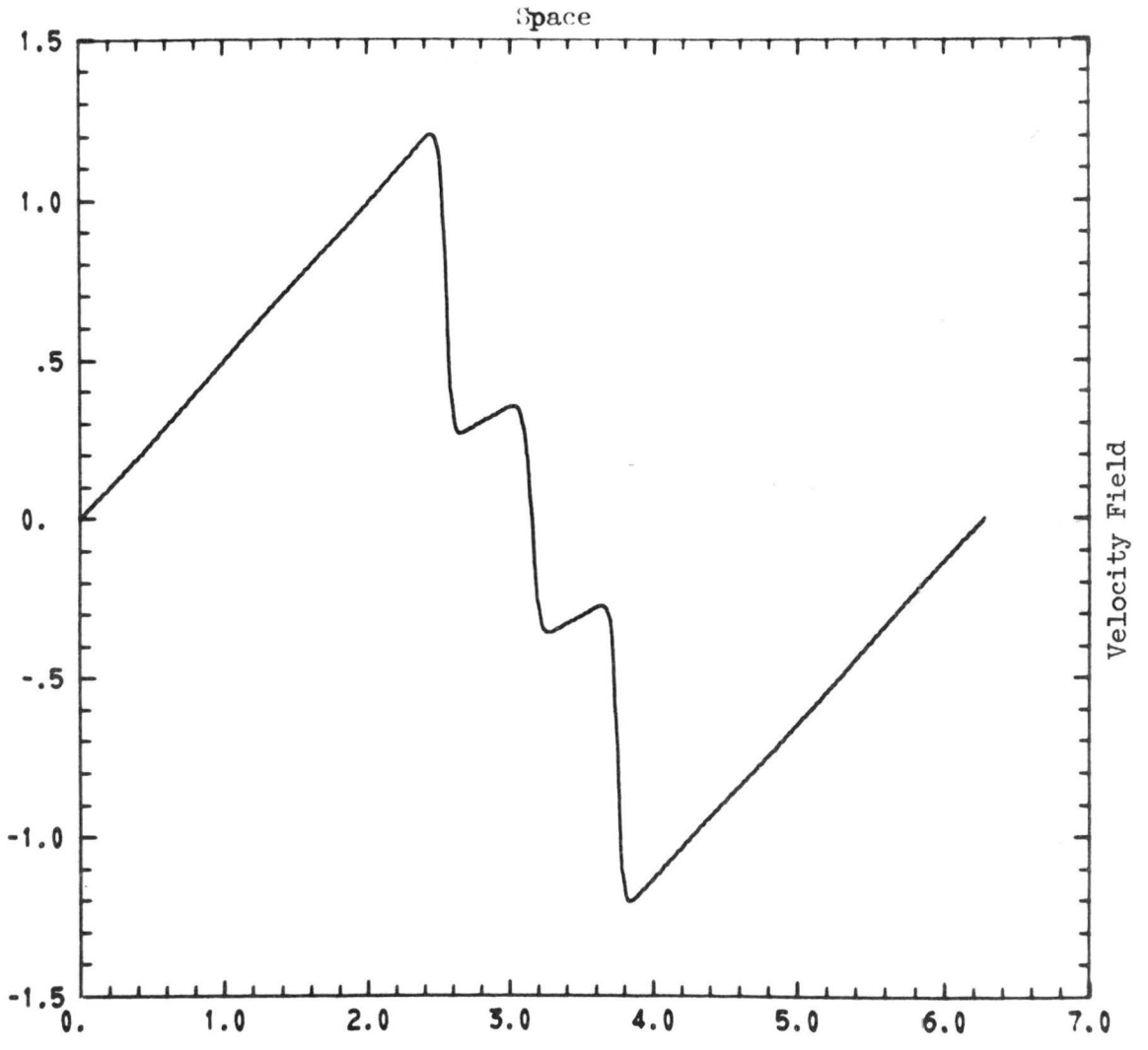

Figure 39. First realization in physical space at τ =1.669

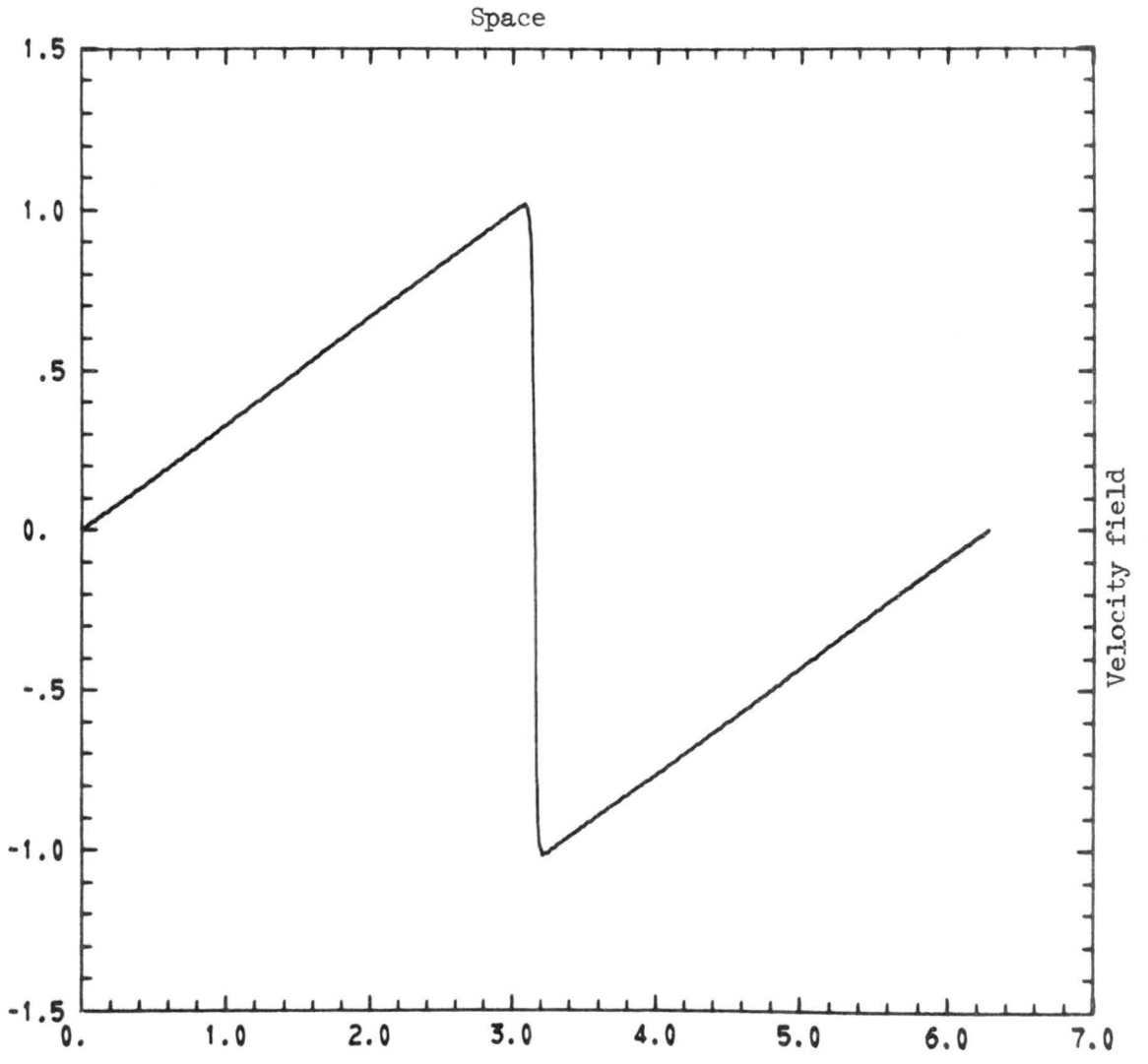

Figure 40. First realization in physical space at τ =2.664

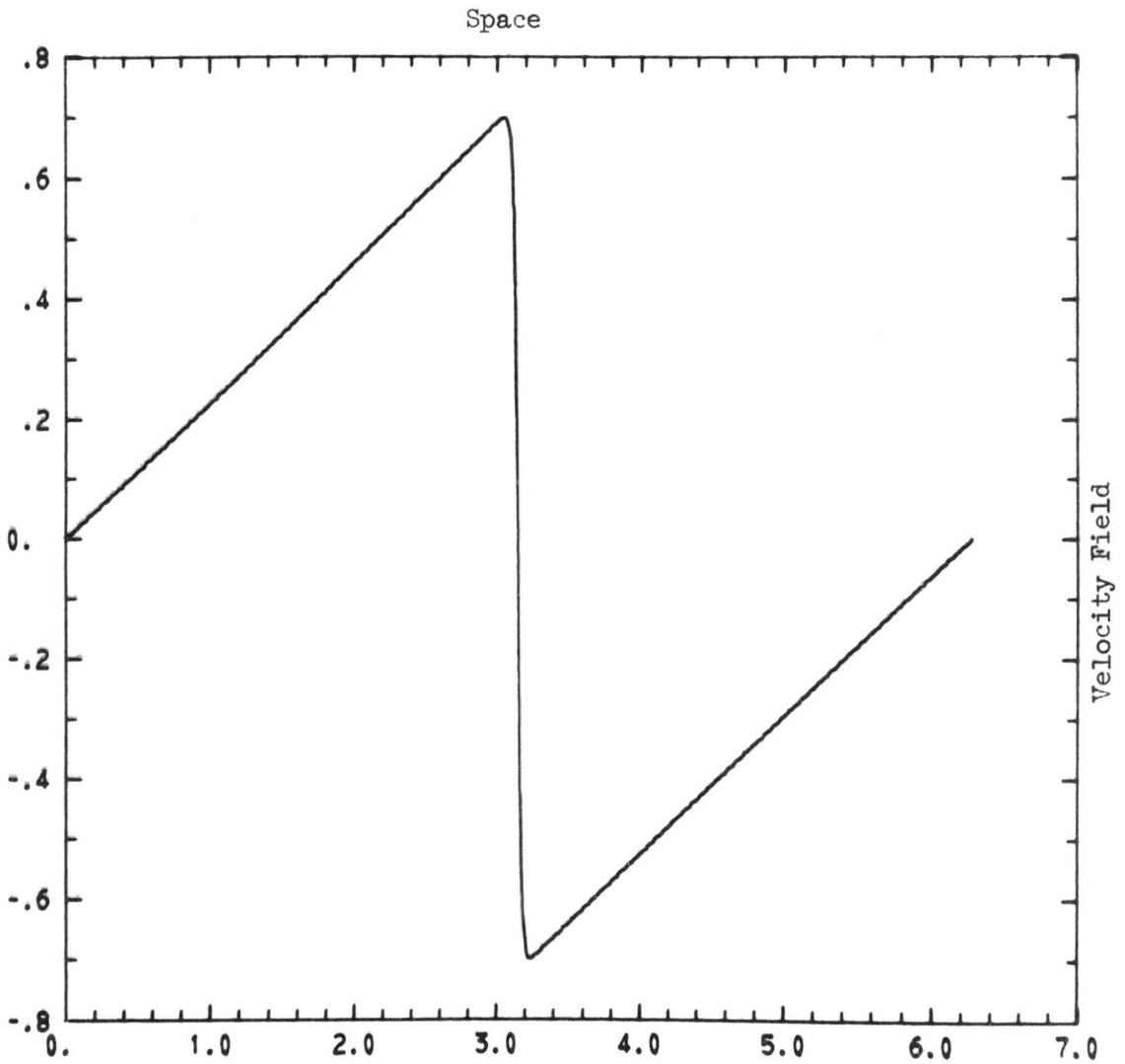

Figure 41. First realization in physical space at τ =4.014.

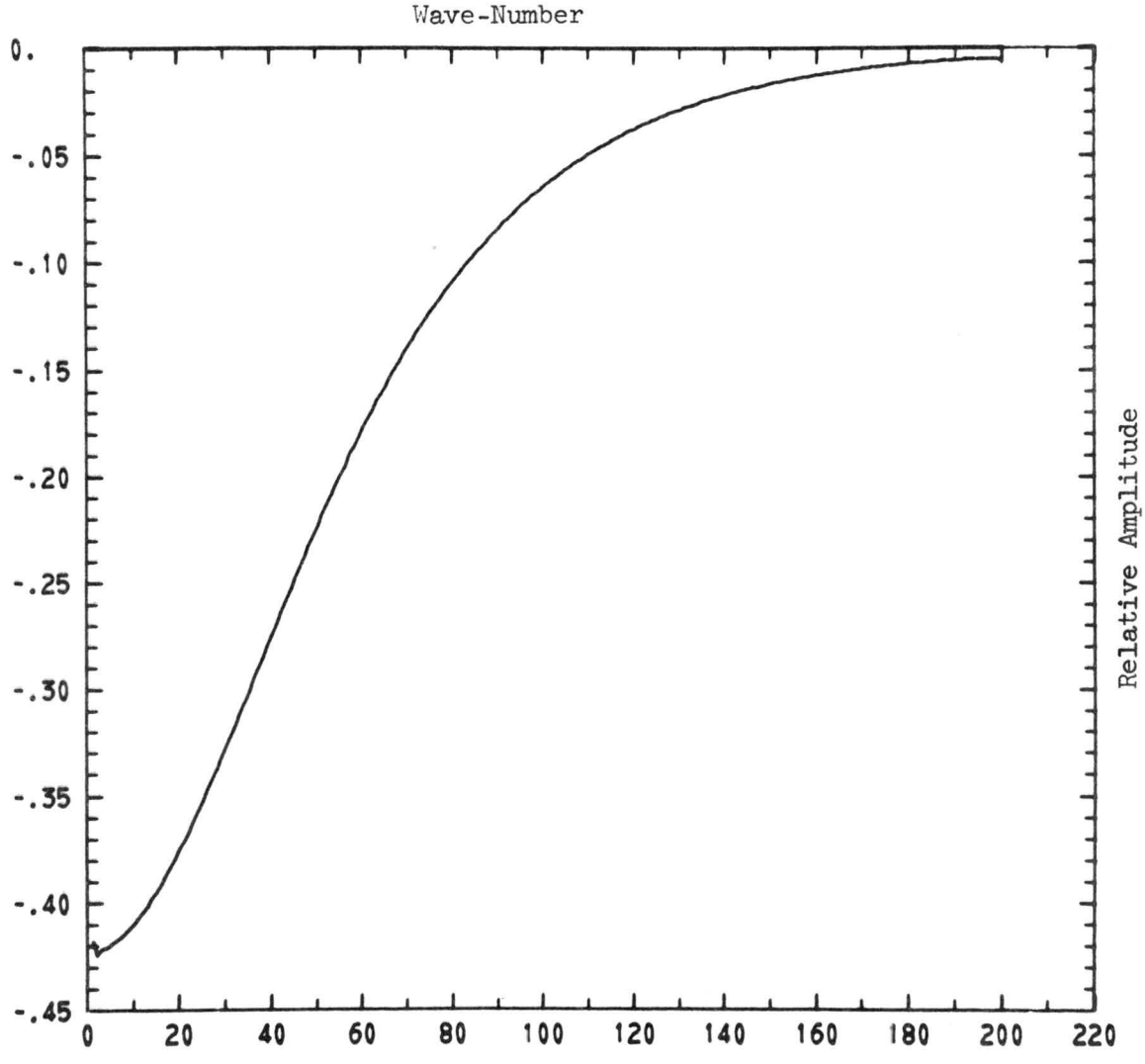

Figure 42. Second realization in Fourier space.

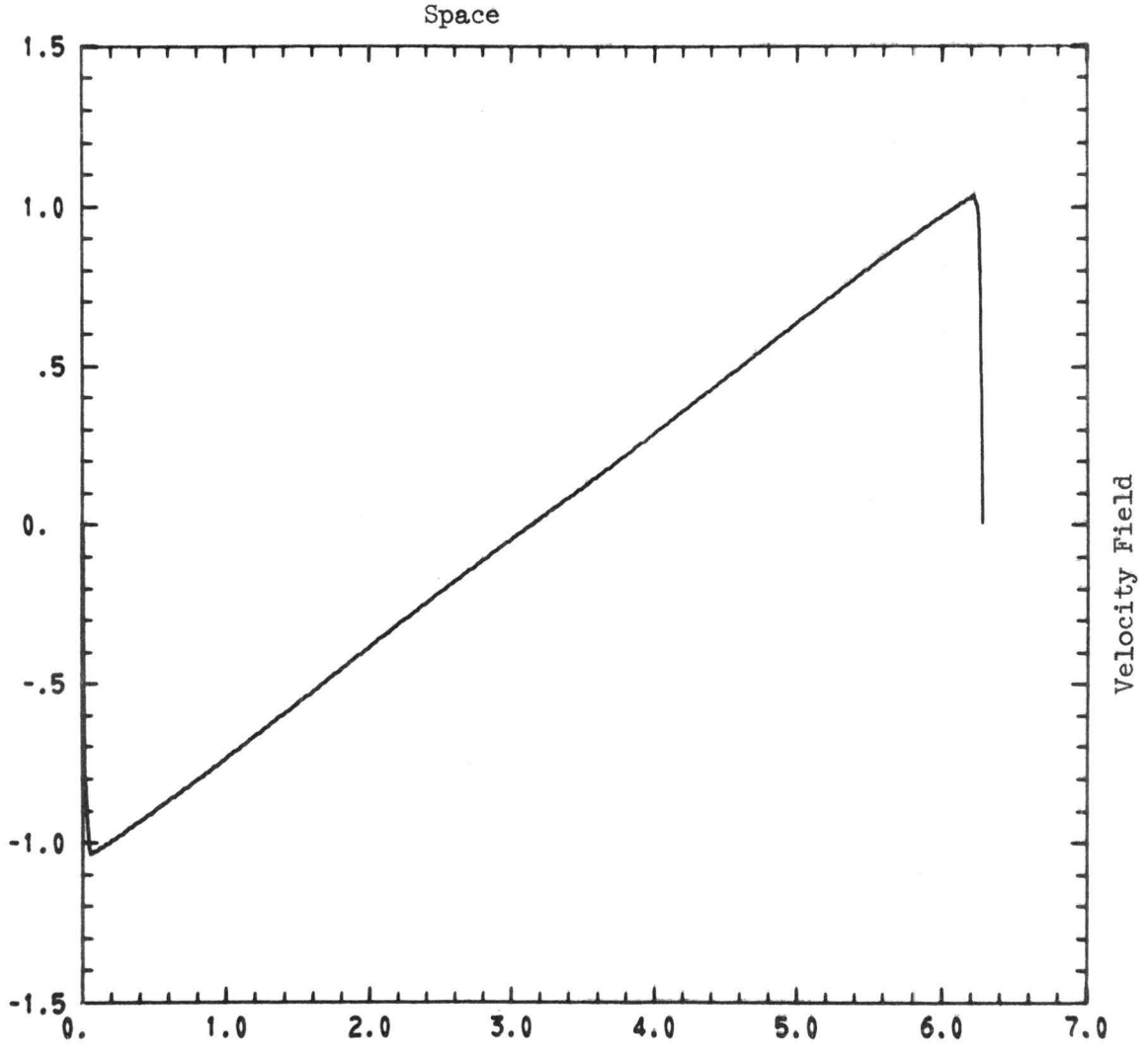

Figure 43. Second realization in physical space.

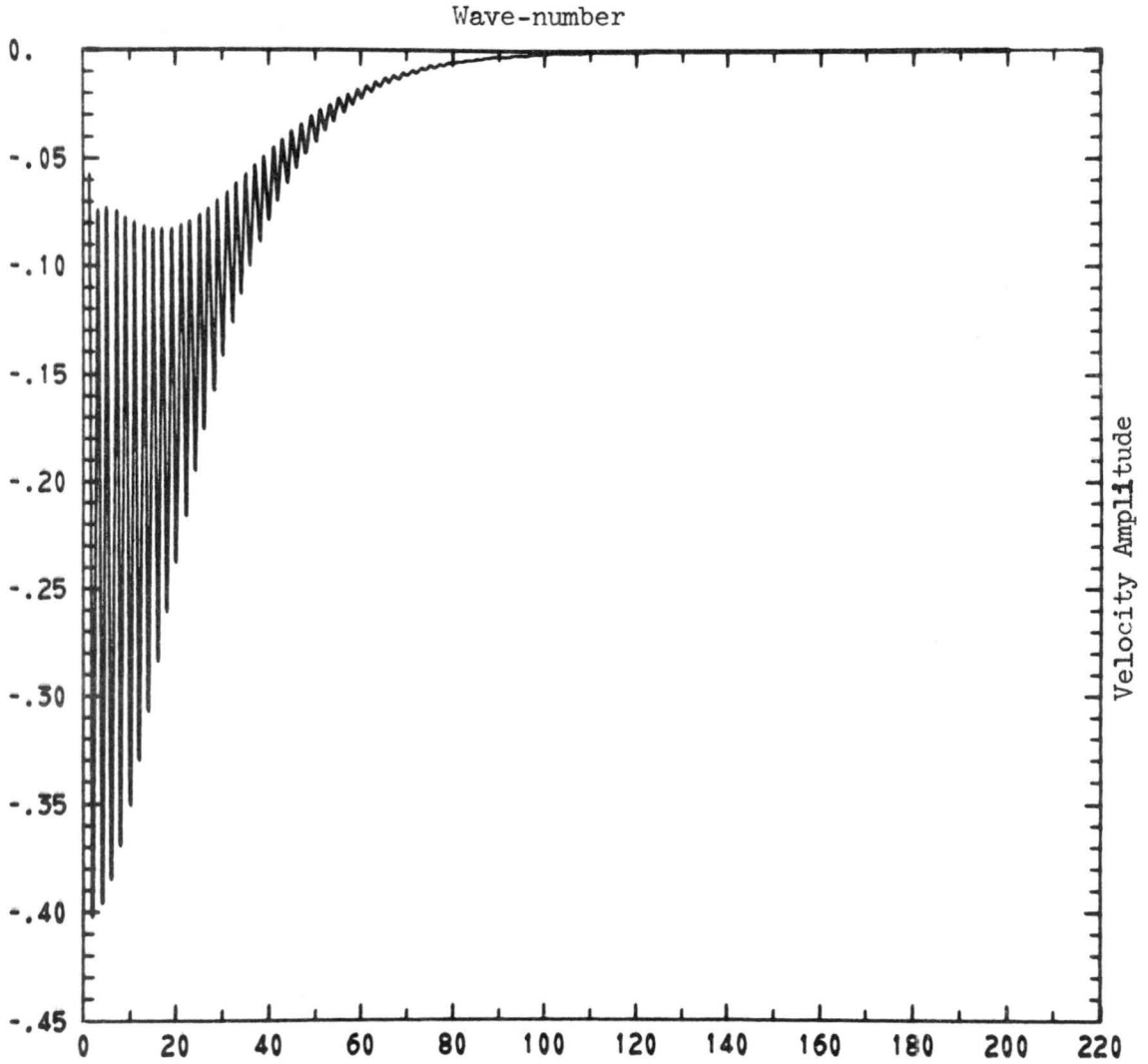

Figure 44. Third realization in Fourier space.

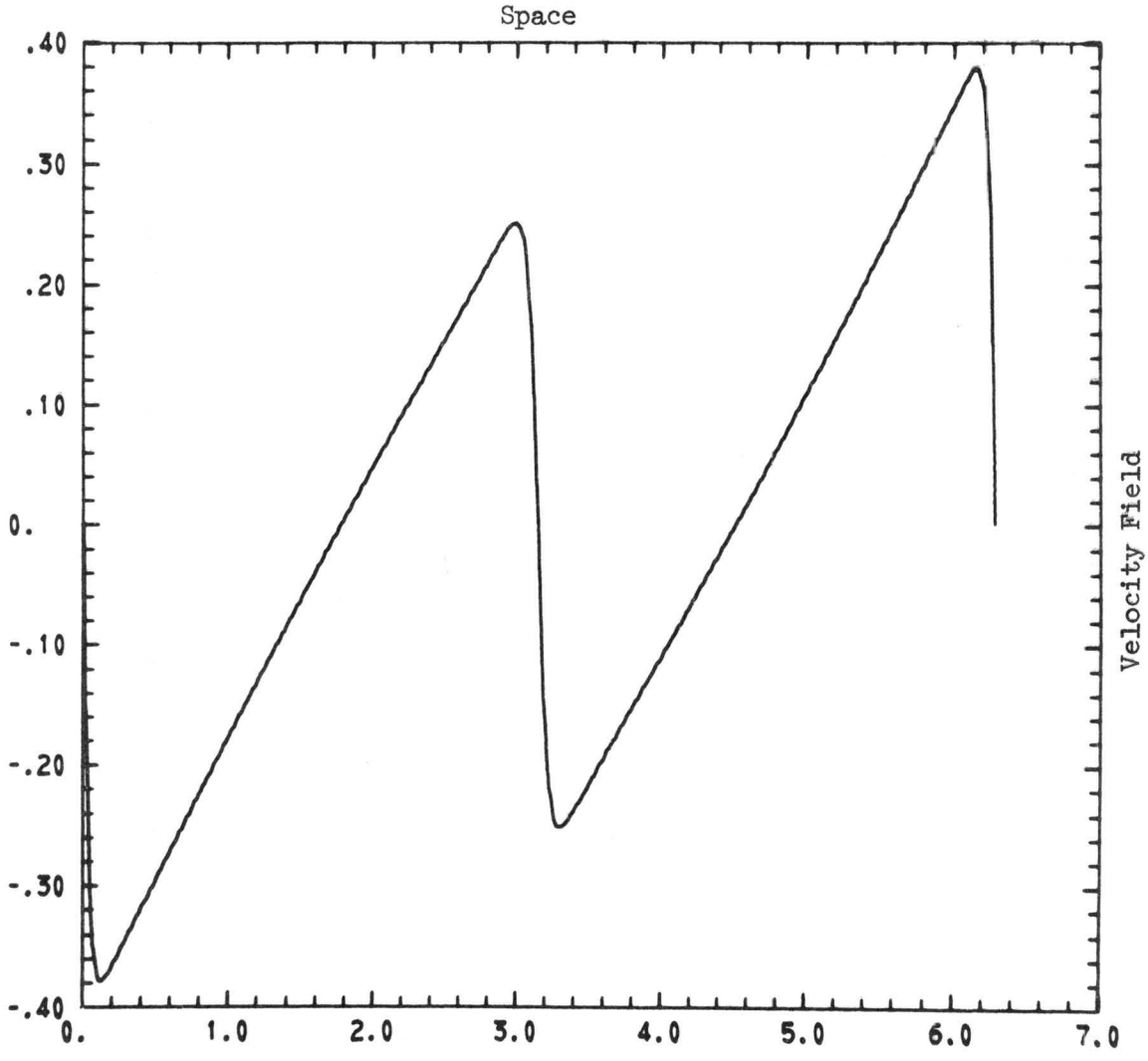

Figure 45. Third realization in physical space.

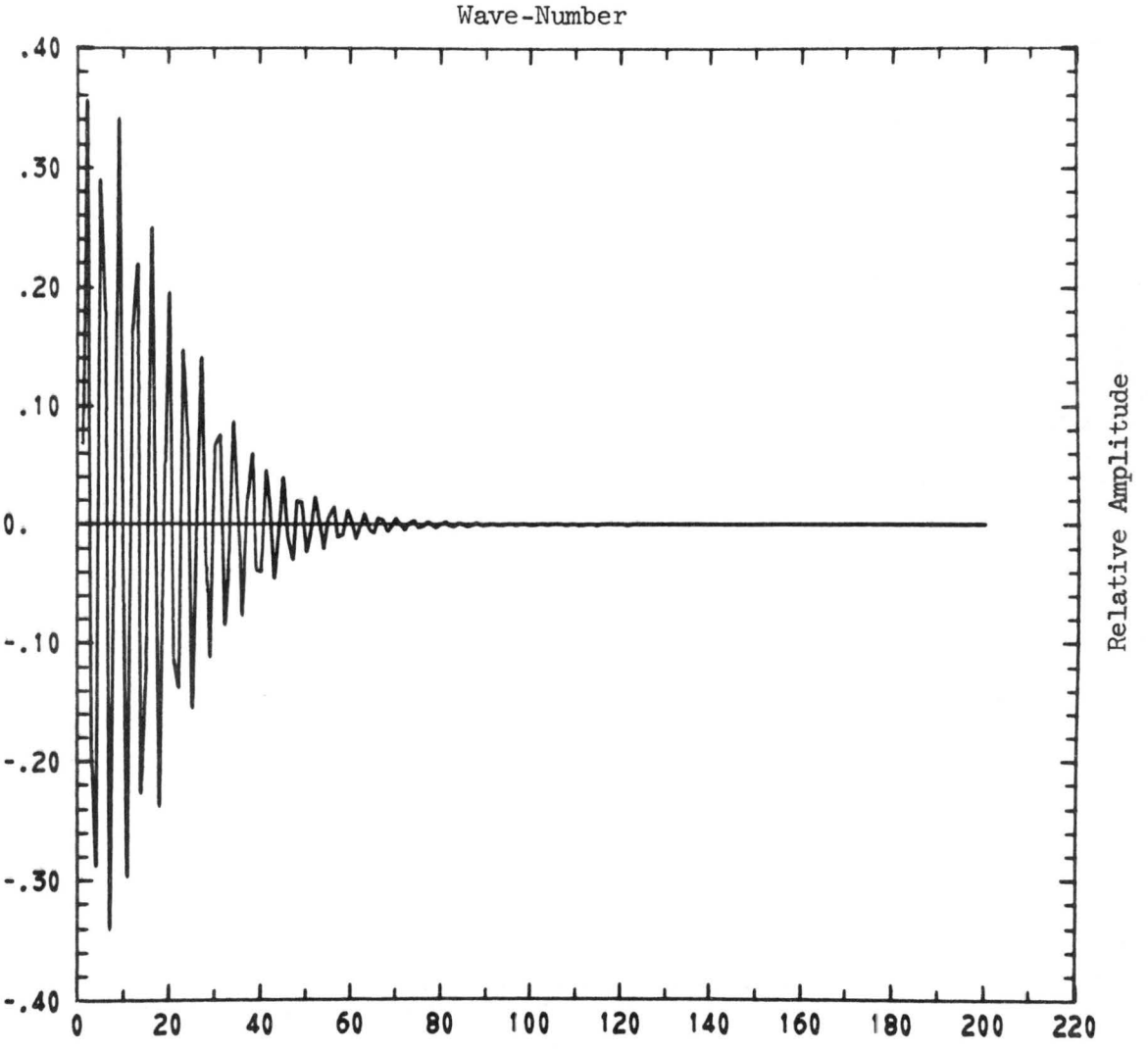

Figure 46. Fourth realization in Fourier space.

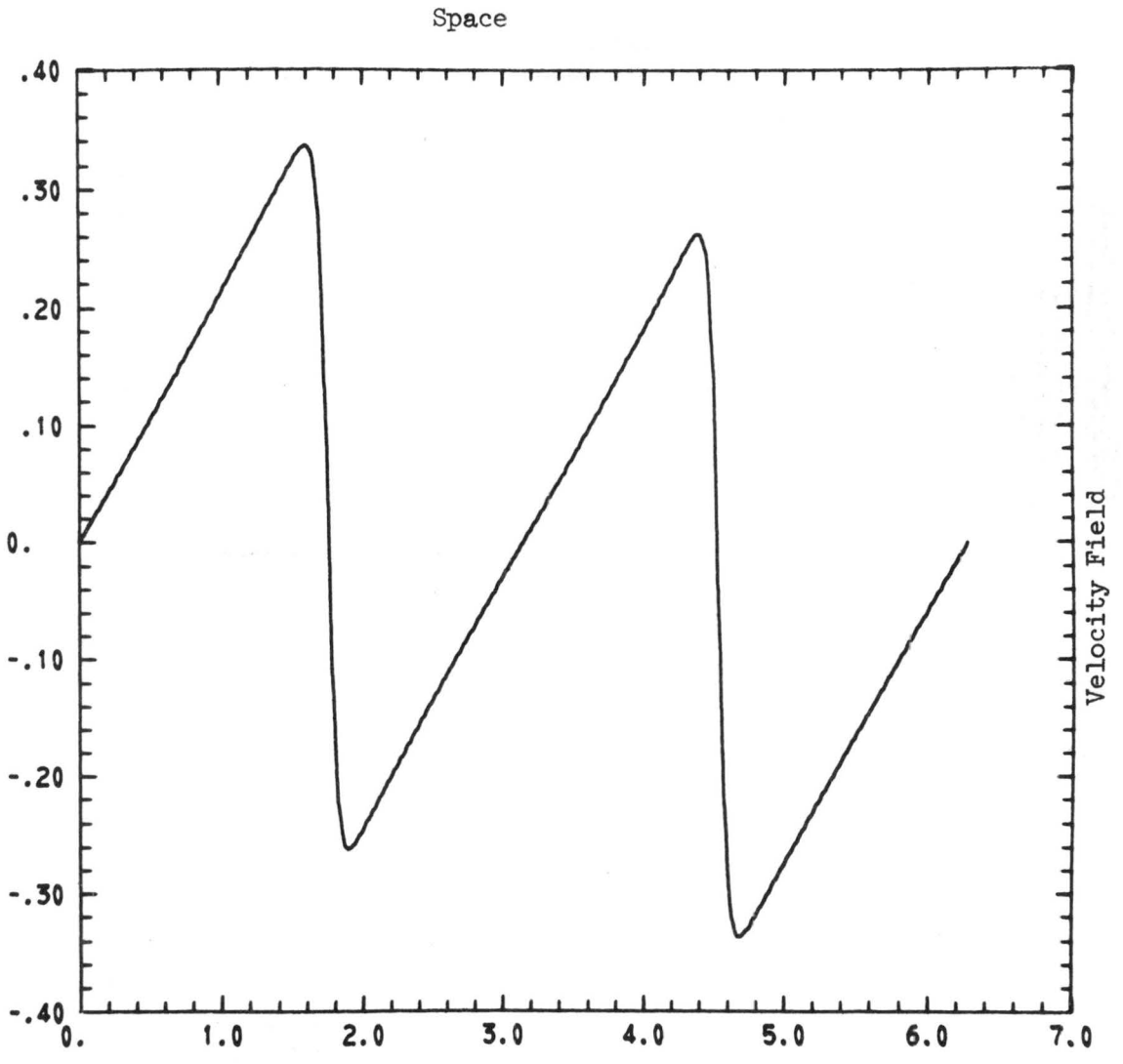

Figure 47. Fourth realization in physical space.

v(1,0)

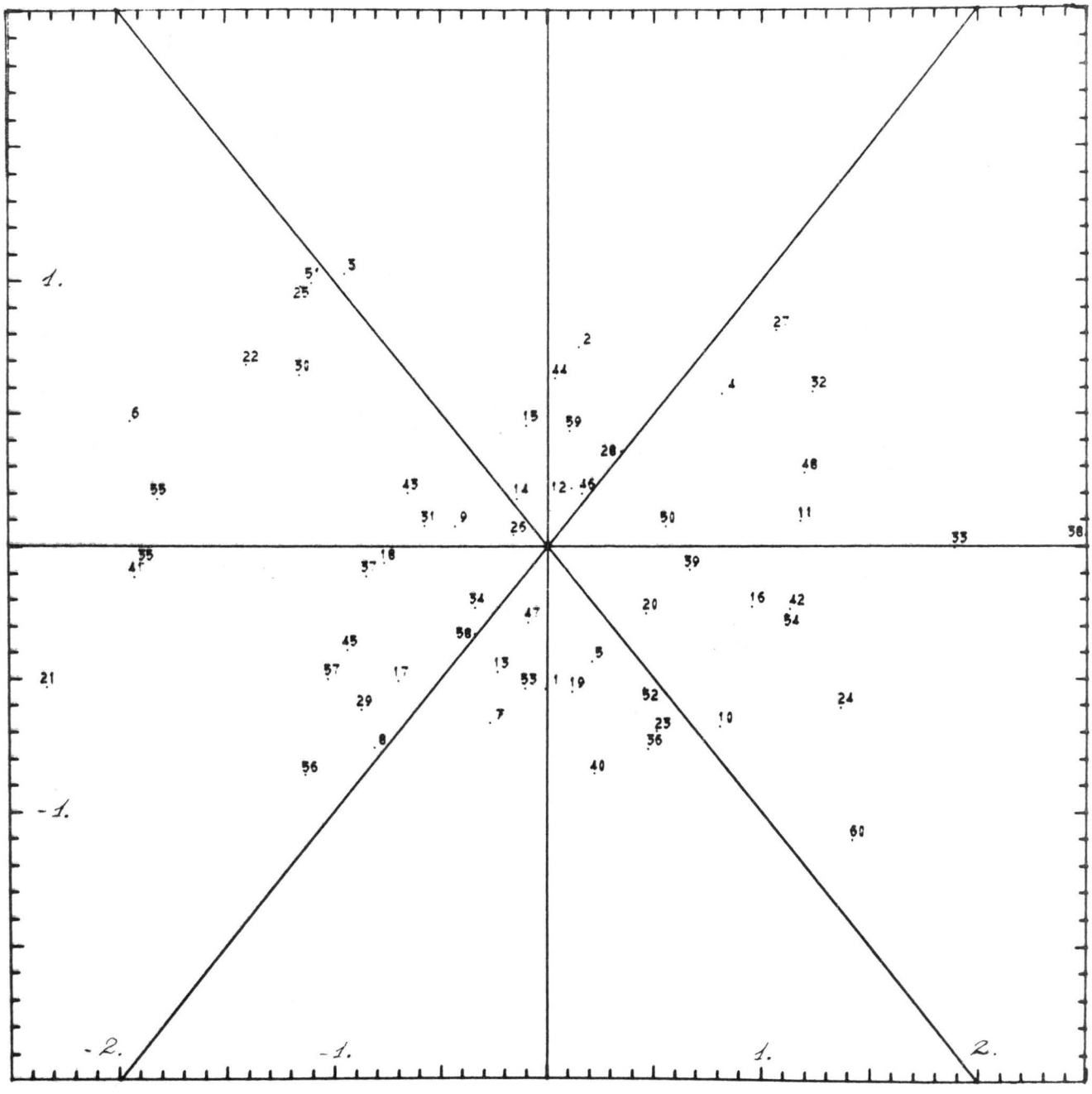

Fig. 48 - Distribution of the points (v(1,0), v(2,0)) for the 60 realizations.

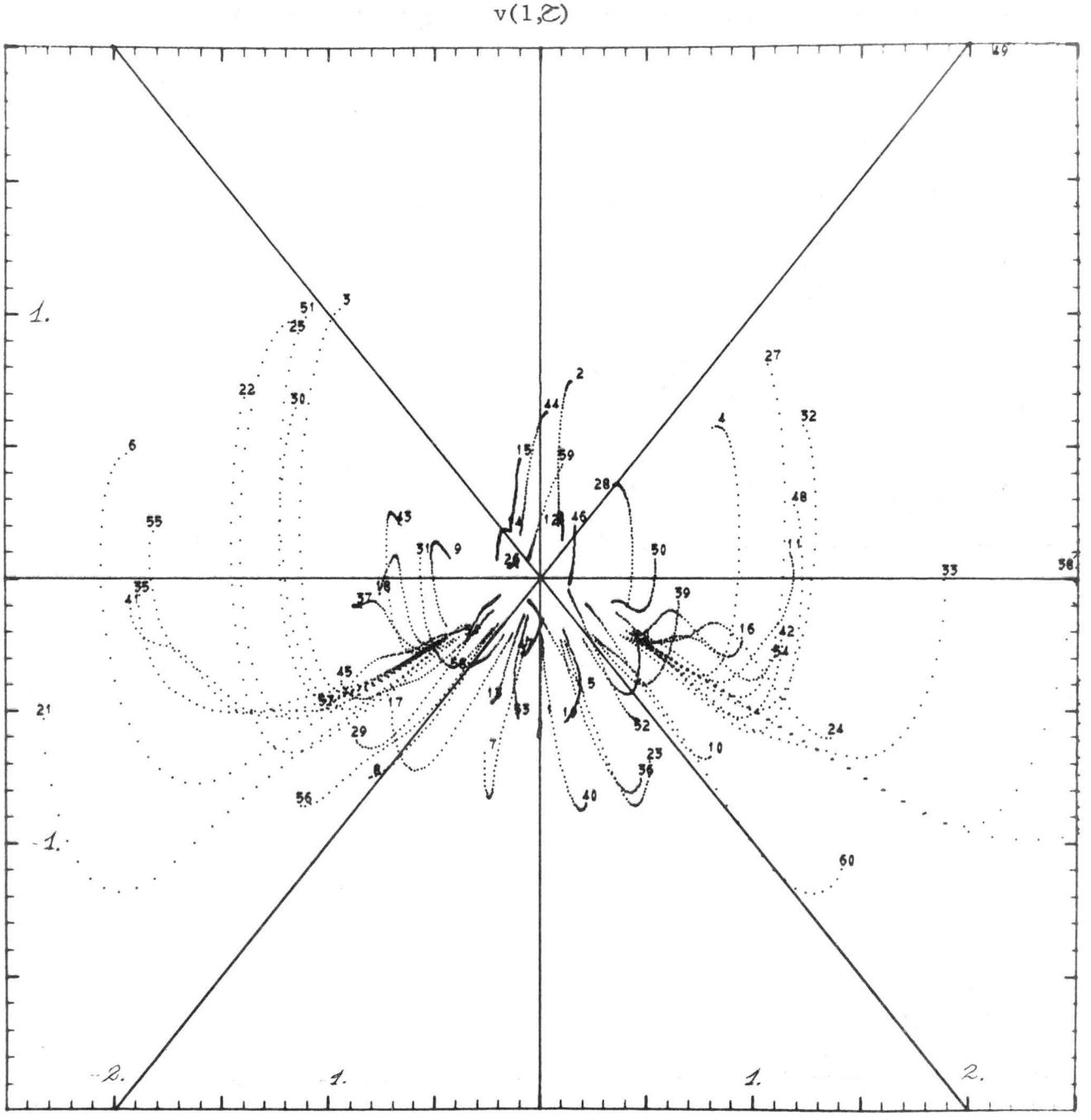

Fig. 49 - Trajectories of the point (v(1,τ), v(2,τ)) for the 60 realizations.

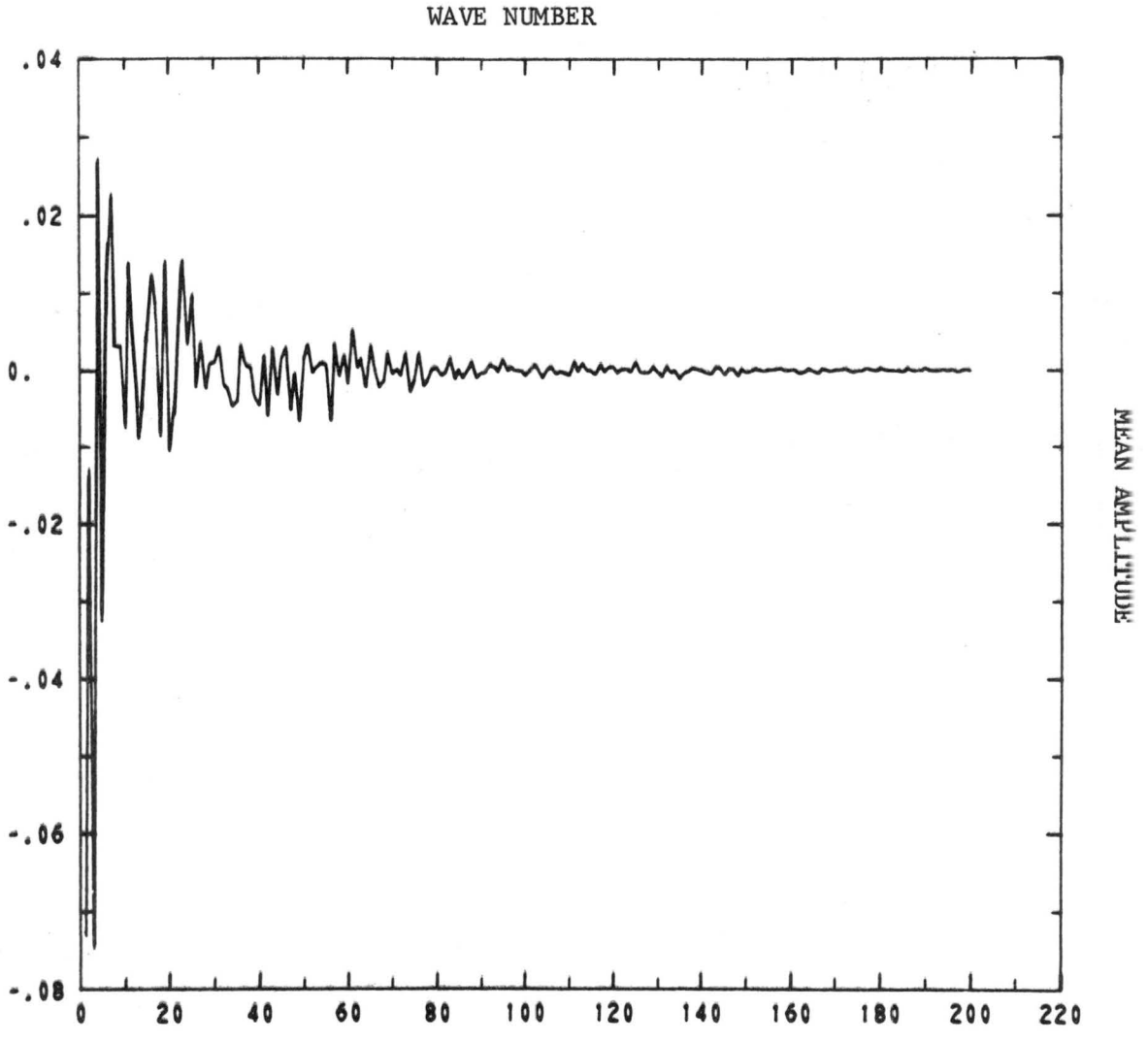

Fig. 50 - Mean amplitudes at time τ=0.

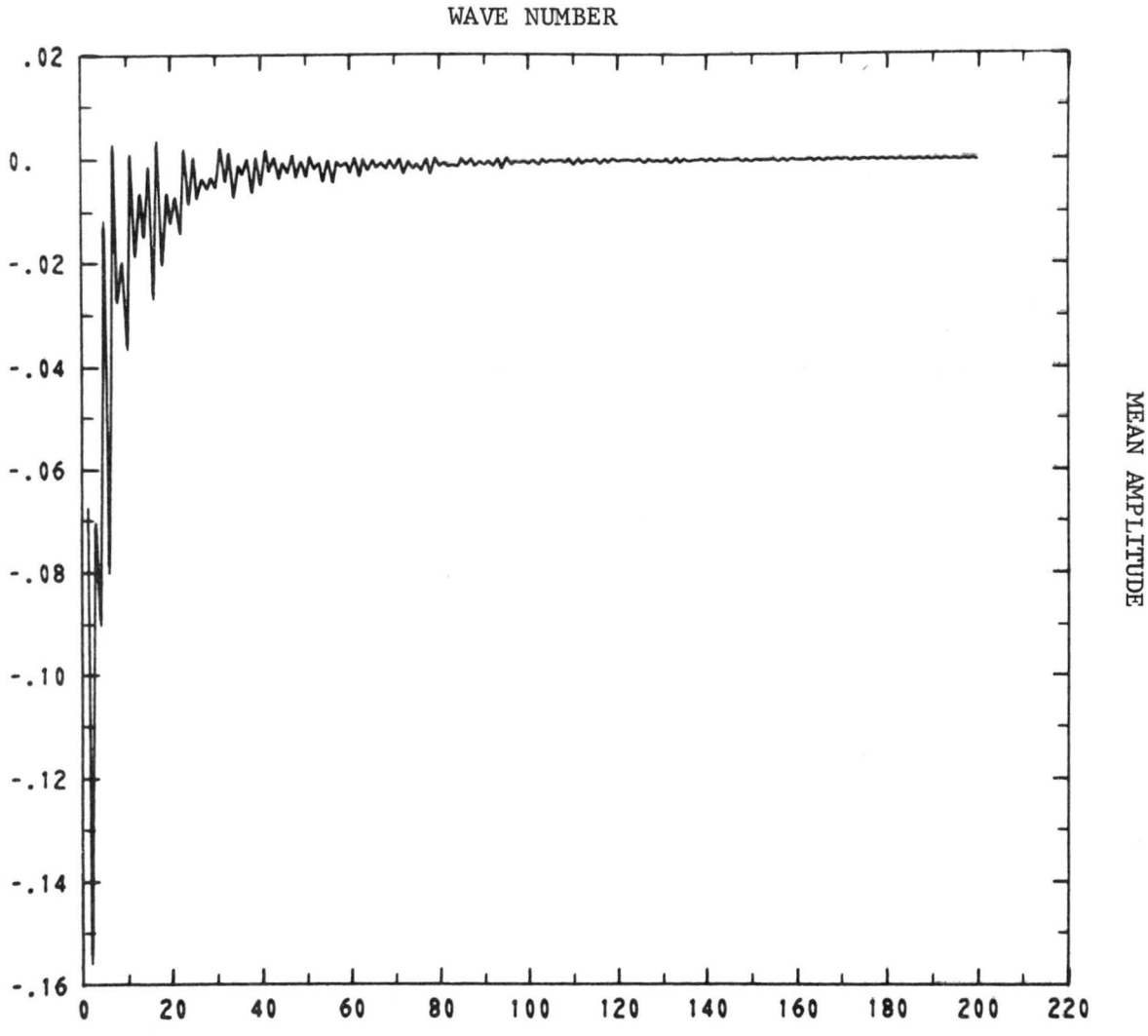

Fig. 51 - Mean amplitudes at time τ=.397

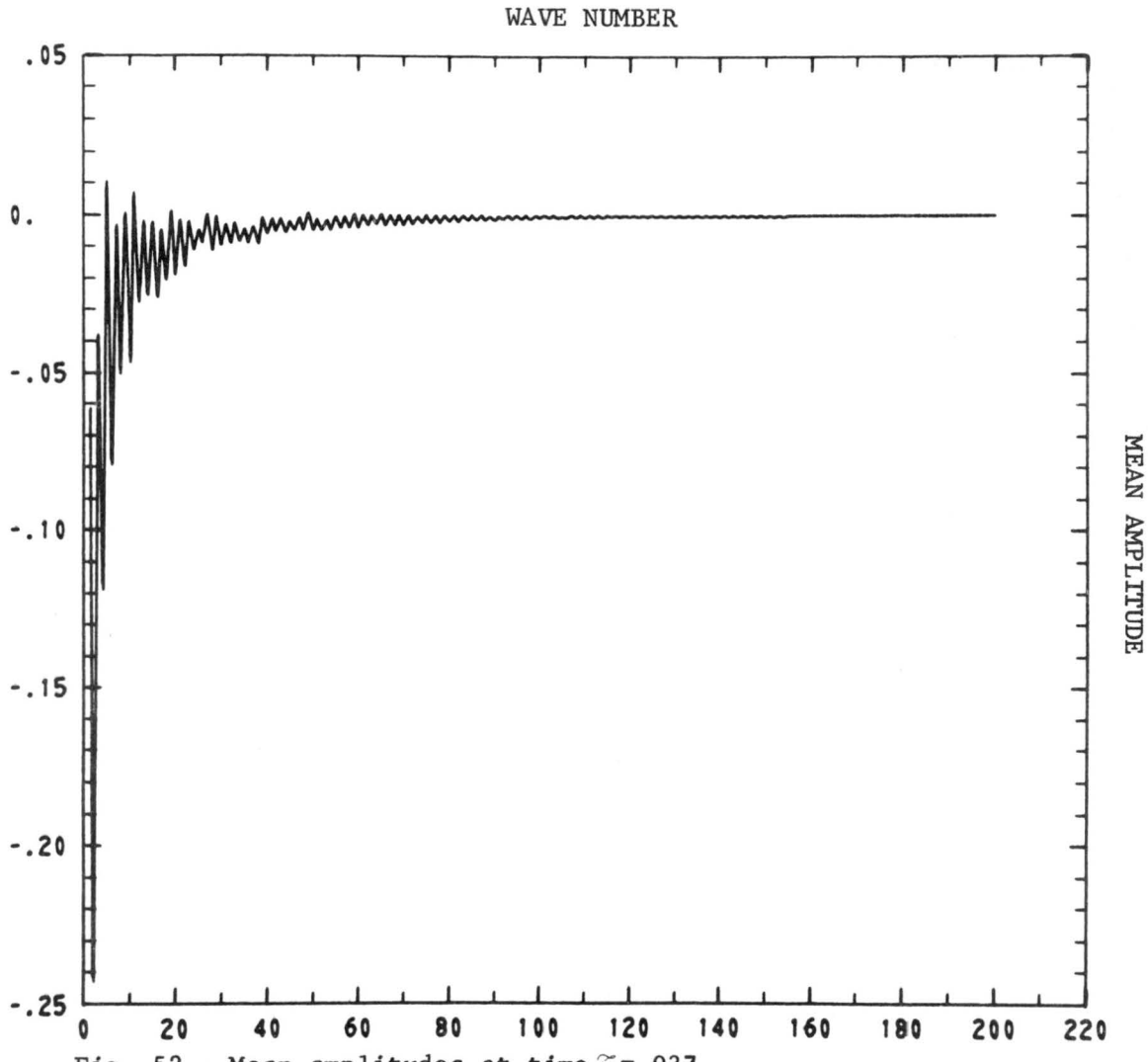

Fig. 52 - Mean amplitudes at time τ=.937

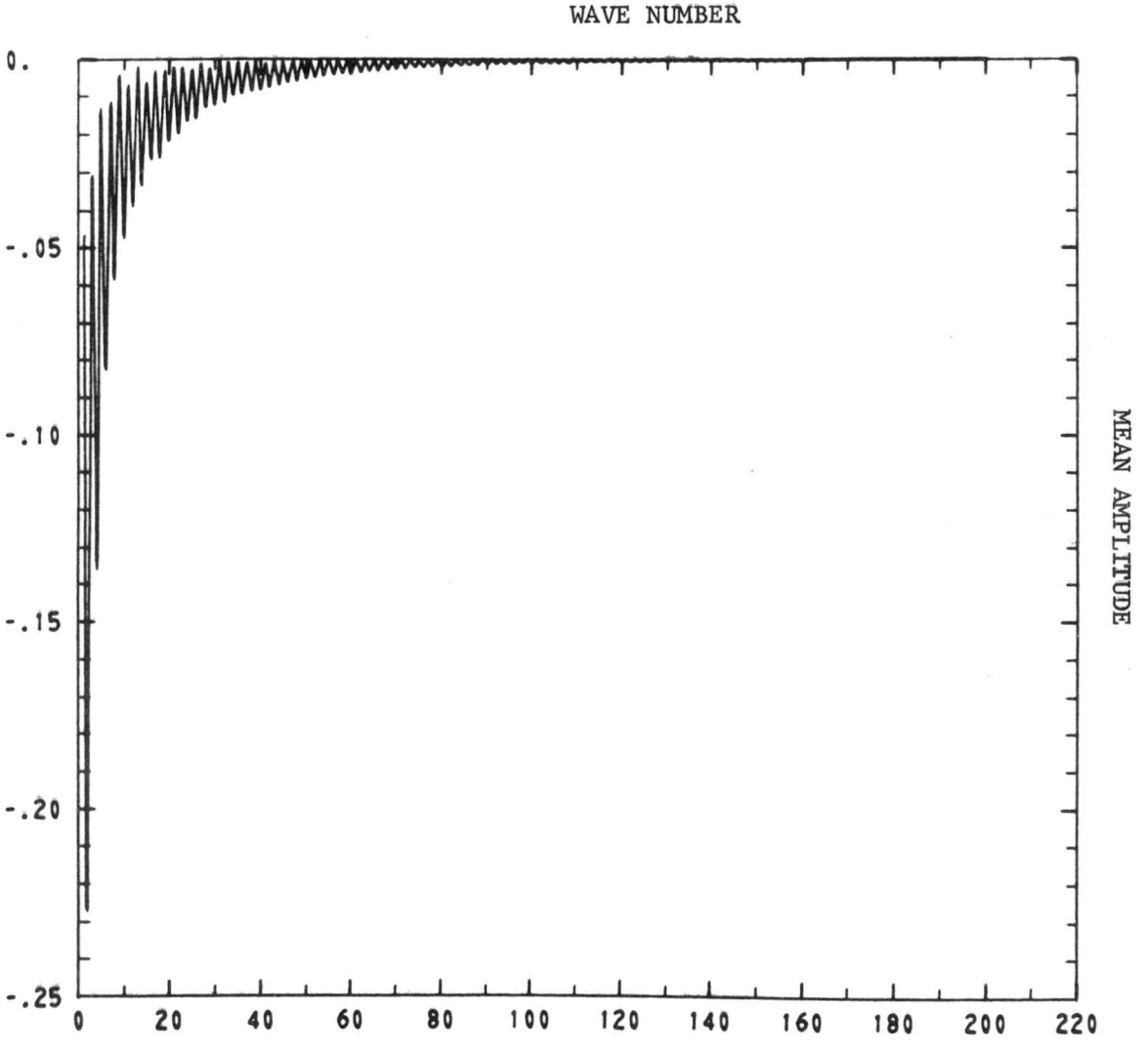

Fig. 53 - Mean amplitudes at time τ=1.669

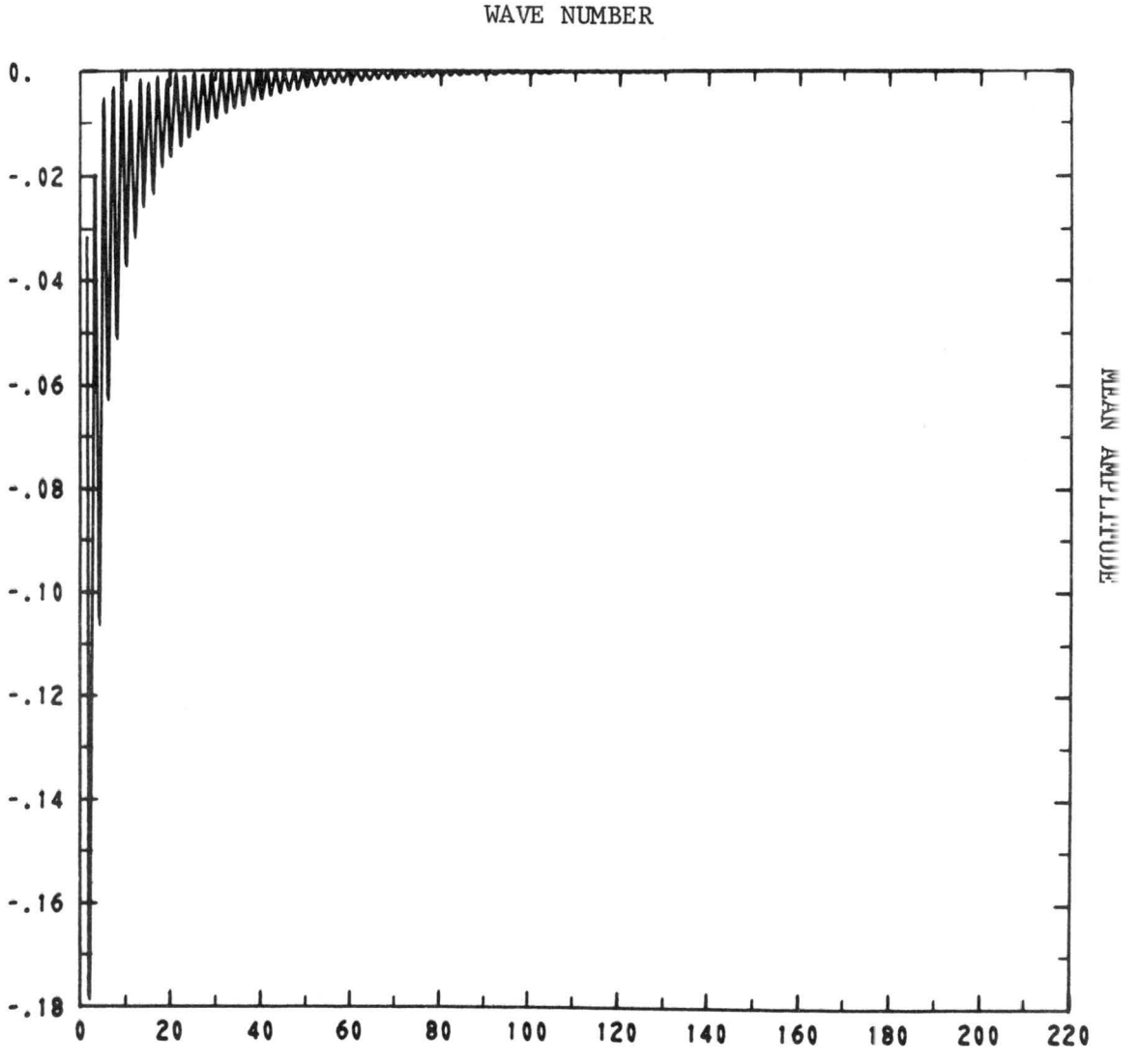

Fig. 54 - Mean amplitudes at time τ=2.664

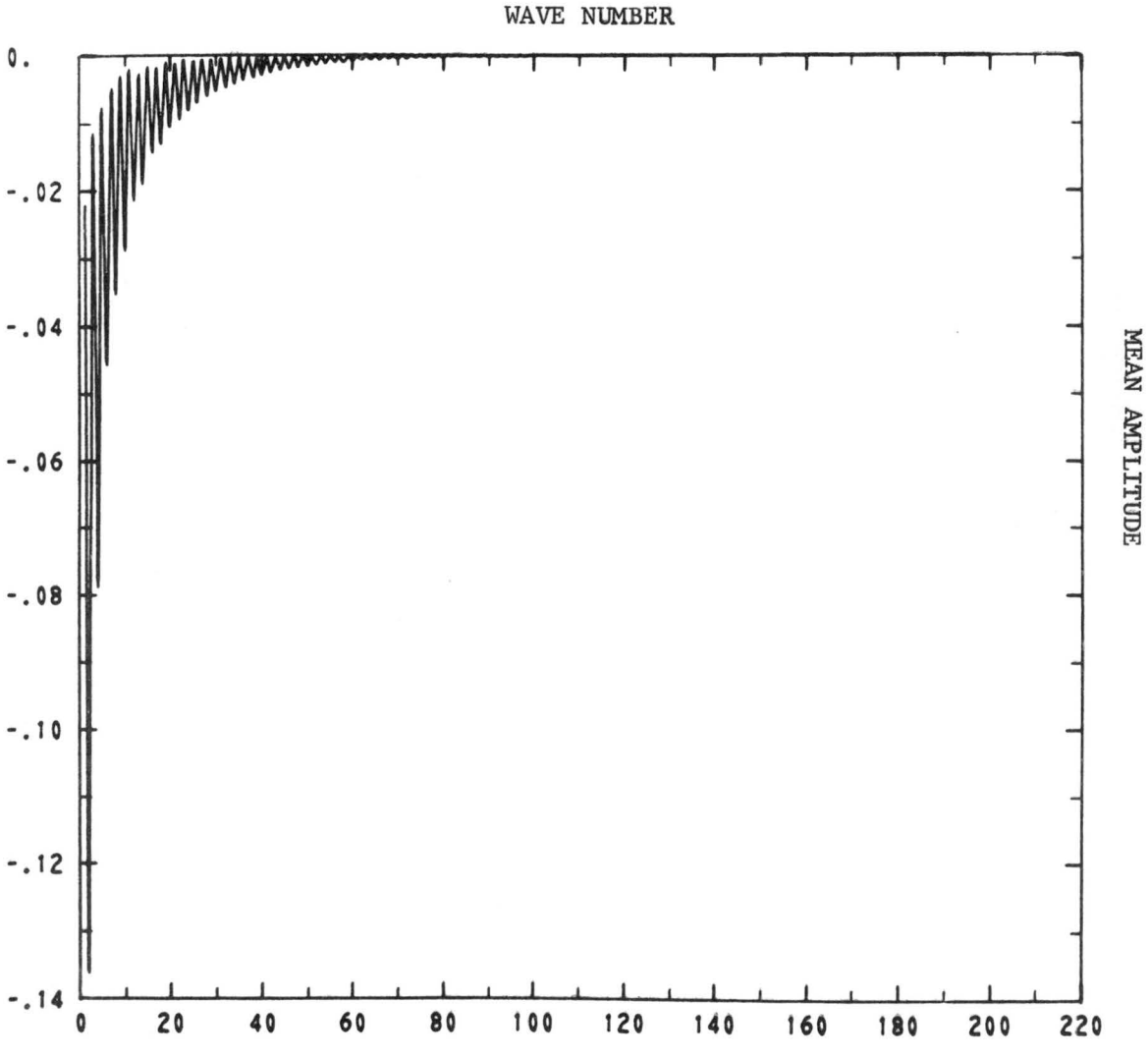

Fig. 55 - Mean amplitudes at time τ=4.014

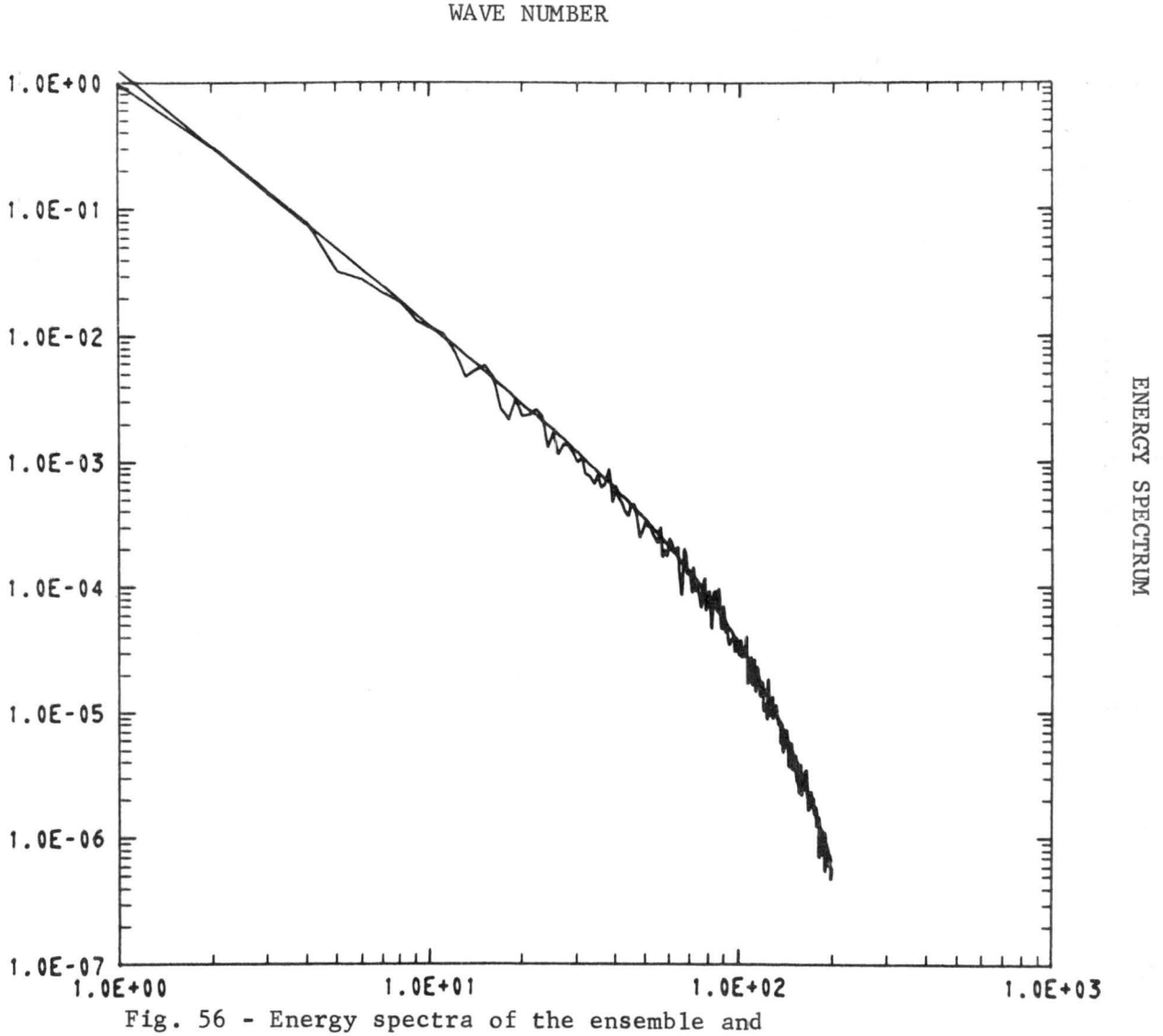

Fig. 56 - Energy spectra of the ensemble and of the reference solution at $t=0$.

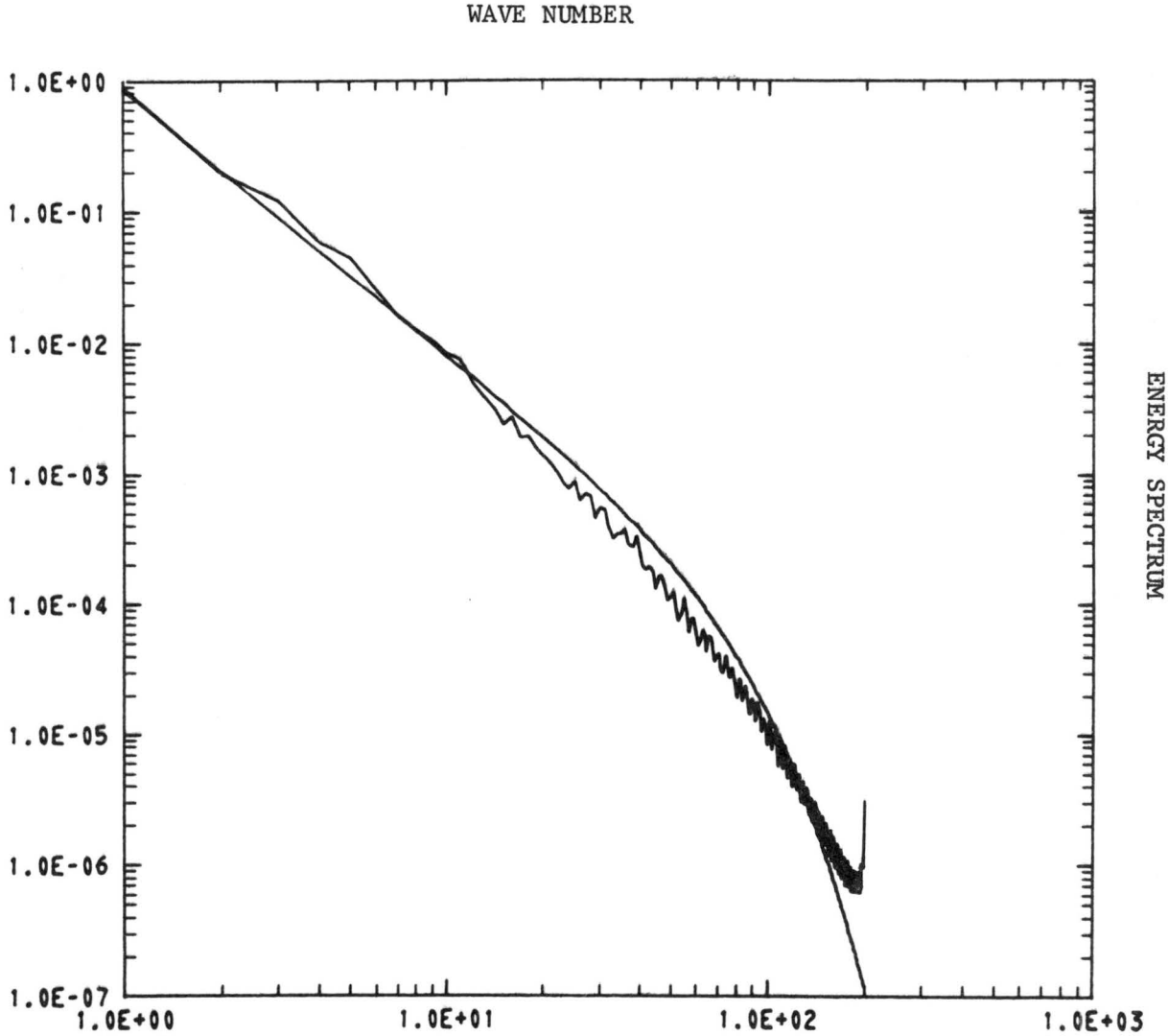

Fig. 57 - Energy specta of the ensemble and of the reference solution at τ=.397

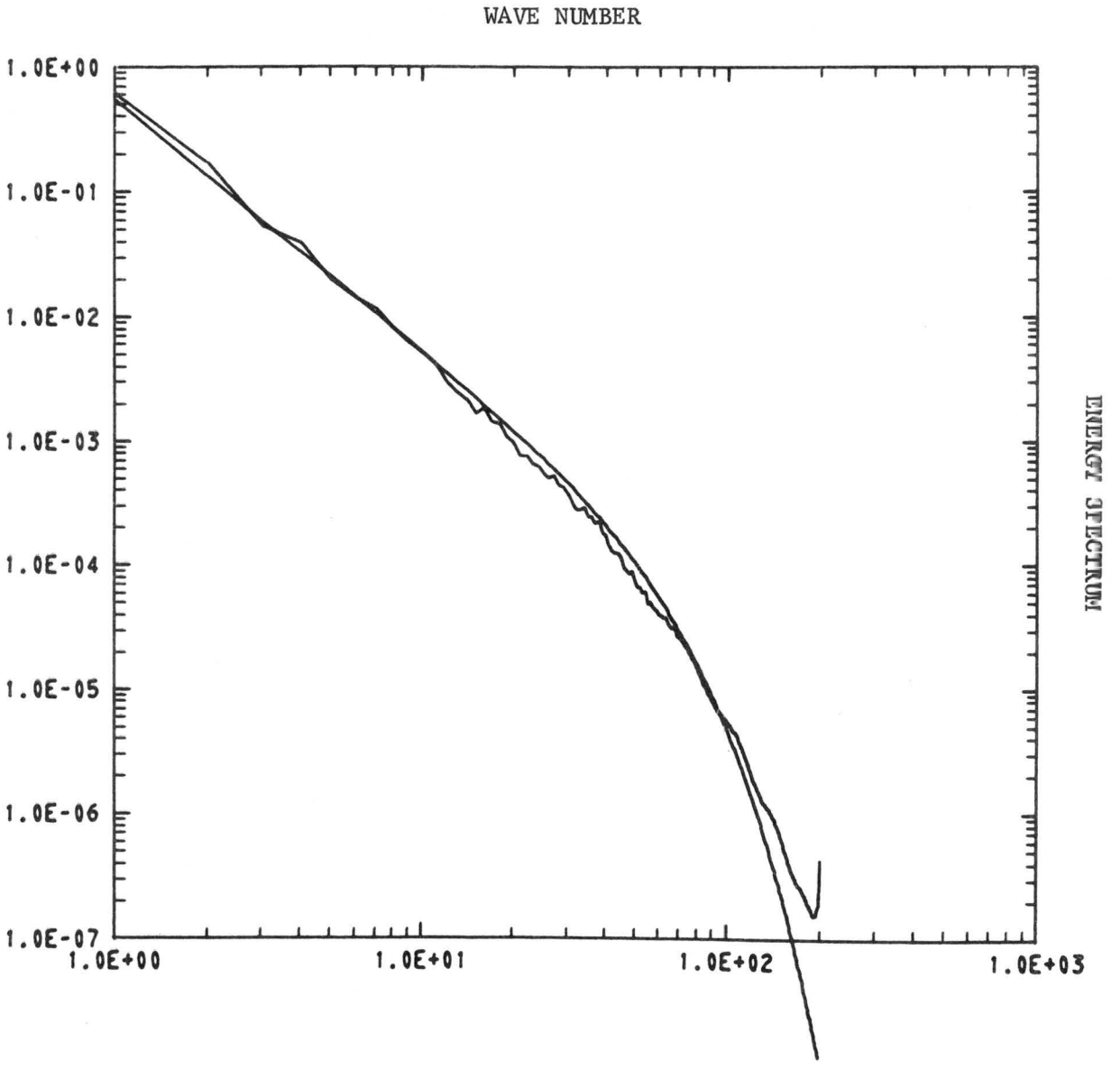

Fig. 58 - Energy spectra of the ensemble and of the reference solution at $\tau = .937$

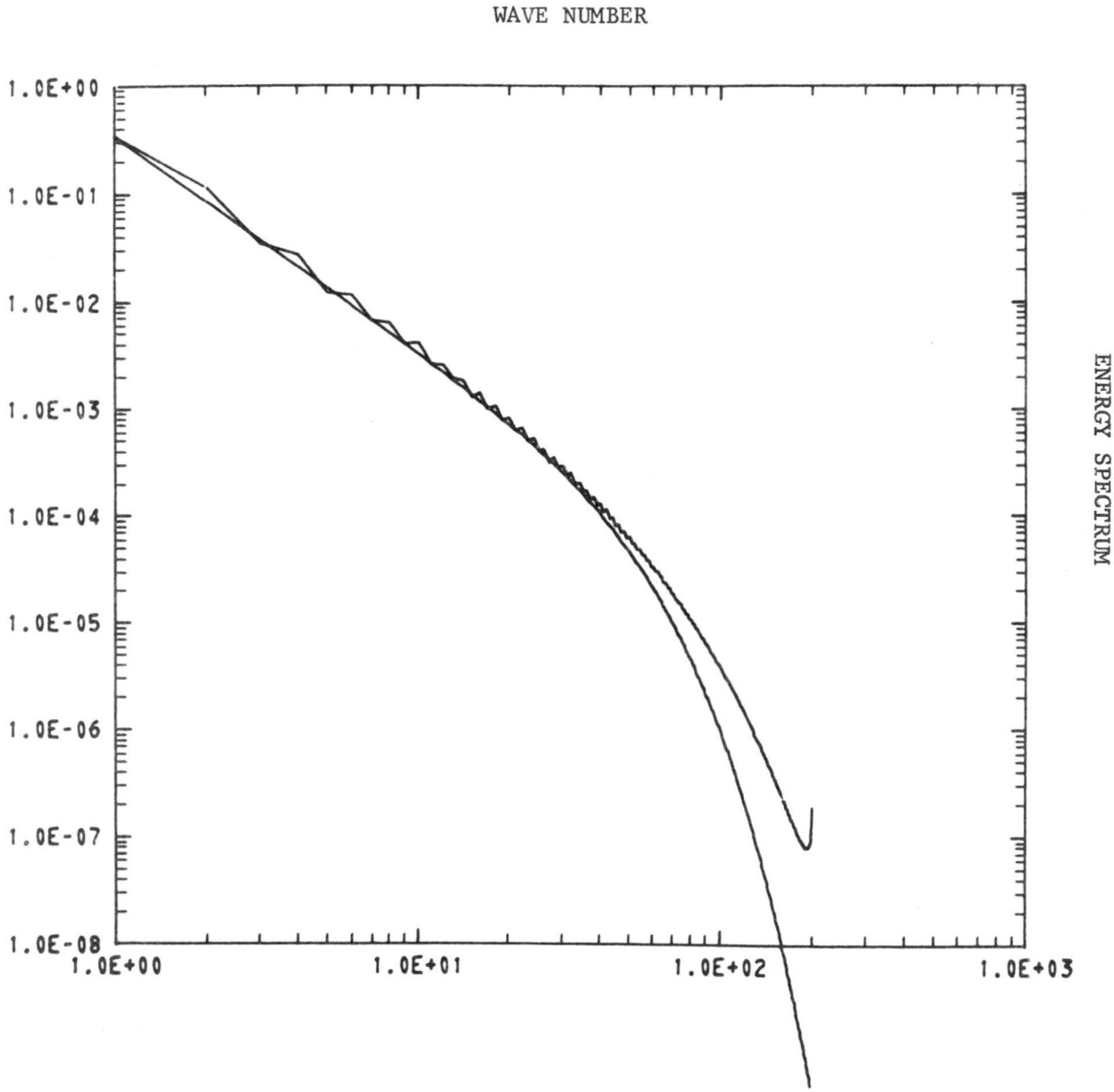

Fig. 59 - Energy spectra of the ensemble and of the reference solution at τ=1.669

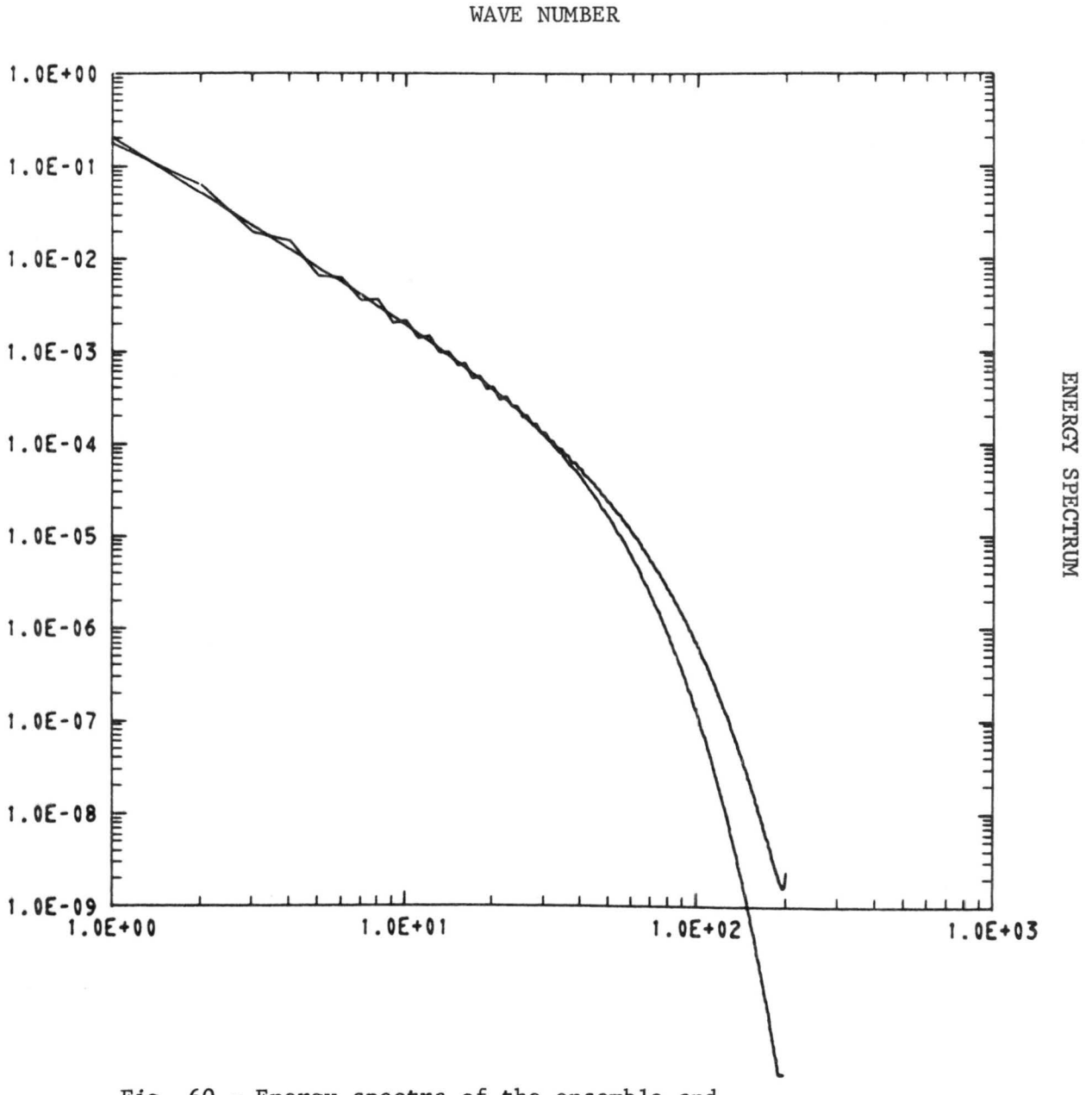

Fig. 60 - Energy spectra of the ensemble and of the reference solution at $t = 2.664$

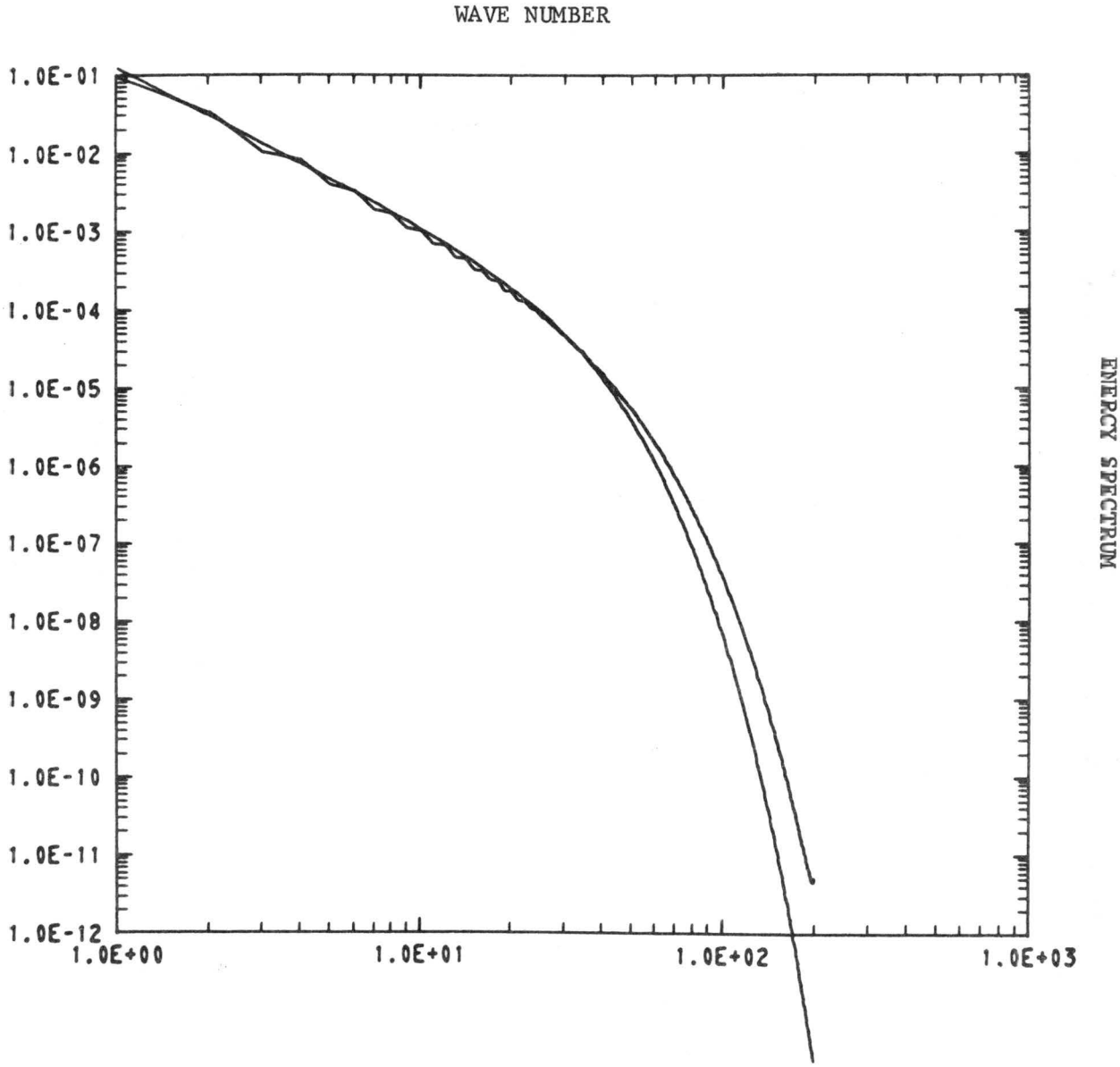

Fig. 61 - Energy spectra of the ensemble and of the reference solution at τ=4.014

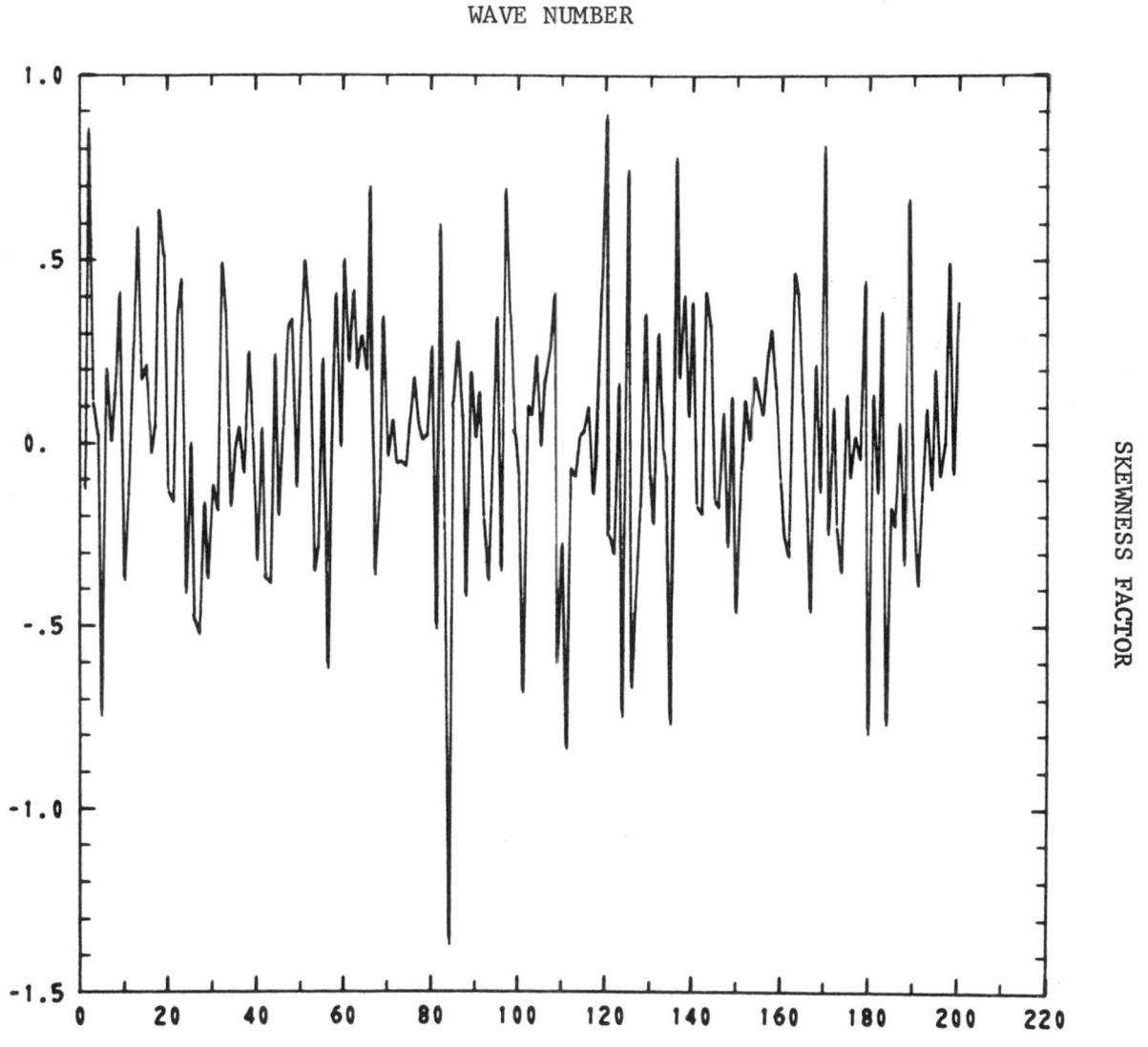

Fig. 62 - Skewness factors at time τ=0.

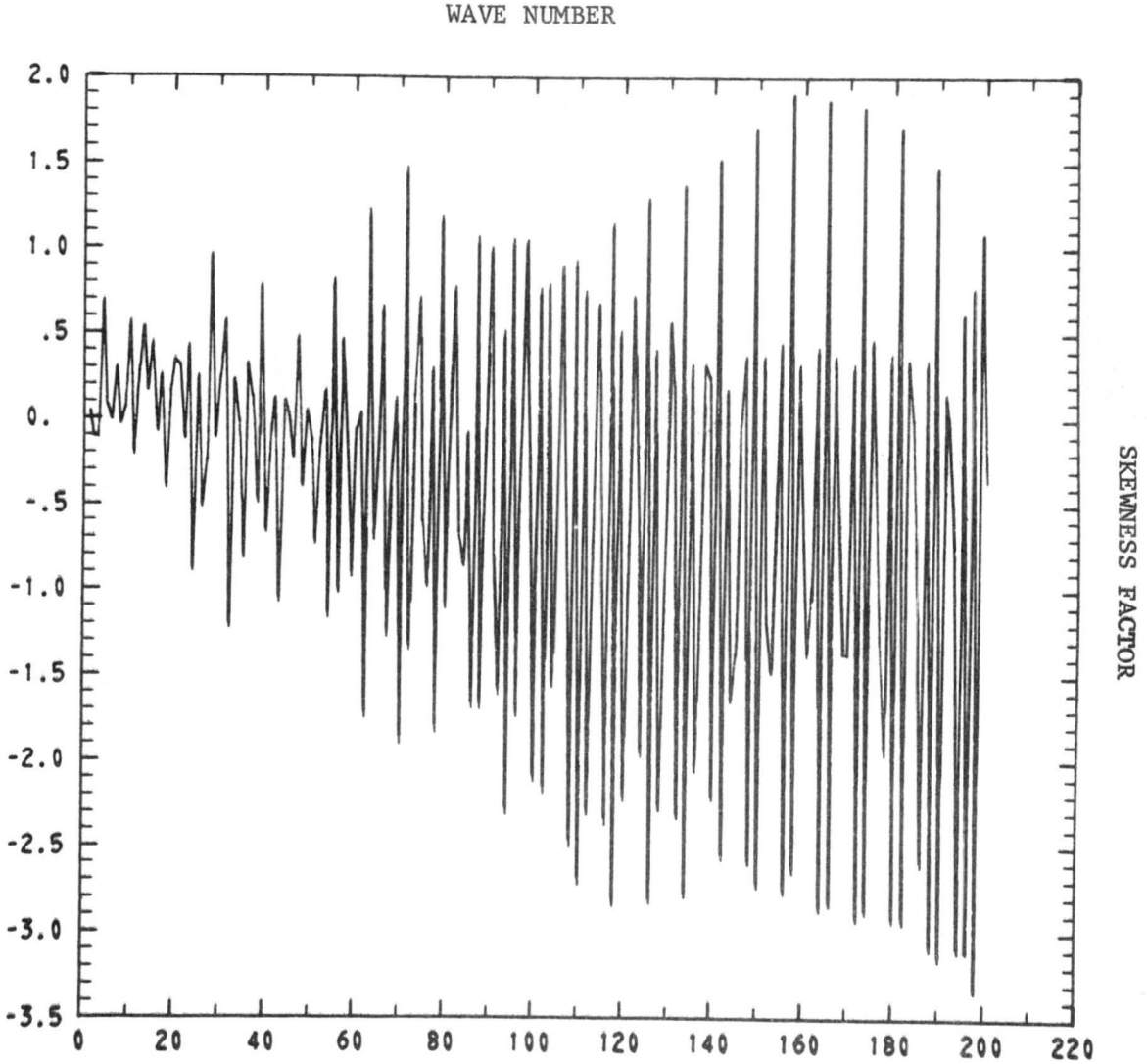

Fig. 63 - Skewness factors at time τ=.397

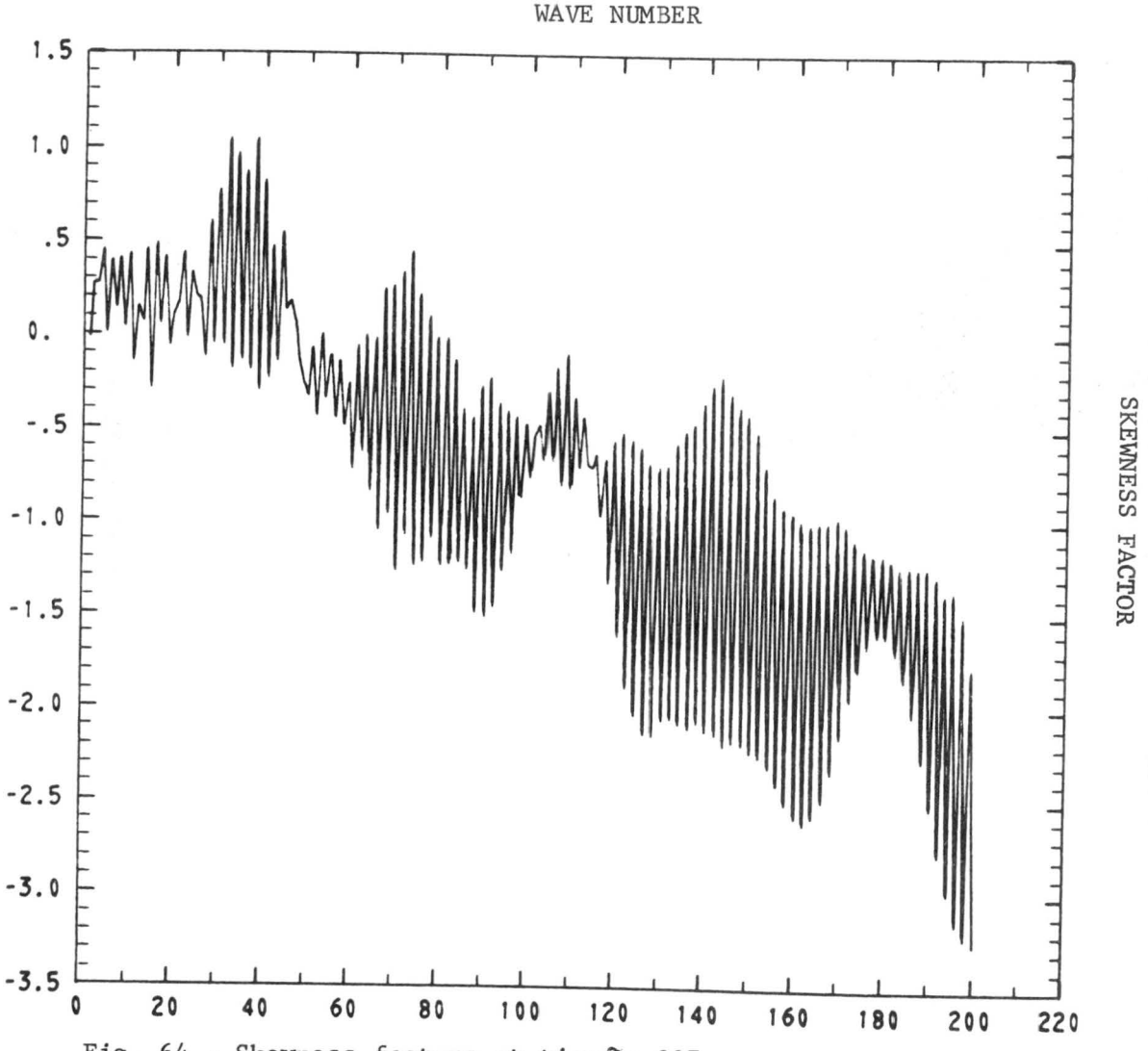

Fig. 64 - Skewness factors at time $\tilde{c}$=.937

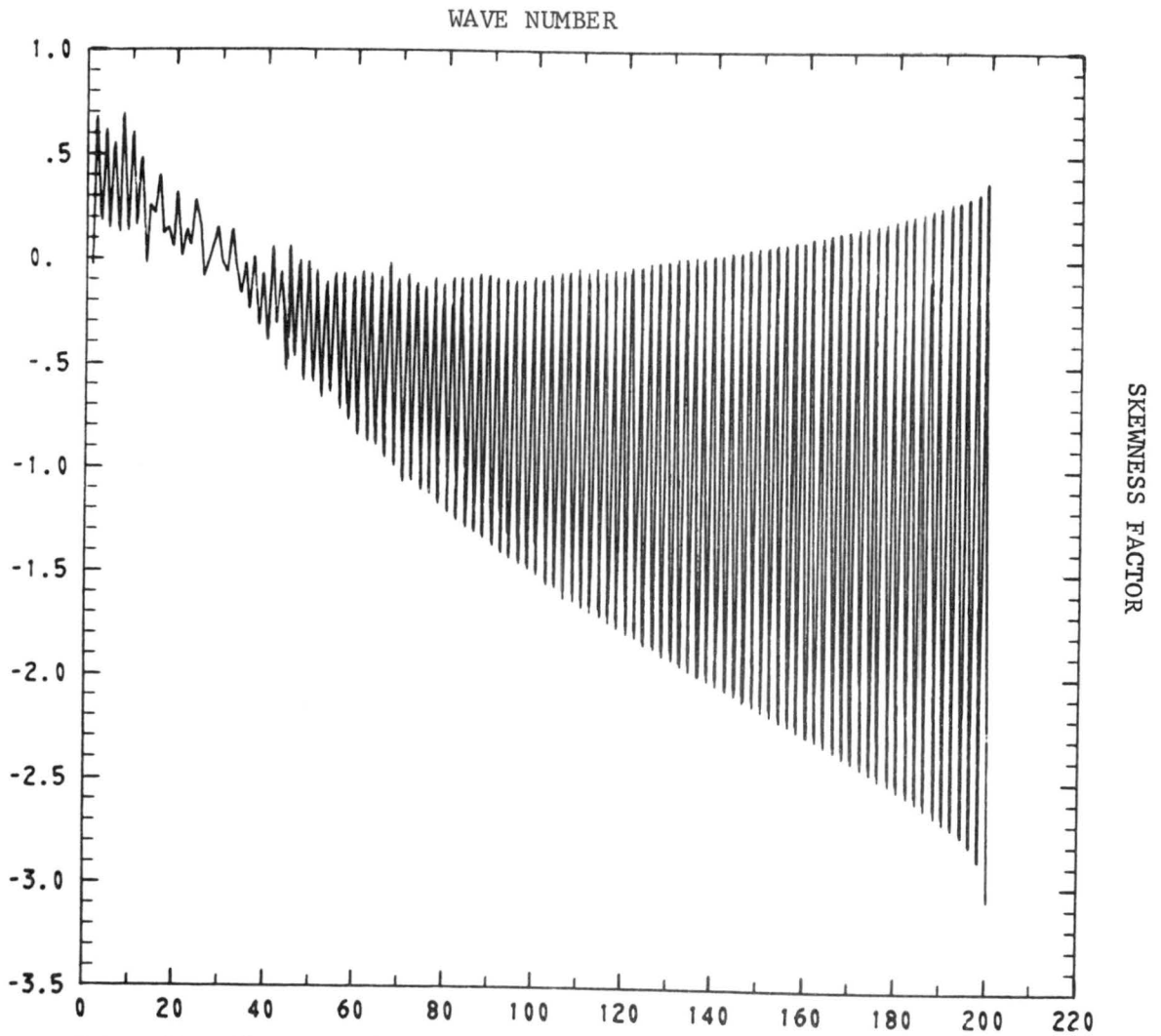

Fig. 65 - Skewness factors at time τ=1.664

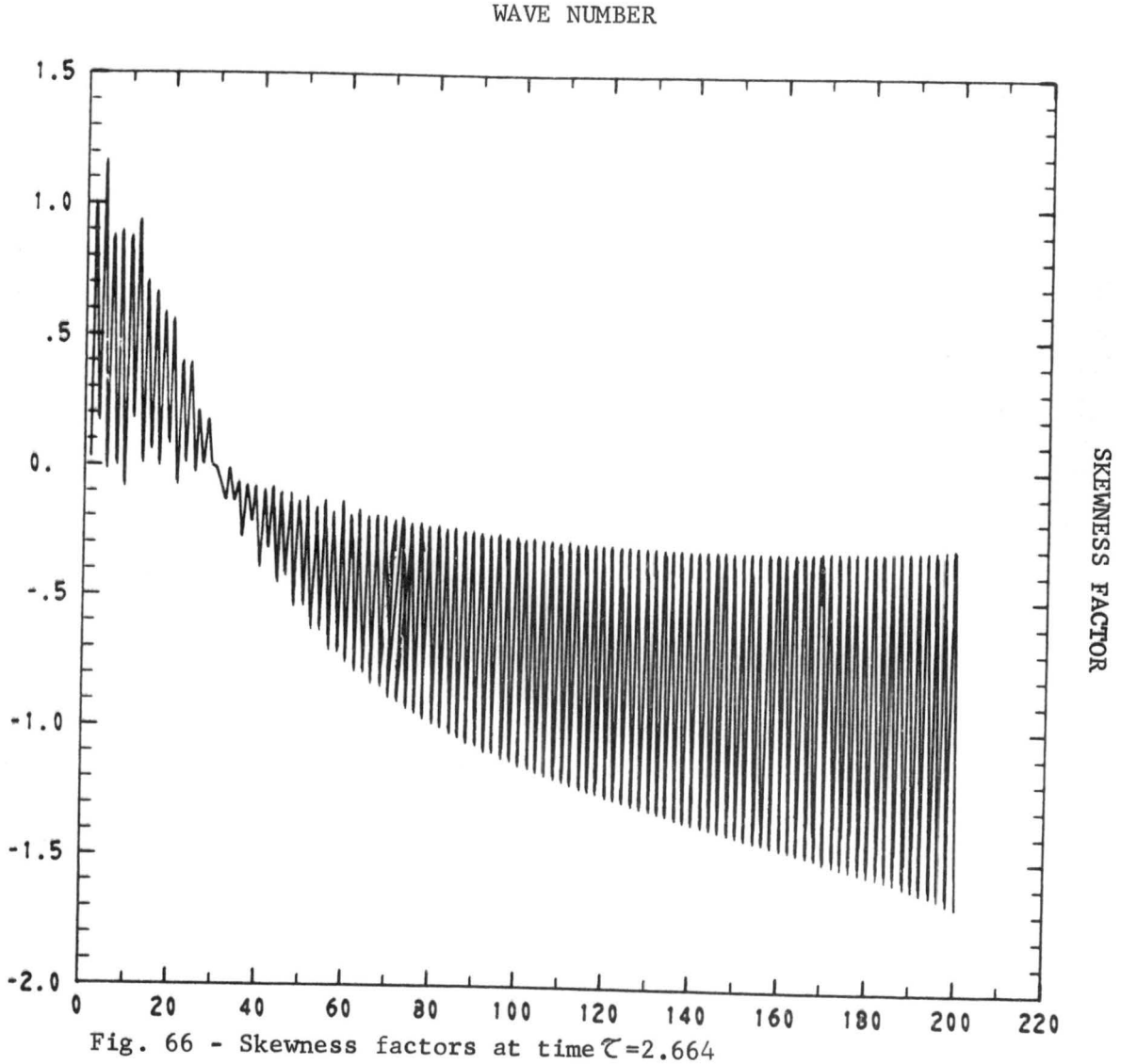

Fig. 66 - Skewness factors at time τ=2.664

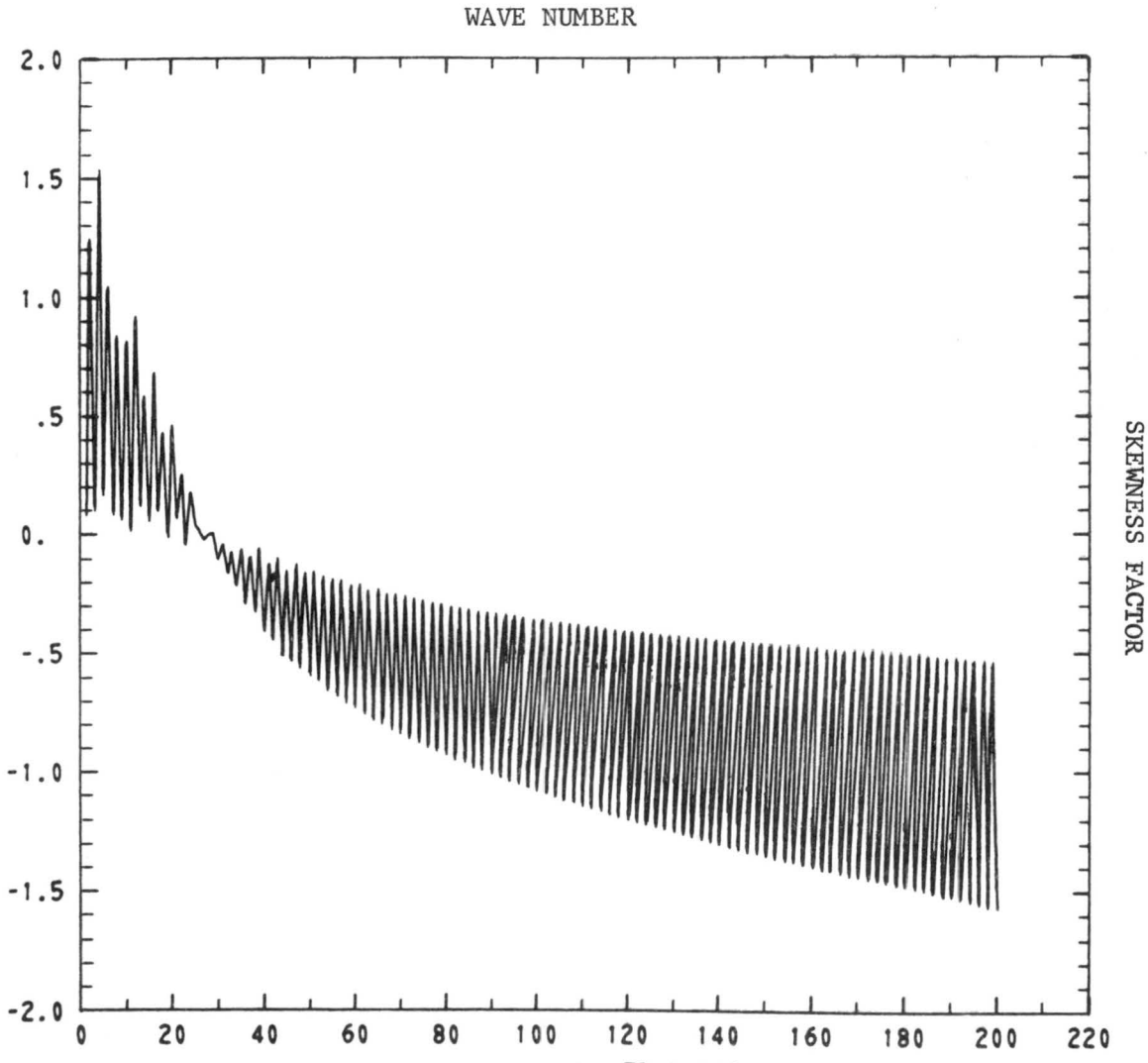

Fig. 67 - Skewness factors at time τ=4.014

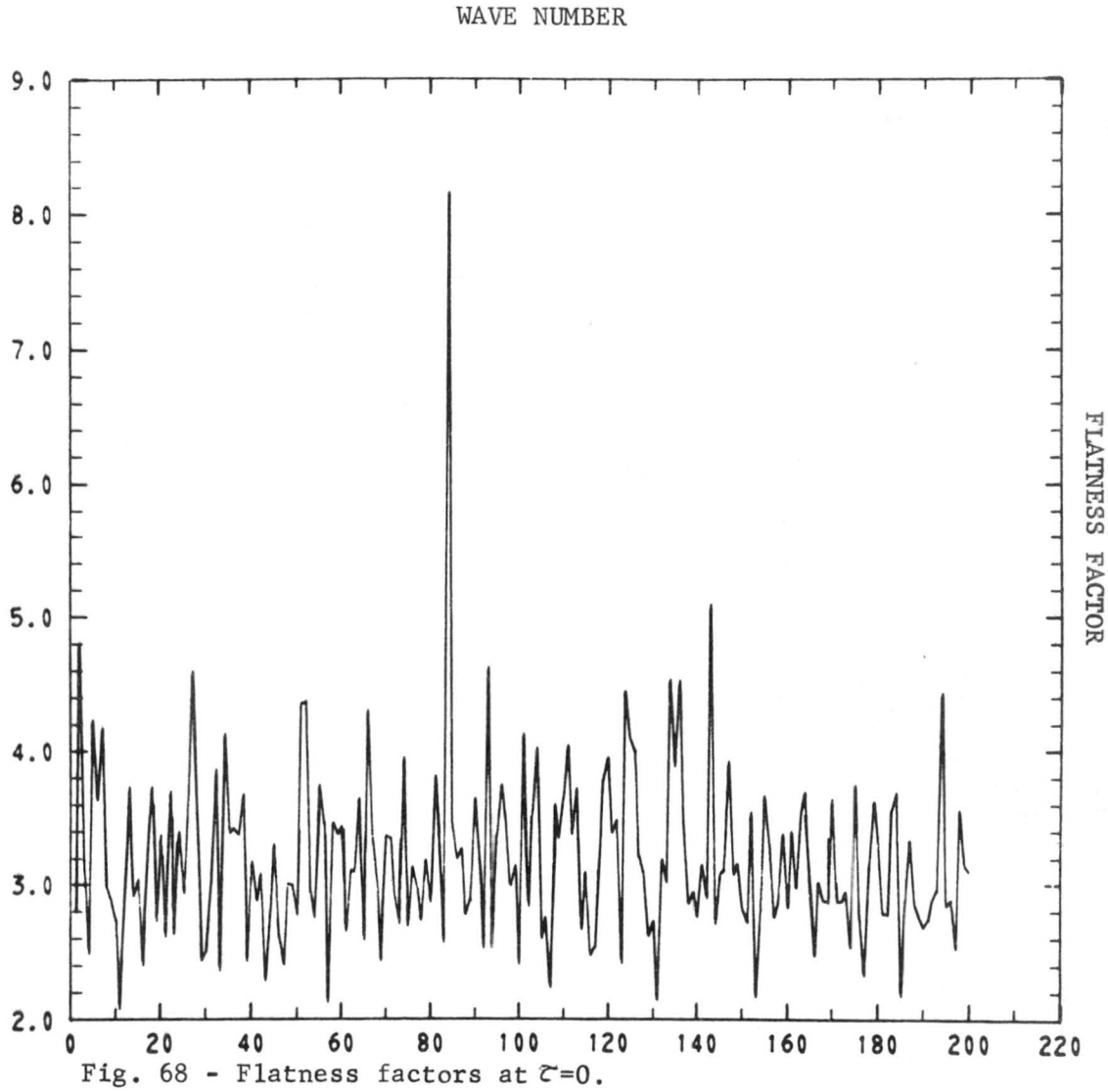

Fig. 68 - Flatness factors at τ=0.

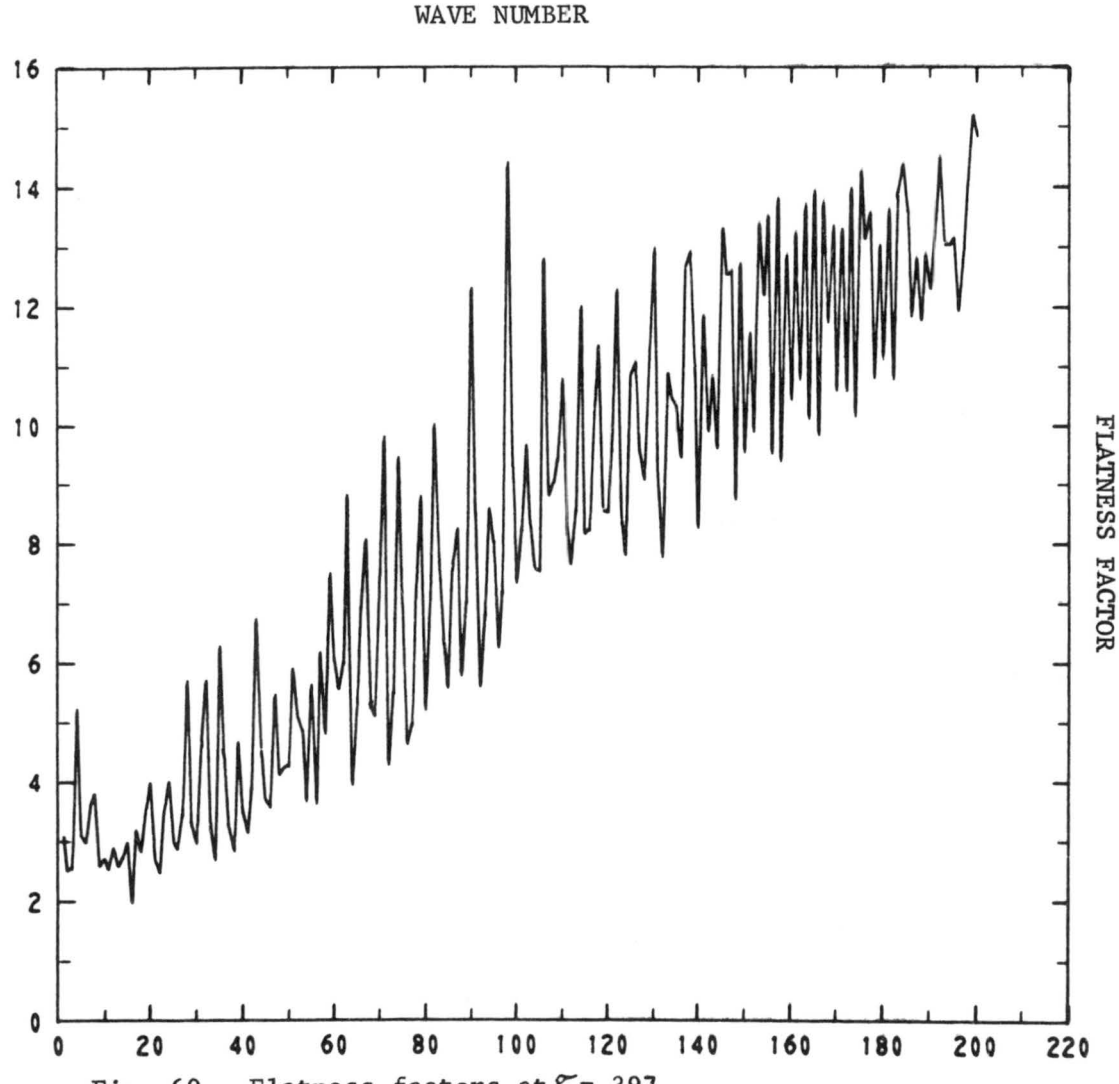

Fig. 69 - Flatness factors at σ=.397

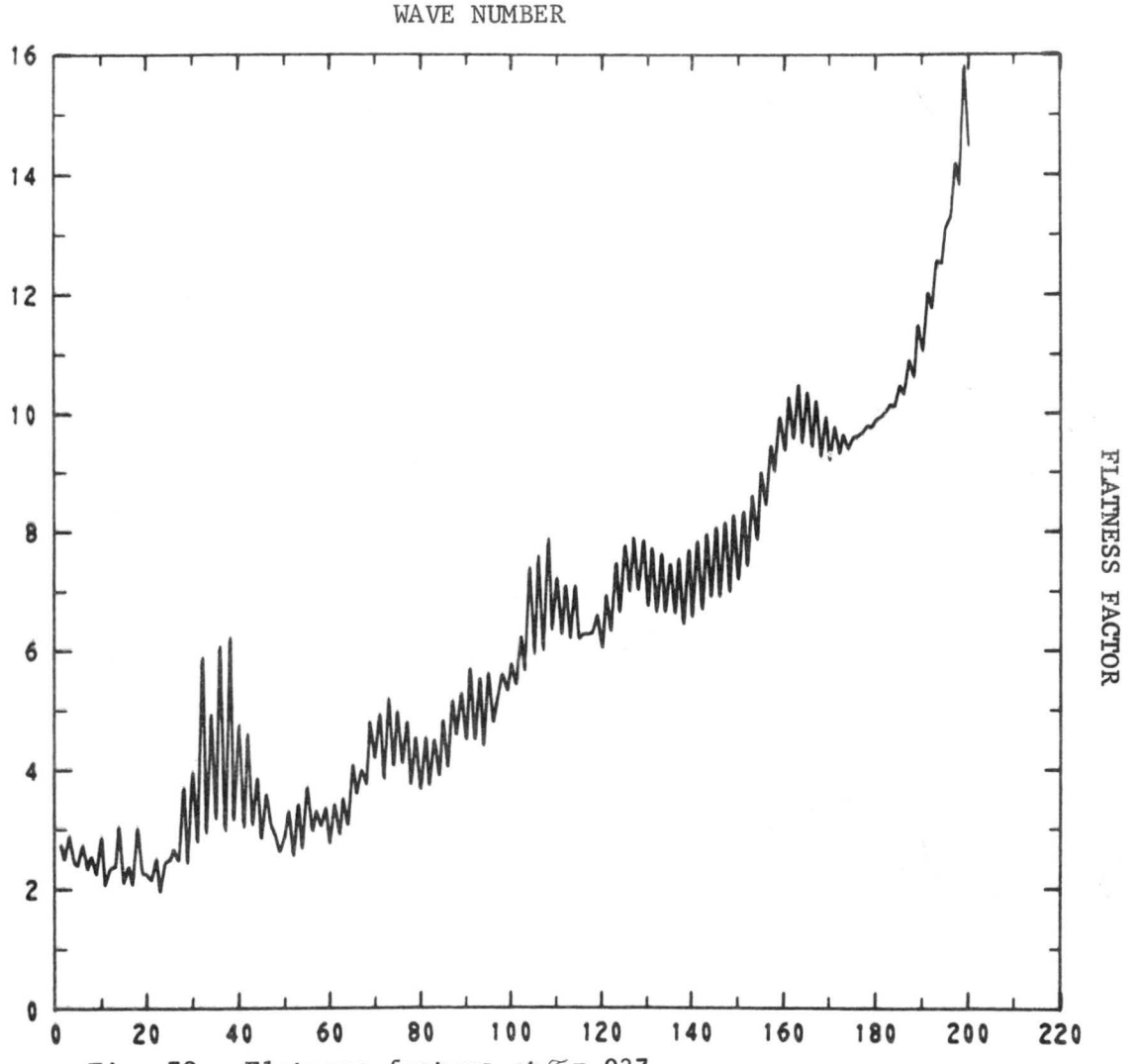

Fig. 70 - Flatness factors at τ=.937

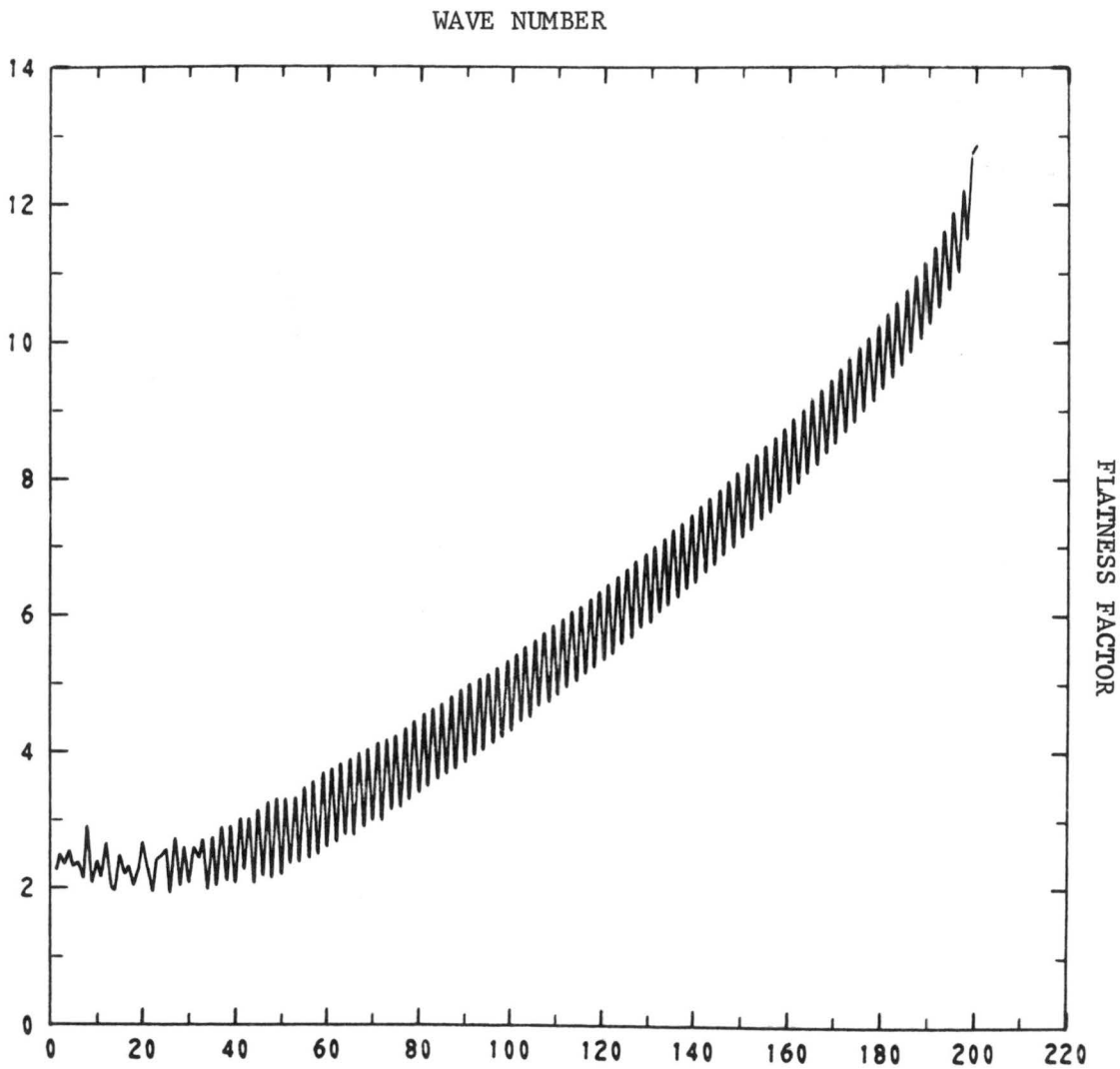

Fig. 71 - Flatness factors at ϵ=1.669

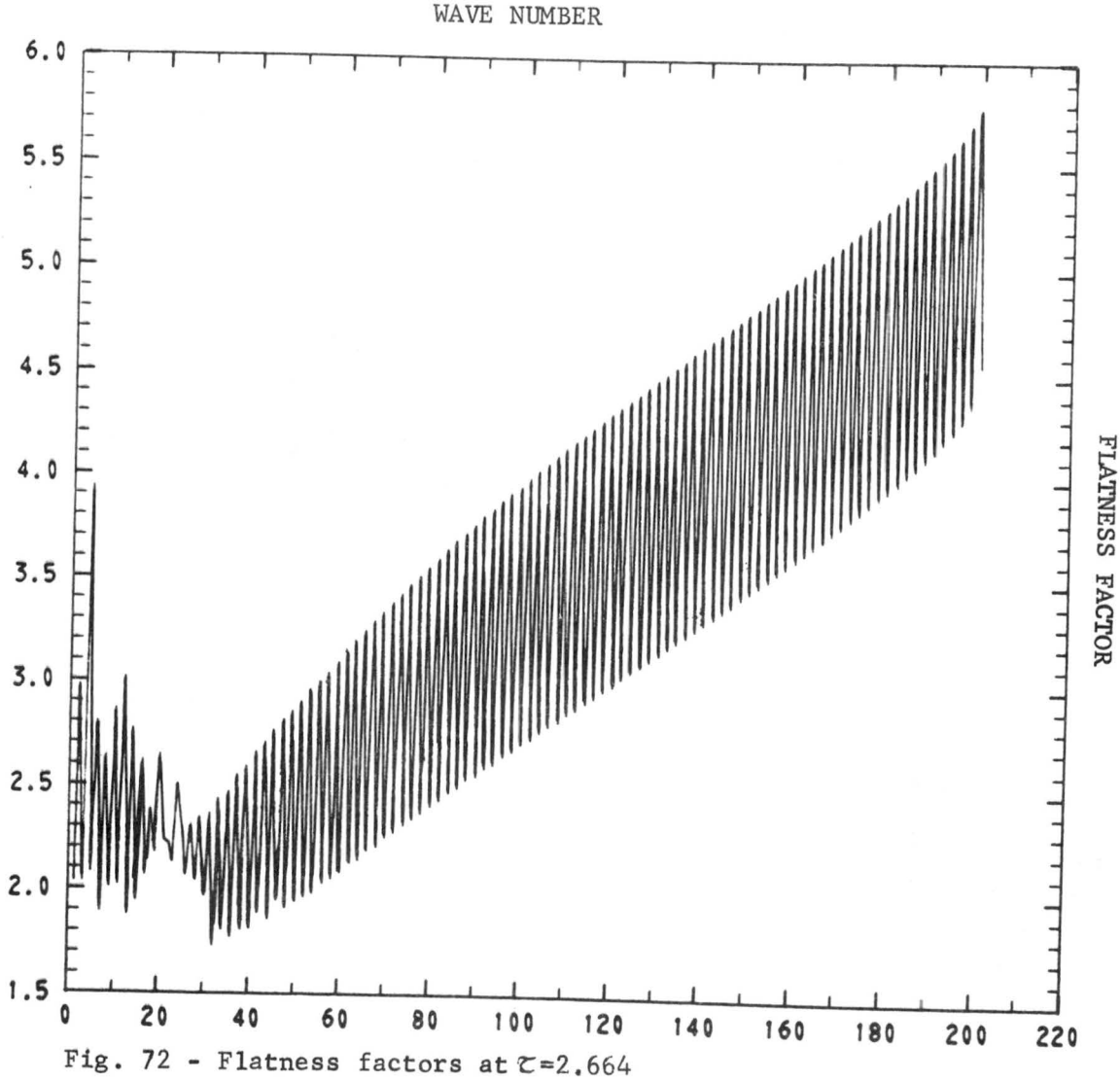

Fig. 72 - Flatness factors at τ=2.664

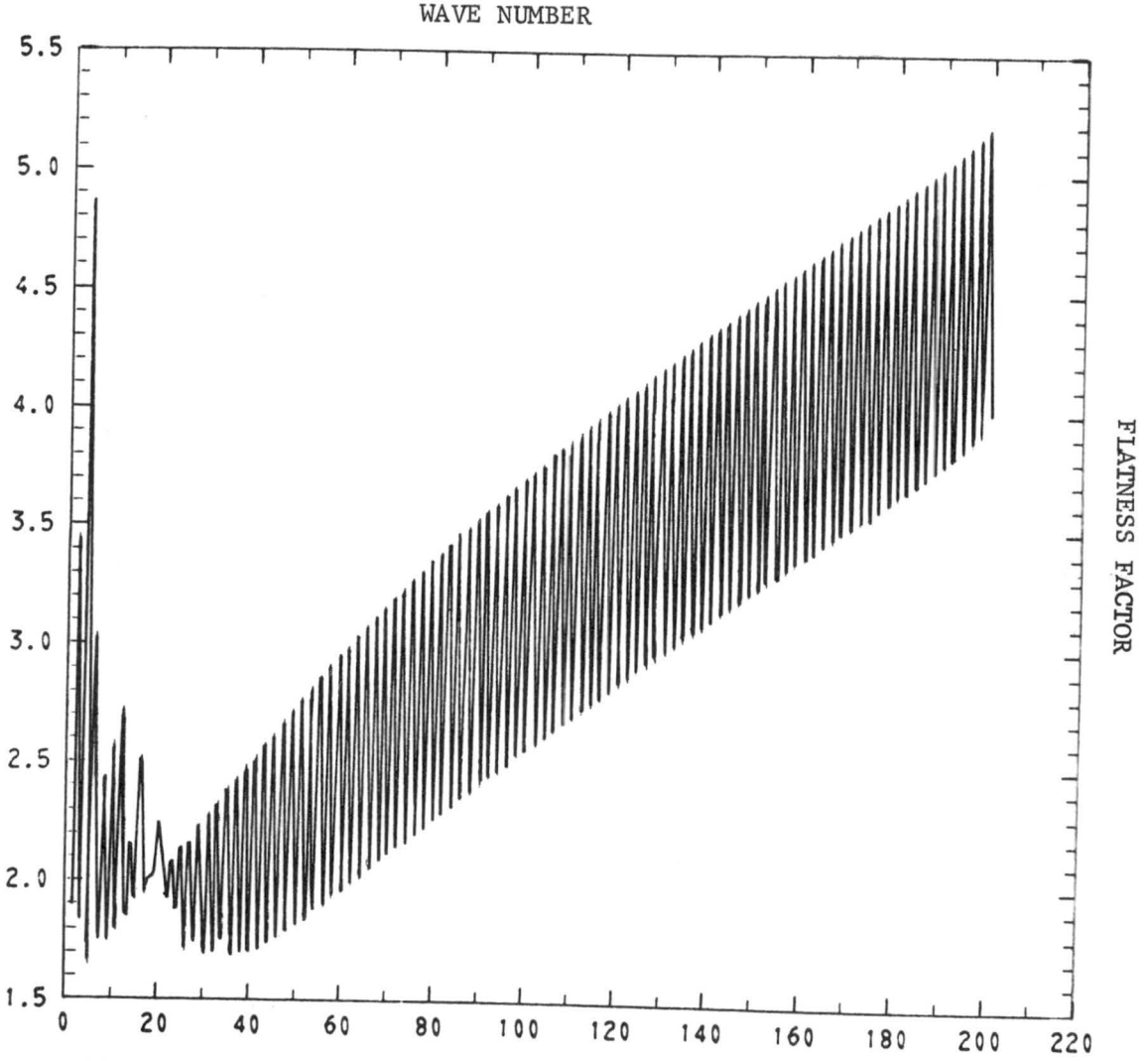

Fig. 73 - Flatness factors at τ=4.014

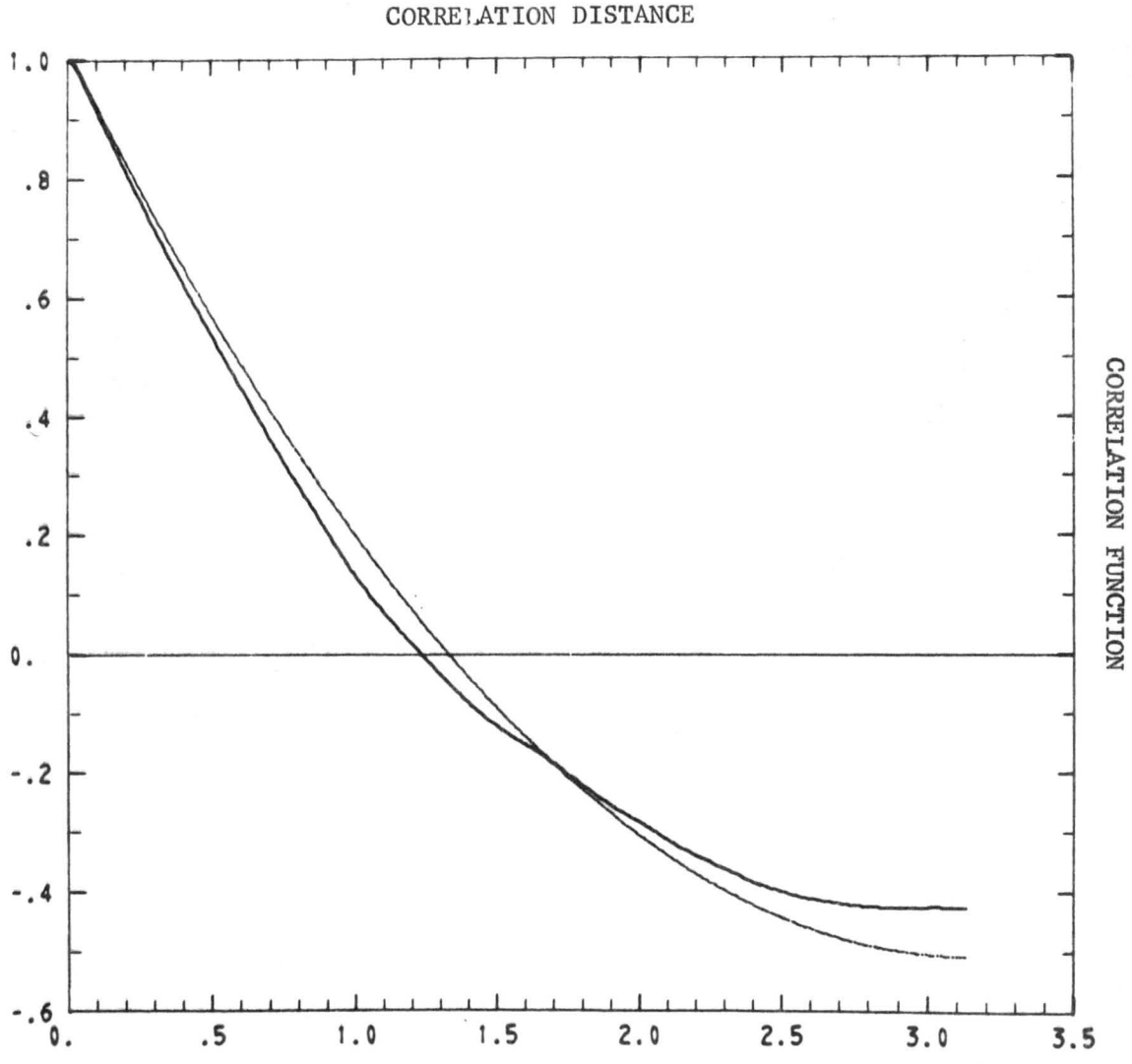

Fig. 74 - Correlation function of the reference solution (RS) and correlation function of the statistical experiment at τ=0.

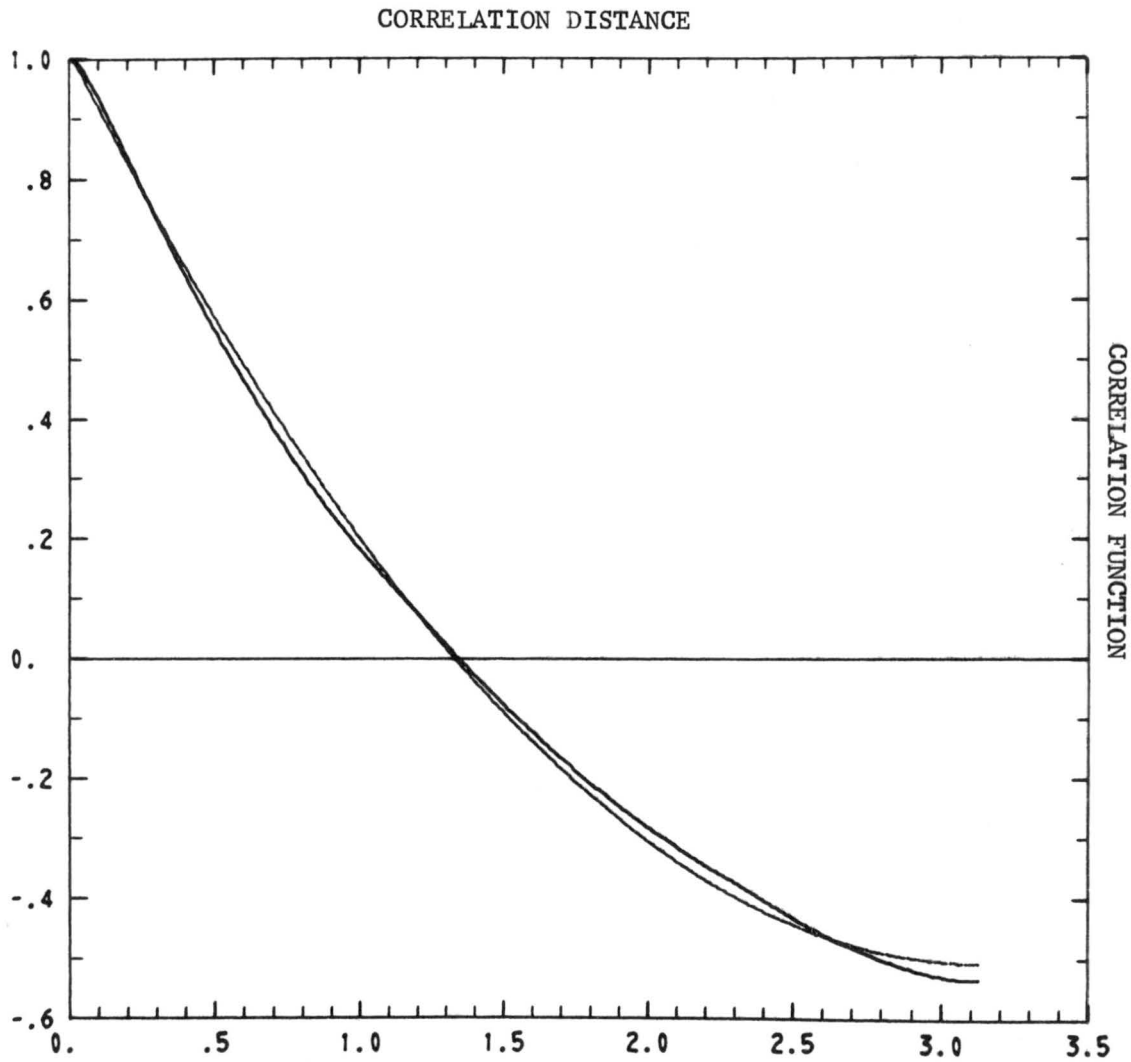

Fig. 75 - Correlation function of the reference solution (RS) and correlation function of the statistical experiment at τ=.397

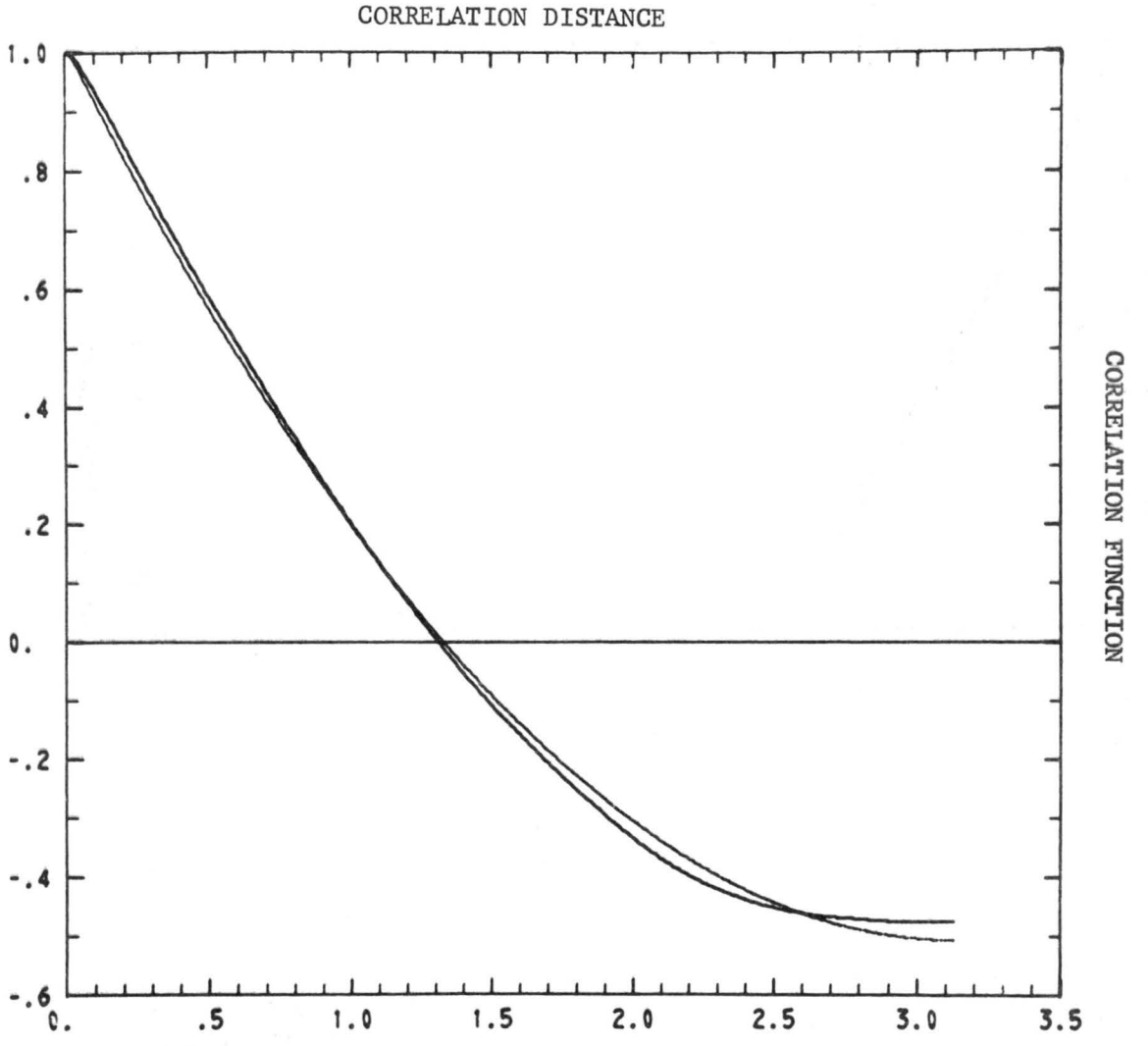

Fig. 76 - Correlation function of the reference solution (RS) and correlation function of the statistical experiment at $\tau = .937$

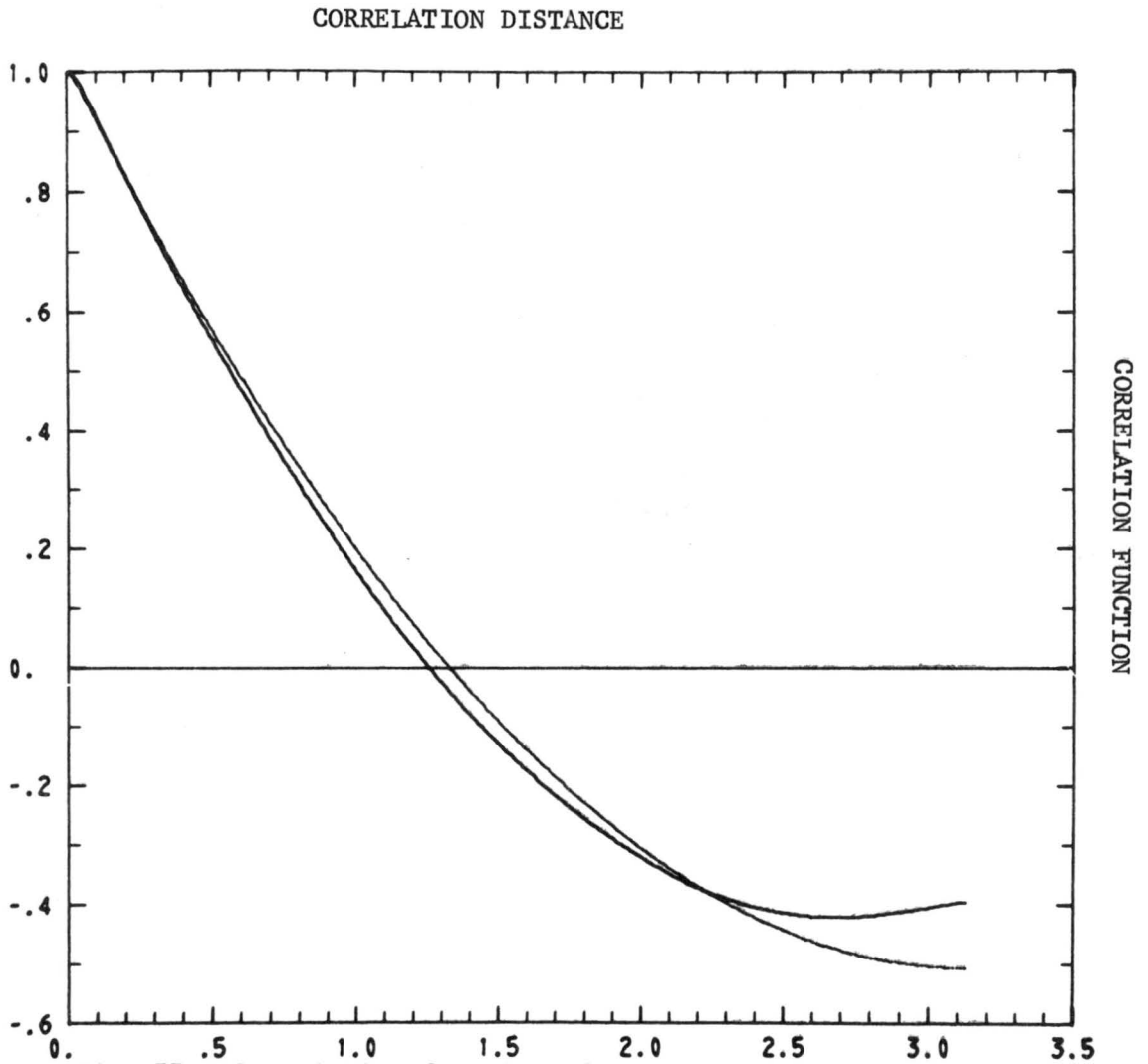

Fig. 77 - Correlation function of the reference solution (RS) and correlation function of the statistical experiment at τ=1.669

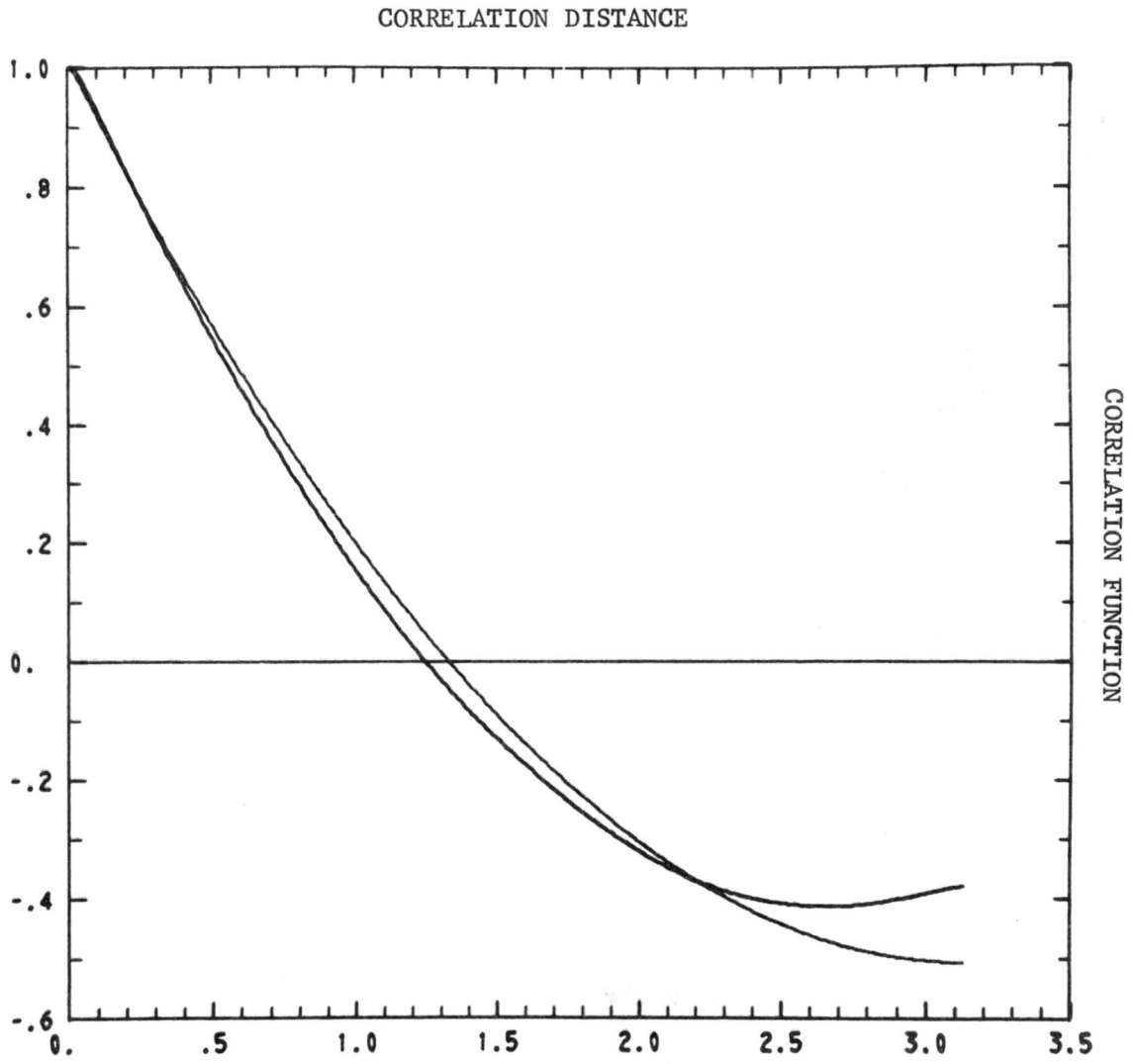

Fig. 78 - Correlation function of the reference solution (RS) and correlation function of the statistical experiment at τ=2.664

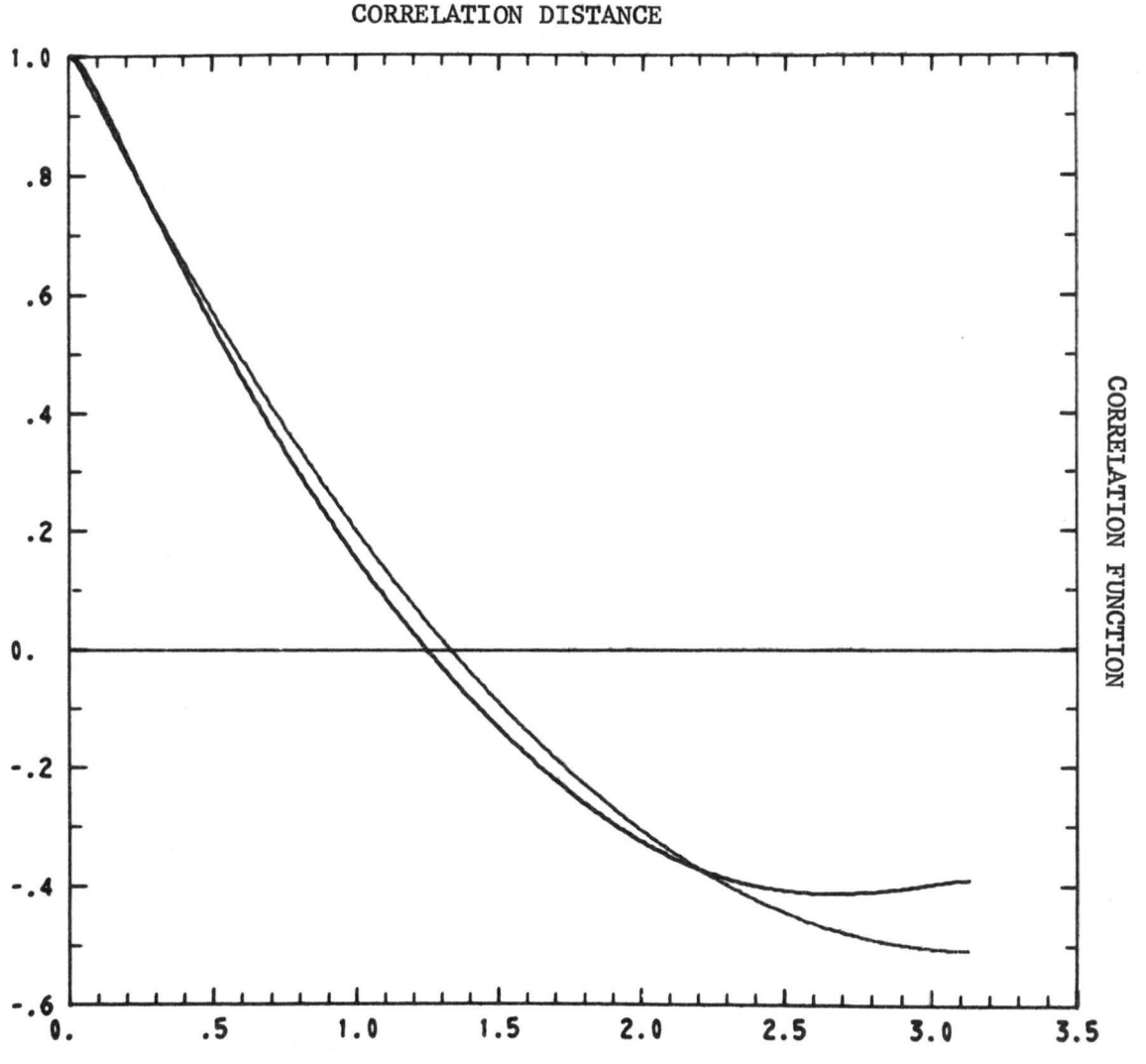

Fig. 79 - Correlation function of the reference solution (RS) and correlation function of the statistical experiment at τ=4.014

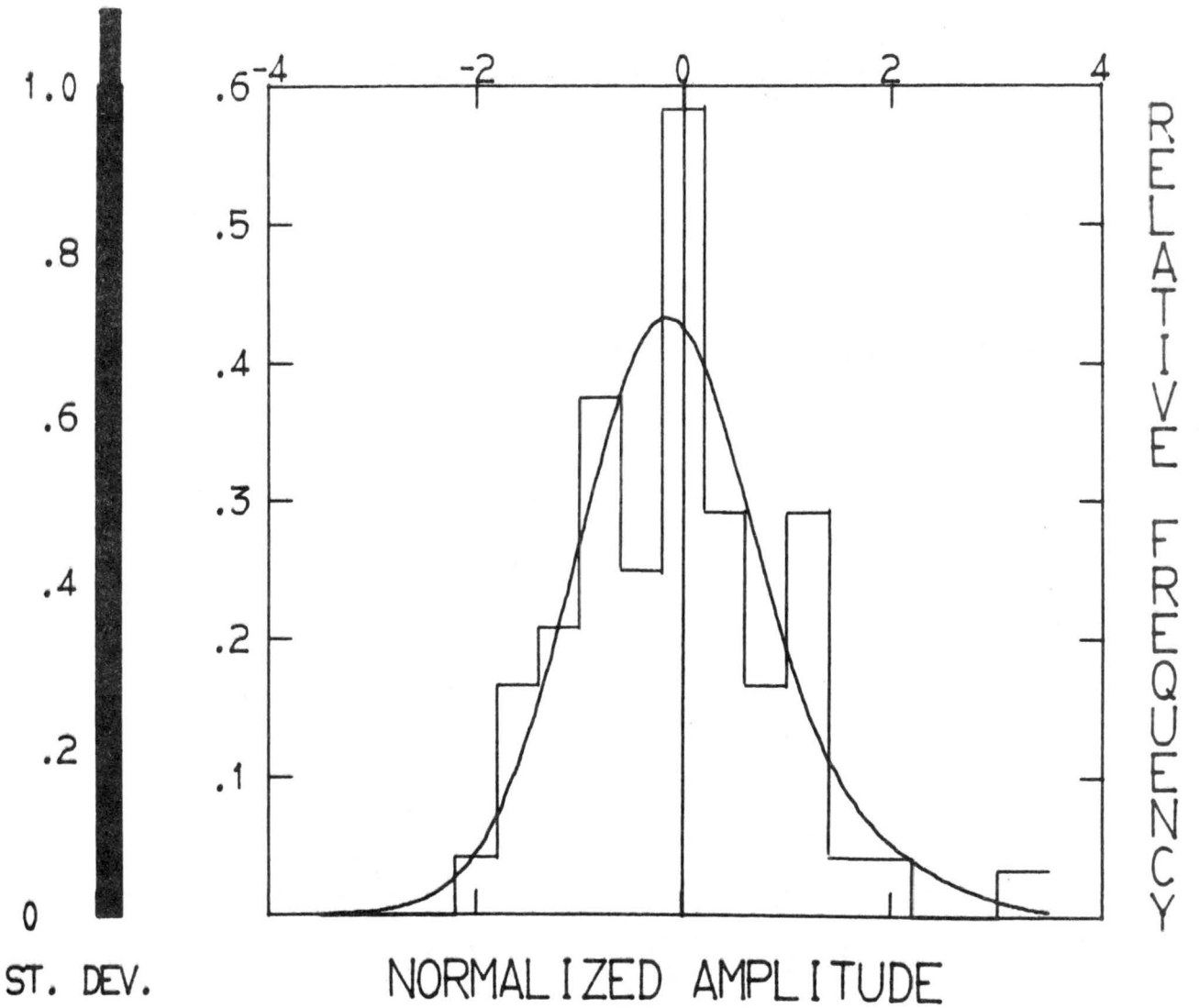

Figure 80. Wave-number 1, σ=.0.

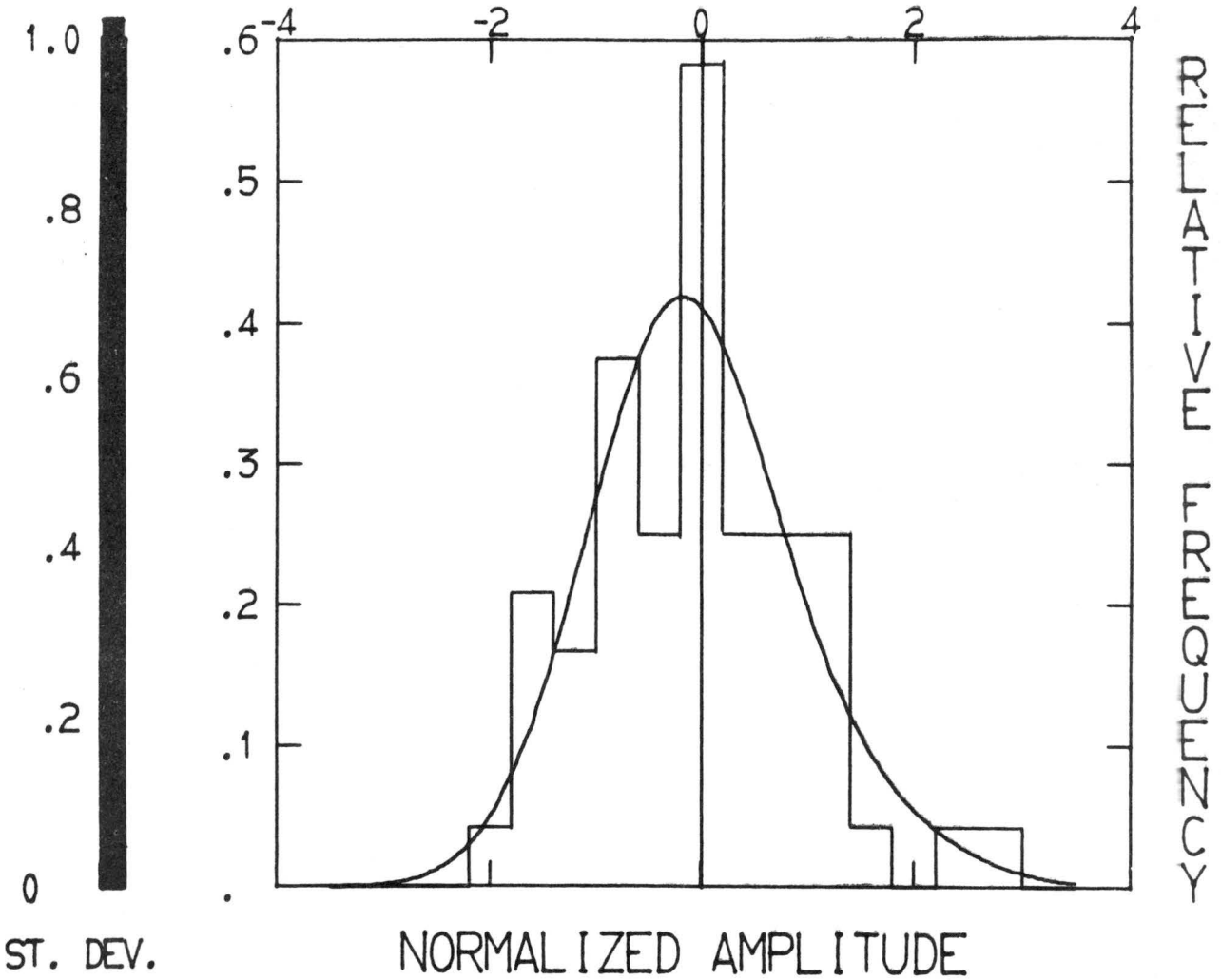

Figure 81. Wave-number 1, σ =.397.

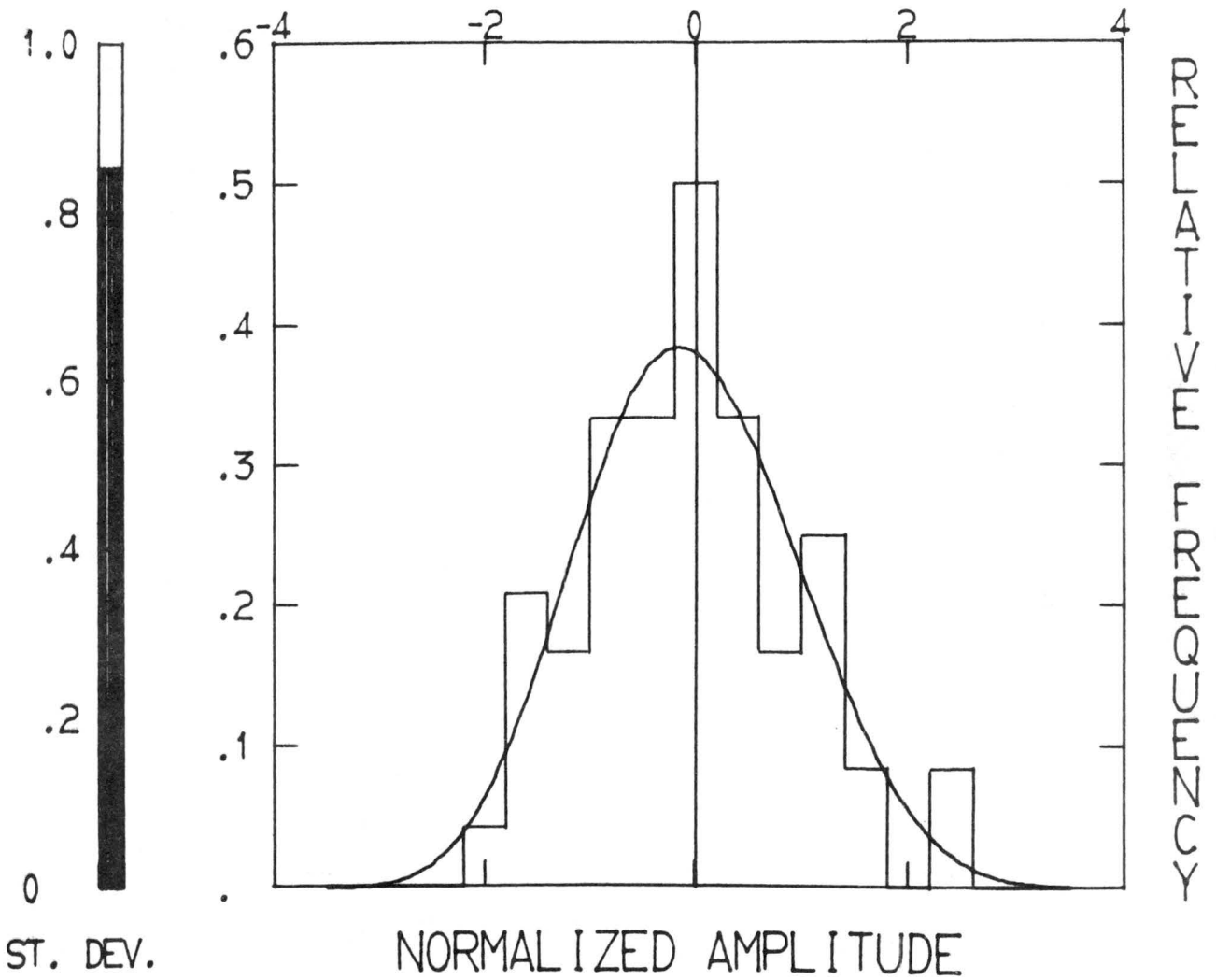

Figure 82. Wave-number 1, τ =937.

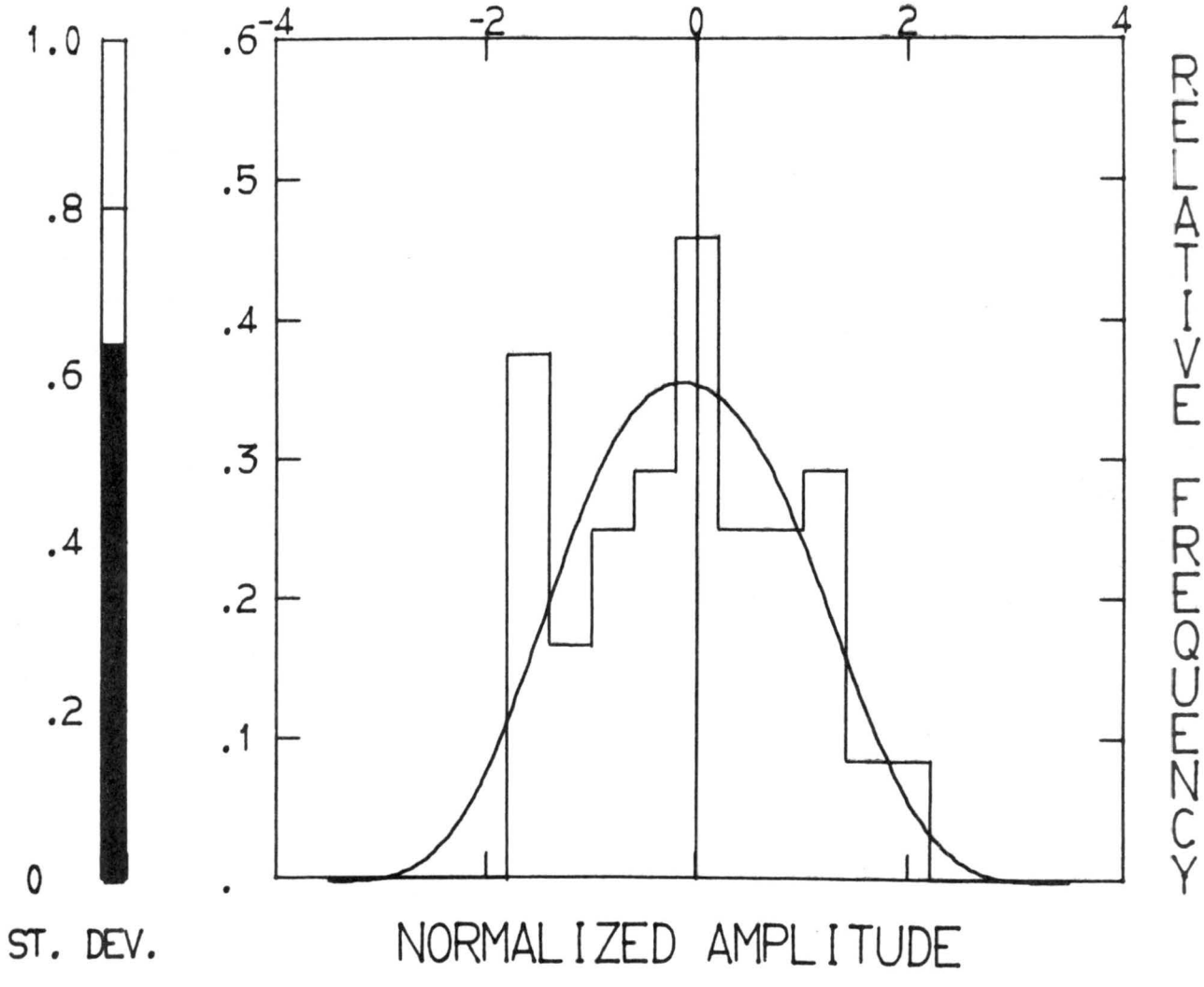

Figure 83. Wave-number 1, τ=1.669.

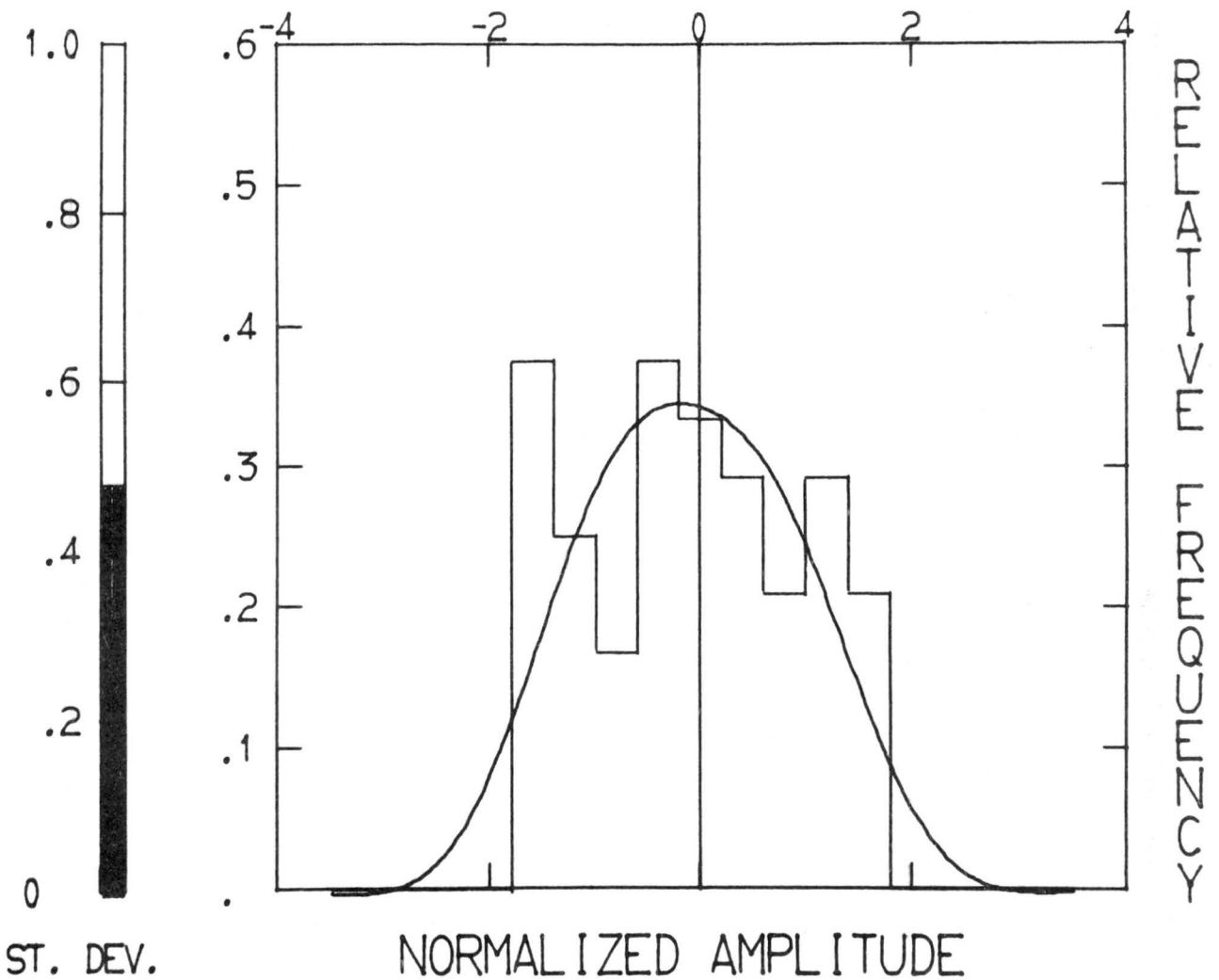

Figure 84. Wave-number 1, σ =2.664.

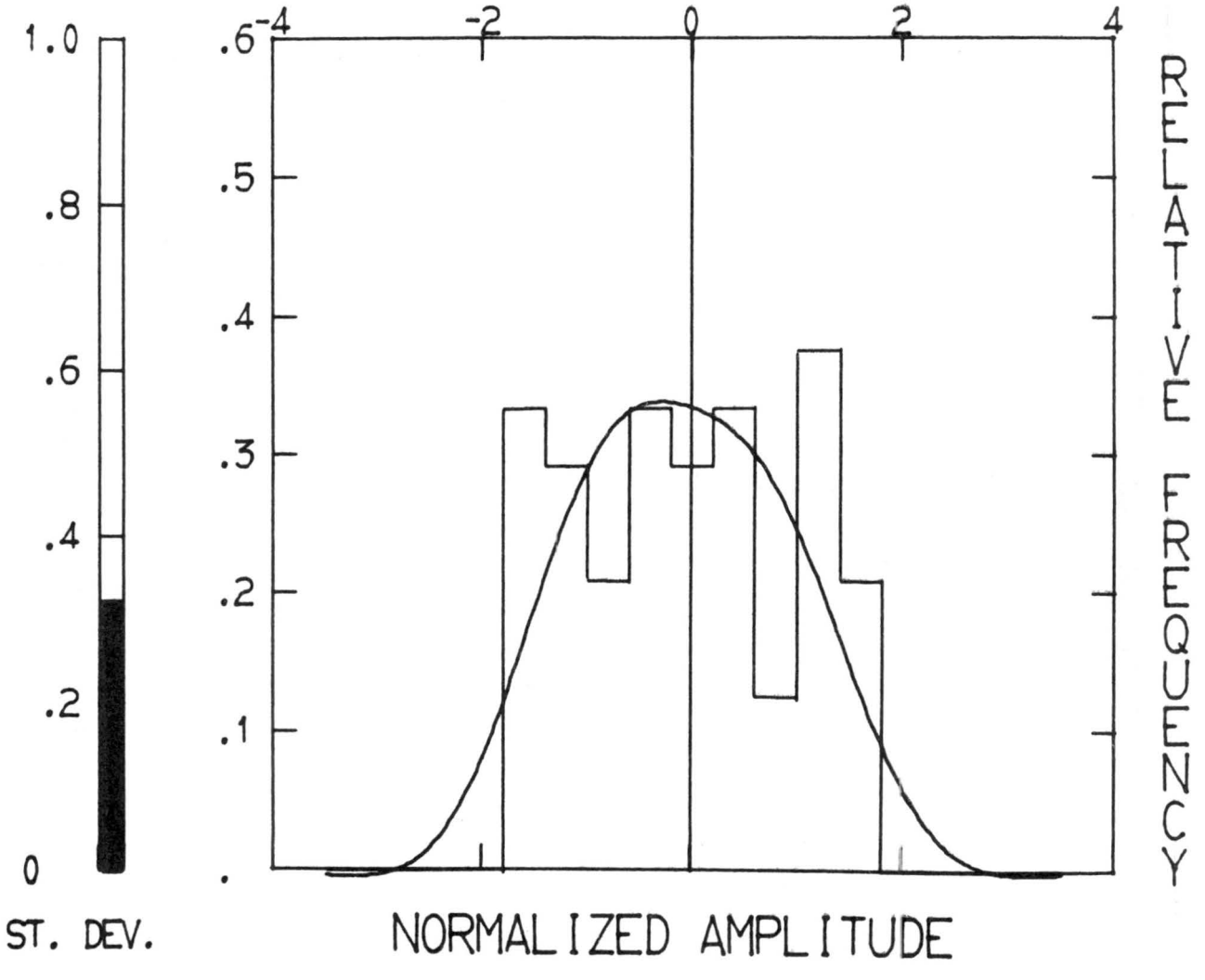

Figure 85. Wave-number 1, $\bar{z}$ =4.014.

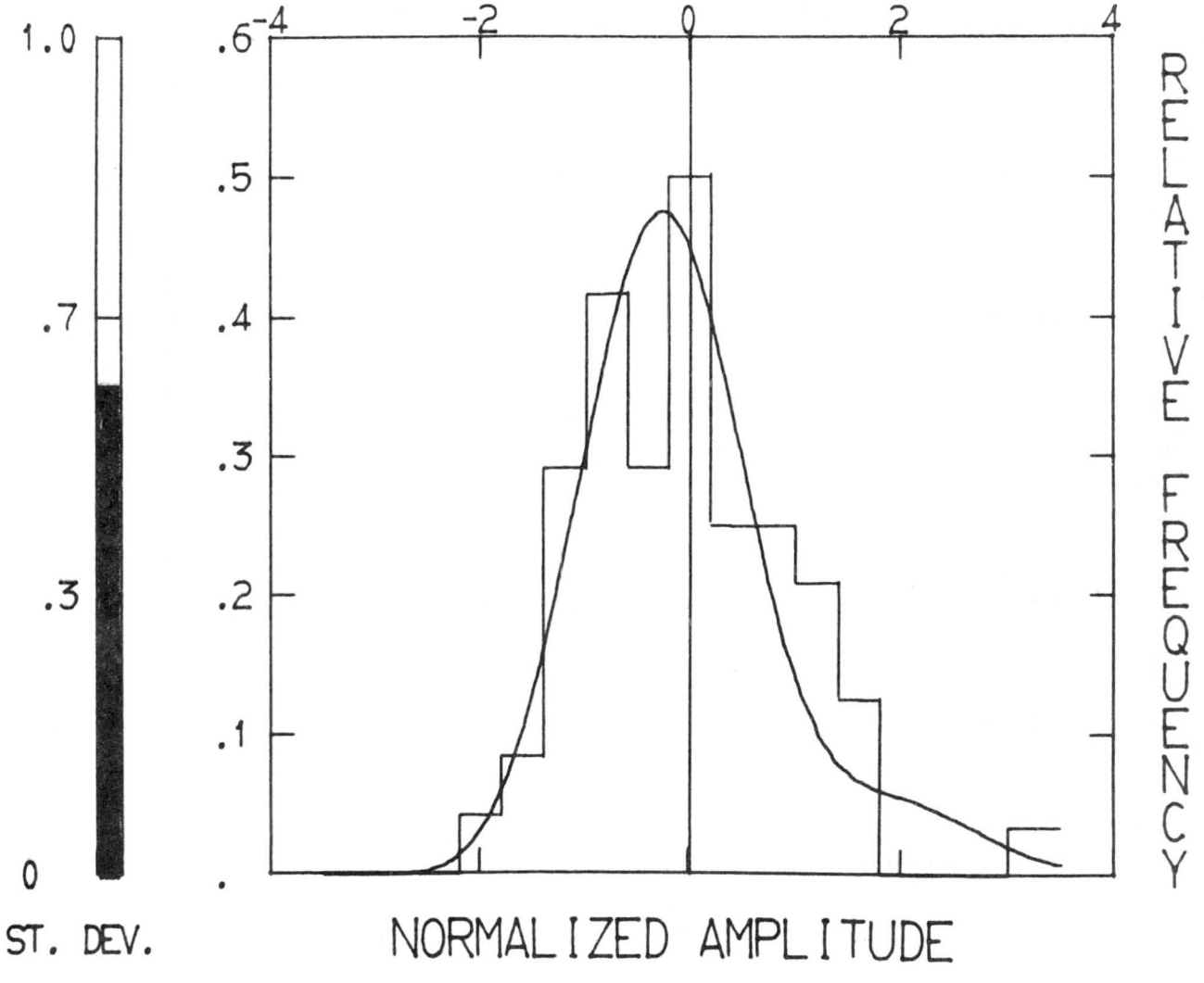

Figure 86. Wave-number 2, $\mathfrak{C}$=.0.

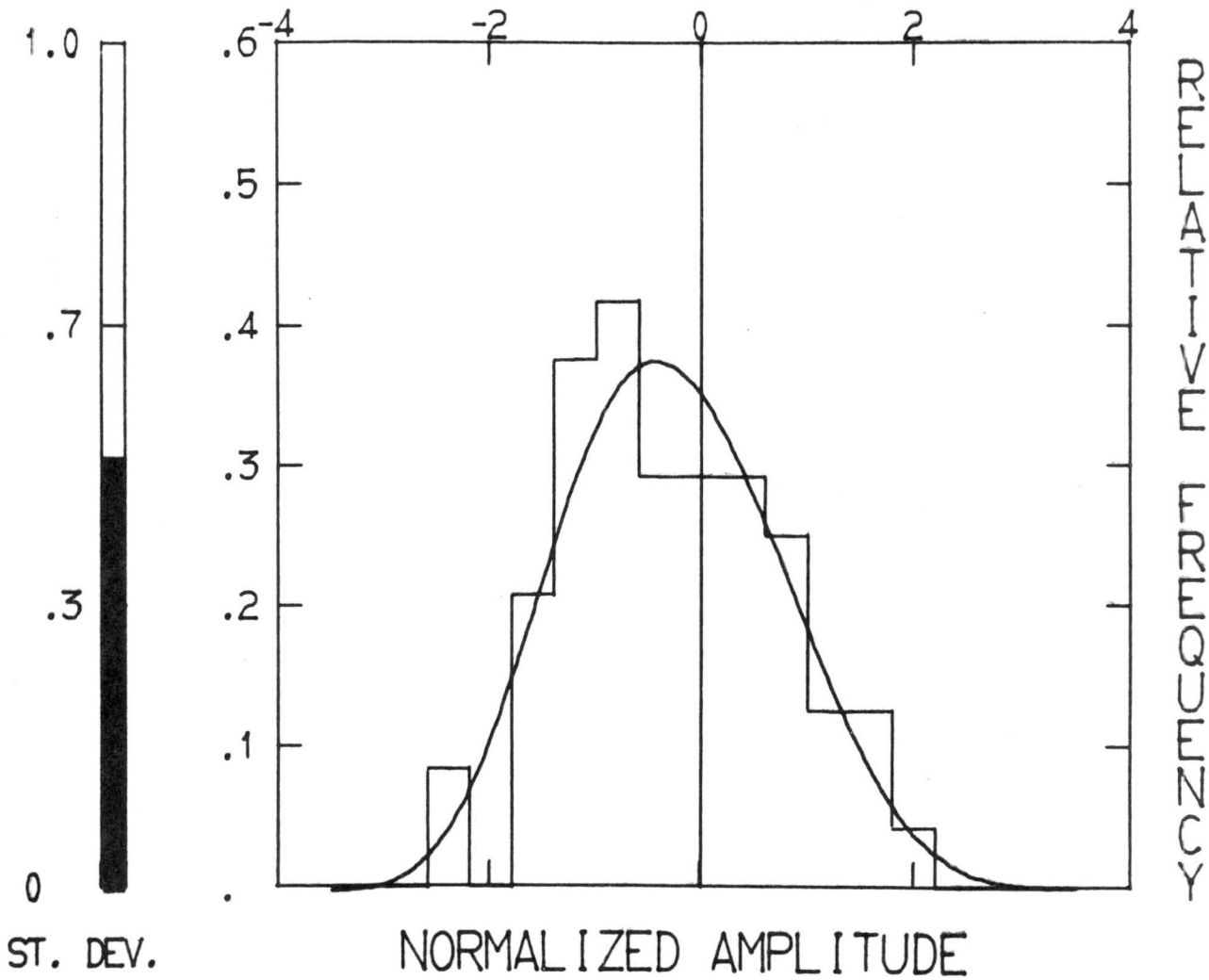

Figure 87. Wave-number 2, $\tau = .397$.

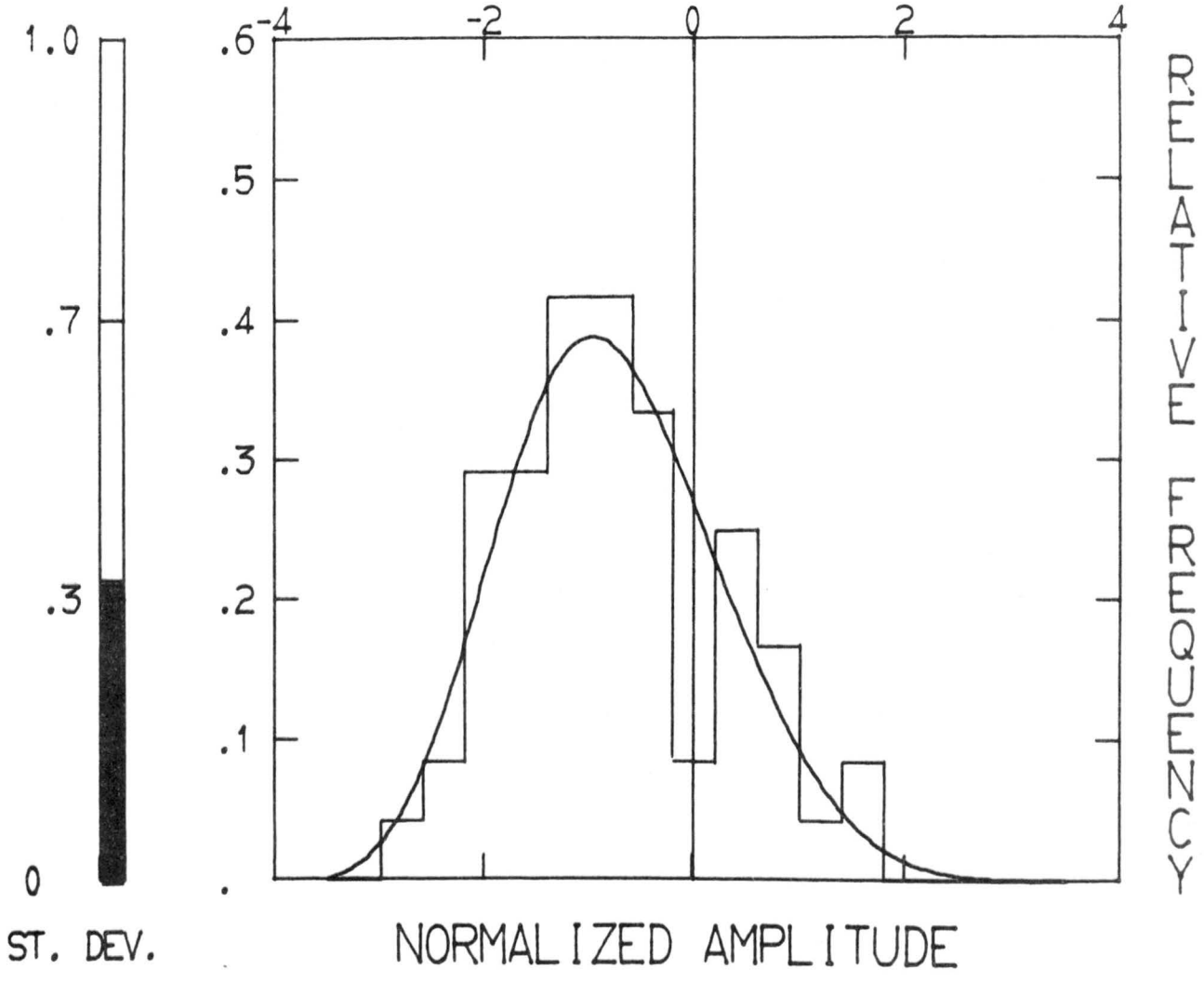

Figure 88. Wave-number 2, $\sigma = .937$.

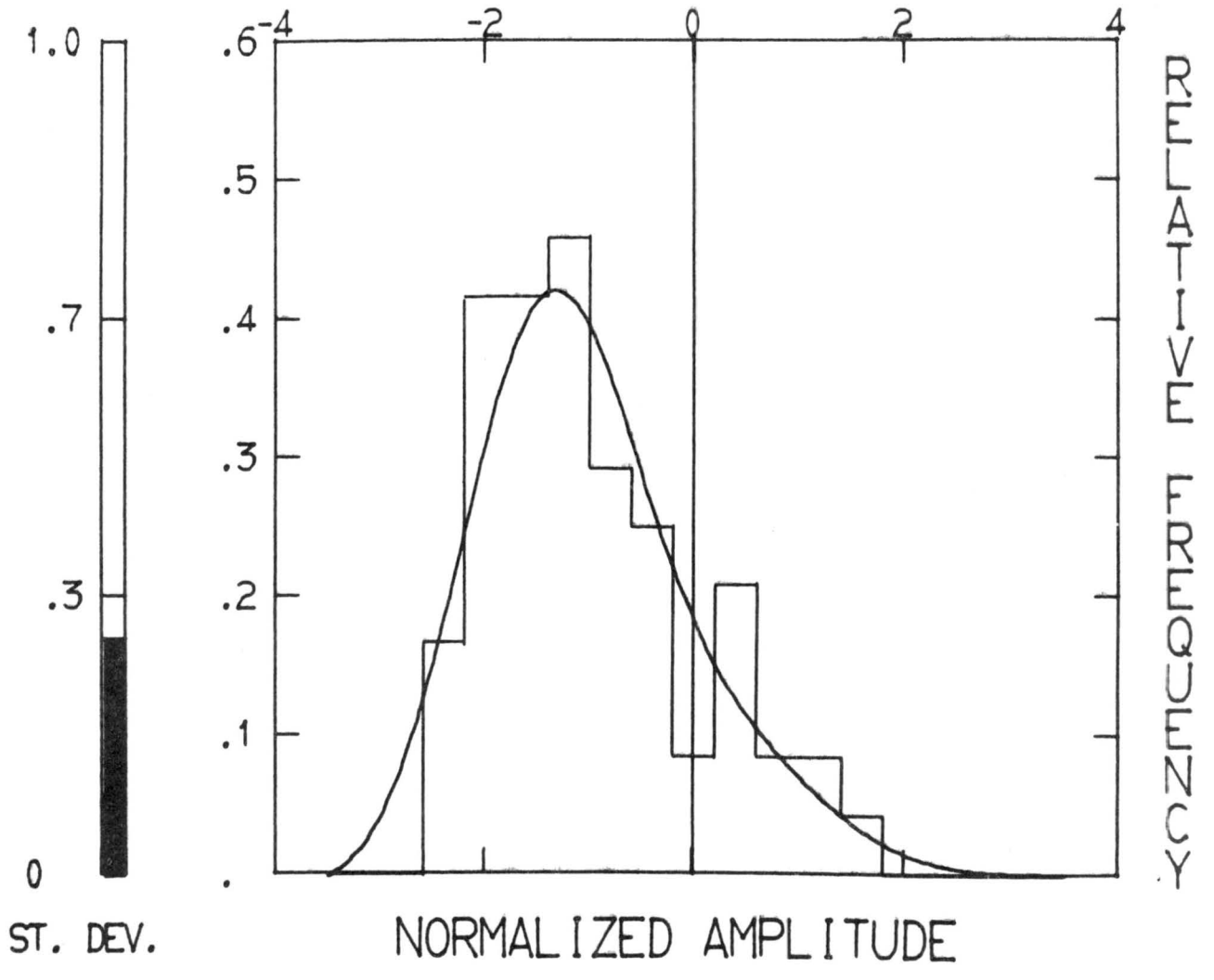

Figure 89. Wave-number 2, σ=1.669.

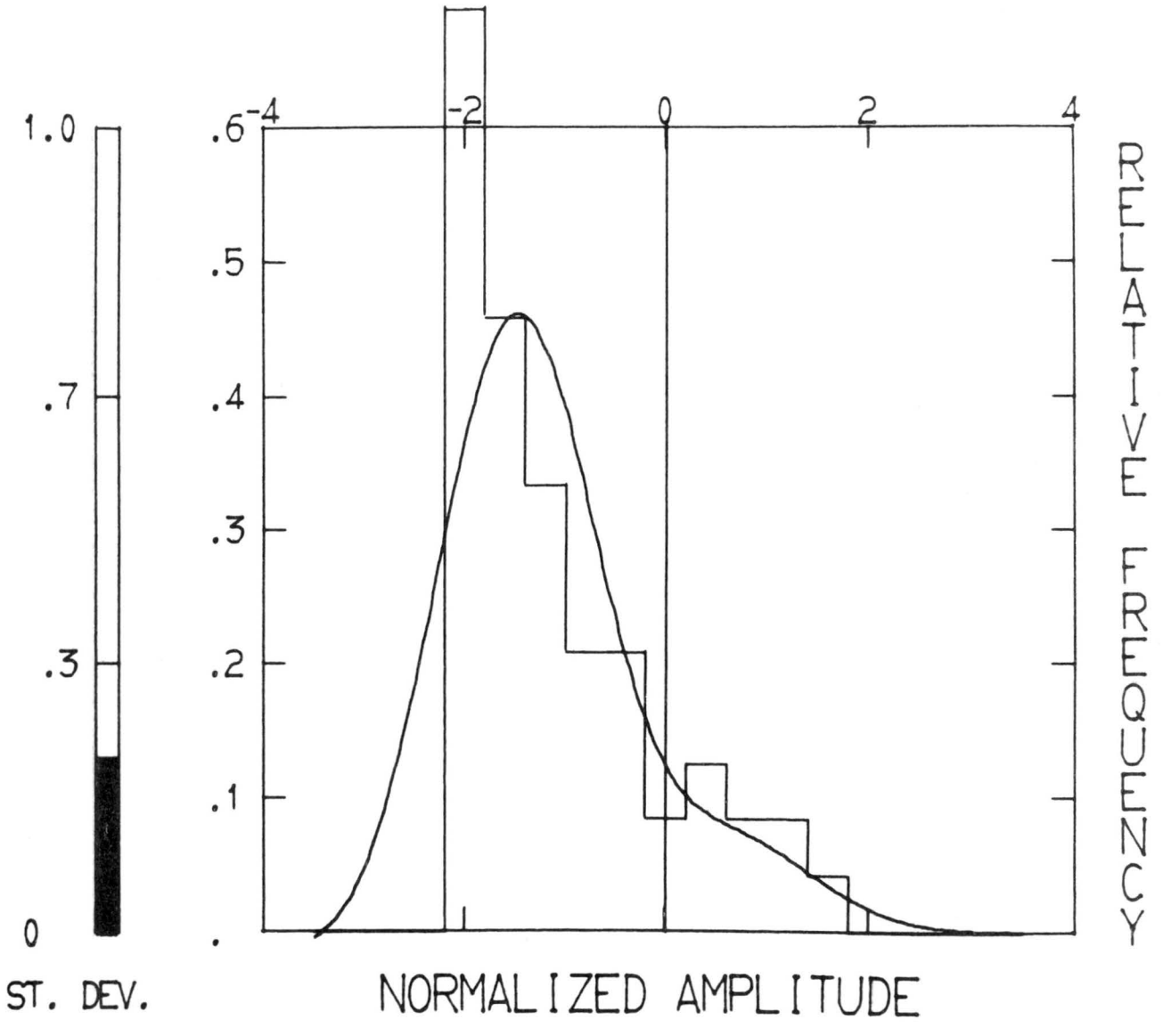

Figure 90. Wave-number 2, τ =2.664.

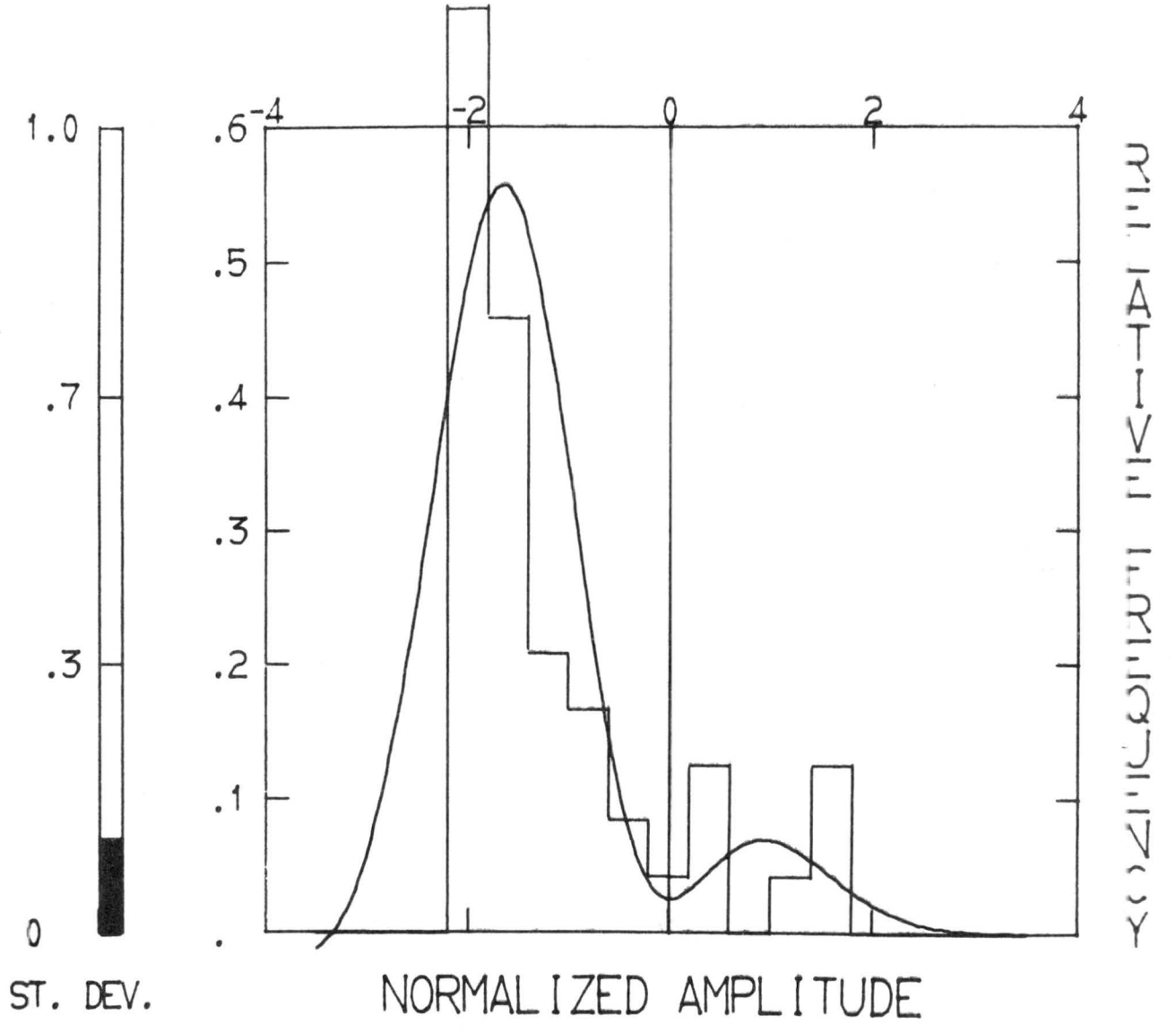

Figure 91. Wave-number 2, τ =4.014.

Unclassified
Security Classification

DOCUMENT CONTROL DATA - R&D

(Security classification of title, body of abstract and indexing annotation must be entered when the overall report is classified)

1. ORIGINATING ACTIVITY *(Corporate author)*

Fluid Mechanics Program, College of Engineering
Colorado State University, Fort Collins, Colorado

2a. REPORT SECURITY CLASSIFICATION

Unclassified

2b. GROUP

3. REPORT TITLE

A NUMERICAL EXPERIMENT ON A TURBULENCE MODEL

4. DESCRIPTIVE NOTES *(Type of report and inclusive dates)*

Technical Report

5. AUTHOR(S) *(Last name, first name, initial)*

Giorgini, Aldo

6. REPORT DATE	7a. TOTAL NO. OF PAGES	7b. NO. OF REFS
December 1967	123	2

8a. CONTRACT OR GRANT NO.

DA-AMC-28-043-65-G20

b. PROJECT NO.

2246

c.

d.

9a. ORIGINATOR'S REPORT NUMBER(S)

CER67-68AG49

9b. OTHER REPORT NO(S) *(Any other numbers that may be assigned this report)*

10. AVAILABILITY/LIMITATION NOTICES

Distribution of This Document is Unlimited.

11. SUPPLEMENTARY NOTES

12. SPONSORING MILITARY ACTIVITY

U.S. Army Materiel Command

13. ABSTRACT

Burgers' equation is Fourier-analyzed to obtain a system of a discrete infinity of equations in a discrete infinity of variables. This system is studied numerically and the response to random initial conditions is obtained by use of a CDC 6600 digital computer.

The 60 realizations obtained were used to obtain mean amplitudes, average energy spectra, skewness factors, flatness factors, and correlation functions.

DD FORM 1 JAN 64 1473

Unclassified
Security Classification

14. KEY WORDS	LINK A		LINK B		LINK C	
	ROLE	WT	ROLE	WT	ROLE	WT
Turbulence Fluid Mechanics Numerical Experiments Burgers' Equation						

INSTRUCTIONS

1. ORIGINATING ACTIVITY: Enter the name and address of the contractor, subcontractor, grantee, Department of Defense activity or other organization *(corporate author)* issuing the report.

2*a*. REPORT SECURITY CLASSIFICATION: Enter the overall security classification of the report. Indicate whether "Restricted Data" is included. Marking is to be in accordance with appropriate security regulations.

2*b*. GROUP: Automatic downgrading is specified in DoD Directive 5200.10 and Armed Forces Industrial Manual. Enter the group number. Also, when applicable, show that optional markings have been used for Group 3 and Group 4 as authorized.

3. REPORT TITLE: Enter the complete report title in all capital letters. Titles in all cases should be unclassified. If a meaningful title cannot be selected without classification, show title classification in all capitals in parenthesis immediately following the title.

4. DESCRIPTIVE NOTES: If appropriate, enter the type of report, e.g., interim, progress, summary, annual, or final. Give the inclusive dates when a specific reporting period is covered.

5. AUTHOR(S): Enter the name(s) of author(s) as shown on or in the report. Enter last name, first name, middle initial. If military, show rank and branch of service. The name of the principal author is an absolute minimum requirement.

6. REPORT DATE: Enter the date of the report as day, month, year; or month, year. If more than one date appears on the report, use date of publication.

7*a*. TOTAL NUMBER OF PAGES: The total page count should follow normal pagination procedures, i.e., enter the number of pages containing information.

7*b*. NUMBER OF REFERENCES: Enter the total number of references cited in the report.

8*a*. CONTRACT OR GRANT NUMBER: If appropriate, enter the applicable number of the contract or grant under which the report was written.

8*b*, 8*c*, & 8*d*. PROJECT NUMBER: Enter the appropriate military department identification, such as project number, subproject number, system numbers, task number, etc.

9*a*. ORIGINATOR'S REPORT NUMBER(S): Enter the official report number by which the document will be identified and controlled by the originating activity. This number must be unique to this report.

9*b*. OTHER REPORT NUMBER(S): If the report has been assigned any other report numbers *(either by the originator or by the sponsor)*, also enter this number(s).

10. AVAILABILITY/LIMITATION NOTICES: Enter any limitations on further dissemination of the report, other than those imposed by security classification, using standard statements such as:

(1) "Qualified requesters may obtain copies of this report from DDC."

(2) "Foreign announcement and dissemination of this report by DDC is not authorized."

(3) "U. S. Government agencies may obtain copies of this report directly from DDC. Other qualified DDC users shall request through _____."

(4) "U. S. military agencies may obtain copies of this report directly from DDC. Other qualified users shall request through _____."

(5) "All distribution of this report is controlled. Qualified DDC users shall request through _____."

If the report has been furnished to the Office of Technical Services, Department of Commerce, for sale to the public, indicate this fact and enter the price, if known.

11. SUPPLEMENTARY NOTES: Use for additional explanatory notes.

12. SPONSORING MILITARY ACTIVITY: Enter the name of the departmental project office or laboratory sponsoring *(paying for)* the research and development. Include address.

13. ABSTRACT: Enter an abstract giving a brief and factual summary of the document indicative of the report, even though it may also appear elsewhere in the body of the technical report. If additional space is required, a continuation sheet shall be attached.

It is highly desirable that the abstract of classified reports be unclassified. Each paragraph of the abstract shall end with an indication of the military security classification of the information in the paragraph, represented as *(TS)*, *(S)*, *(C)*, *or (U)*.

There is no limitation on the length of the abstract. However, the suggested length is from 150 to 225 words.

14. KEY WORDS: Key words are technically meaningful terms or short phrases that characterize a report and may be used as index entries for cataloging the report. Key words must be selected so that no security classification is required. Identifiers, such as equipment model designation, trade name, military project code name, geographic location, may be used as key words but will be followed by an indication of technical context. The assignment of links, rules, and weights is optional.

MINIMUM BASIC DISTRIBUTION LIST FOR USAMC SCIENTIFIC AND TECHNICAL REPORTS IN METEOROLOGY AND ATMOSPHERIC SCIENCES

Commanding General (1)
U. S. Army Materiel Command
Attn: AMCRD-RV-A
Washington, D. C. 20315

Commanding General (1)
U. S. Army Electronics Command
Attn: AMSEL-EW
Fort Monmouth, New Jersey 07703

Commanding General (1)
U. S. Army Test and Evaluation Command
Attn: NBC Directorate
Aberdeen Proving Ground, Maryland 21005

Commanding Officer (1)
U. S. Army Ballistics Research Laboratories
Attn: AMXBR-IA
Aberdeen Proving Ground, Maryland 21005

Chief, Atmospheric Physics Division (2)
Atmospheric Sciences Laboratory
U. S. Army Electronics Command
Fort Monmouth, New Jersey 07703

U. S. Army Munitions Command (1)
Attn: Irving Solomon
Operations Research Group
Edgewood Arsenal, Maryland 21010

Commanding Officer (1)
U. S. Army Dugway Proving Ground
Attn: Meteorology Division
Dugway, Utah 84022

Commanding Officer (1)
U. S. Army CDC, CBR Agency
Attn: Mr. N. W. Bush
Fort McClellan, Alabama 36205

Commanding General (1)
U. S. Army Test and Evaluation Command
Attn: AMSTE-EL
Aberdeen Proving Ground, Maryland 21005

Commandant (1)
U. S. Army Signal School
Attn: Meteorological Department
Fort Monmouth, New Jersey 07703

Assistant Chief of Staff for Force Development (1)
CBR Nuclear Operations Directorate
Department of the Army
Washington, D. C. 20310

Director (1)
Atmospheric Sciences Programs
National Sciences Foundation
Washington, D. C. 20550

Assistant Secretary of Defense (1)
Research and Engineering
Attn: Technical Library
Washington, D. C. 20301

R. A. Taft Sanitary Engineering Center (1)
Public Health Service
4676 Columbia Parkway
Cincinnati, Ohio

Dr. Hans A. Panofsky (1)
Department of Meteorology
The Pennsylvania State University
University Park, Pennsylvania

Commanding General (1)
U. S. Continental Army Command
Attn: Reconnaissance Branch ODCS
for Intelligence
Fort Monroe, Virginia 23351

Commander (1)
Air Force Cambridge Research Laboratories
Attn: CRZW
1065 Main Street
Waltham, Massachusetts

President (1)
U. S. Army Artillery Board
Fort Sill, Oklahoma 73504

National Center for Atmospheric Research (1)
Attn: Library
Boulder, Colorado

Dr. J. E. Cermak, Head (15)
Fluid Mechanics Program
Colorado State University
Fort Collins, Colorado 80521

Author (1)

Chief of Research and Development (1)
Department of the Army
Attn: CRD/M
Washington, D. C. 20310

Commanding General (1)
U. S. Army Missile Command
Attn: AMSMI-RRA
Redstone Arsenal, Alabama 35809

Commanding General (1)
U. S. Army Natick Laboratories
Attn: Earth Sciences Division
Natick, Massachusetts 01762

Director, U. S. Army Engineer (1)
Waterways Experiment Station
Attn: WES-FV
Vicksburg, Mississippi 39181

Chief, Atmospheric Sciences Research Division (5)
Atmospheric Sciences Laboratory
U. S. Army Electronics Command
Fort Huachuca, Arizona 85613

Commanding Officer (1)
U. S. Army Frankford Arsenal
Attn: SMUFA-1140
Philadelphia, Pennsylvania 19137

Commandant (1)
U. S. Army Artillery and Missile School
Attn: Target Acquisition Department
Fort Sill, Oklahoma 73504

Commanding General (1)
U. S. Army Electronics Proving Ground
Attn: Field Test Department
Fort Huachuca, Arizona 85613

Commanding General (1)
U. S. Army Test and Evaluation Command
Attn: AMSTE-BAF
Aberdeen Proving Ground, Maryland 21005

Office of Chief Communications - Electronics (1)
Department of the Army
Attn: Electronics Systems Directorate
Washington, D. C. 20315

Chief of Naval Operations (1)
Department of the Navy
Attn: Code 427
Washington, D. C. 20350

Director (1)
Bureau of Research and Development
Federal Aviation Agency
Washington, D. C. 20553

Director of Meteorological Systems (1)
Office of Applications (FM)
National Aeronautics and Space Administration
Washington, D. C. 20546

Director (1)
Atmospheric Physics and Chemistry Laboratory
Environmental Science Services Administration
Boulder, Colorado

Andrew Morse (1)
Army Aeronautical Activity
Ames Research Center
Moffett Field, California 94035

Commanding Officer (2)
U. S. Army Cold Regions Research and
Engineering Laboratories
Attn: Environmental Research Branch
Hanover, New Hampshire 03755

Mr. Ned L. Kragness (1)
U. S. Army Aviation Materiel Command
SMOSM-E
12th and Spruce Streets
Saint Louis, Missouri 63166

Commanding Officer, U. S. Army (1)
Artillery Combat Development Agency
Fort Sill, Oklahoma 73504

Commander, USAR Air Weather Service (MATS) (1)
Attn: AWSSS/TIPD
Scott Air Force Base, Illinois

Dr. John Bogusky (1)
7310 Cedardale Drive
Alexandria, Virginia 22308

Commanding General (1)
U. S. Army Combat Development Command
Attn: CDCMR-E
Fort Belvoir, Virginia 22060

Commanding General (1)
U. S. Army Munitions Command
Attn: AMSMU-RE-R
Dover, New Jersey 07801

Commanding Officer (1)
U. S. Army Ballistics Research Laboratories
Attn: AMXBR-B
Aberdeen Proving Ground, Maryland 21005

Director (2)
Atmospheric Sciences Laboratory
U. S. Army Electronics Command
Fort Monmouth, New Jersey 07703

Chief, Atmospheric Sciences Office (2)
Atmospheric Sciences Laboratory
U. S. Army Electronics Command
White Sands Missile Range, New Mexico 88002

Commanding Officer (1)
U. S. Army Picatinny Arsenal
Attn: SMUPA-TV-3
Dover, New Jersey 07801

Commanding Officer (1)
U. S. Army Communications - Electronics
Combat Development Agency
Fort Monmouth, New Jersey 07703

Commanding General (1)
Deseret Test Center
Attn: Design and Analysis Division
Fort Douglas, Utah 84113

Commandant (1)
U. S. Army CBR School Micrometeorological
Section
Fort McClellan, Alabama 36205

Assistant Chief of Staff for Intelligence (1)
Department of the Army
Attn: ACSI-DERSI
Washington, D. C. 20310

Officer in Charge (1)
U. S. Naval Weather Research Facility
U. S. Naval Air Station, Building 4-28
Norfolk, Virginia 23500

Chief, Fallout Studies Branch (1)
Division of Biology and Medicine
Atomic Energy Commission
Washington, D. C. 20545

Director (1)
U. S. Weather Bureau
Attn: Librarian
Washington, D. C. 20235

Dr. Albert Miller (1)
Department of Meteorology
San Jose State College
San Jose, California 95114

Mrs. Francis L. Wheedon (1)
Army Research Office
3045 Columbia Pike
Arlington, Virginia 22201

Commander (1)
Air Force Cambridge Research Laboratories
Attn: CRXL
L. G. Hanscom Field
Bedford, Massachusetts

Harry Moses, Asso. Meteorologist (1)
Radiological Physics Division
Argonne National Laboratory
9700 S. Cass Avenue
Argonne, Illinois 60440

Defense Documentation Center (20)
Cameron Station
Alexandria, Virginia 22314

Office of U. S. Naval Weather Service (1)
U. S. Naval Air Station
Washington, D. C. 20390

Dr. Gerald Gill (1)
University of Michigan
Ann Arbor, Michigan 48103